Study of local heat transfer coefficient on peripheral PWR assembly fuel in the event of touching spacer grids

Final Report

Simon Walker, Simon Lo

Checkendon Hill Ltd
Checkendon Hill House
Streatley
Berks
RG8 9SX

Title	**Study of local heat transfer coefficient on peripheral PWR assembly fuel in the event of touching spacer grids** **Final Report**
Prepared for	Office for Nuclear Regulation
Report No.	CH/ONR/2016/36 v4: Final to ONR (incorporating ONR comments on v3)
Contract:	36 ONR (2016)
Confidentiality, copyright and reproduction	This report is submitted by Checkendon Hill Ltd in connection with a contract to supply goods and services and is submitted on the basis of confidentiality. The contents must not be disclosed to third parties except in accordance with terms of the contract.
Contact Details	Checkendon Hill Ltd Checkendon Hill House Streatley Berks RG8 9SX s.p.walker@checkendonhill.com
Author(s)	S P Walker
	Simon Lo
Reviewed by	Simon Lo
	S P Walker
Approved by	S P Walker

SUMMARY

This report discusses means to assess the propensity to "critical heat flux" for the fuel rods in a PWR on the outer periphery of a subassembly, when that subassembly has bowed such that the outer face of its spacer grid comes into contact with the outer face of the spacer grid of the neighbouring assembly.

We begin with a discussion of the CHF phenomenon itself, and describe the two radically different forms that it takes, of "bubble crowding", and "film dryout". We review the means by which these events are predicted under "normal" geometries, such as uniform tubes or rods bundles, using "non-CFD" methods such as correlations, look up tables, and phenomenological modelling.

The particular and rather difficult geometry of interest has little prospect of being well addressed by these methods, but seems likely to require a more "three-dimensional" capability. Given this, we next review the current capabilities of computational fluid dynamics to predict single and two-phase flows in rod bundles, and in rod bundles incorporating spacer grids. We then turn to the prospects for the extension of this CFD capability to predict the two forms of CHF. The conclusion is broadly the same for both. A great deal of work is being devoted to this, results are encouraging, but a reliable blind *a priori* prediction, for general cases, is still some way off. With that being the case for "normal" geometries, it is still more so for the particularly difficult one of the "downstream of touching spacer grids" circumstances.

Given this assessment of the state-of-the-art, we then consider what useful information could be gained by a pragmatic application of our present capabilities regarding the reduction, if any, of the margin to CHF caused by these conditions.

Having briefly reviewed measurement capabilities, we speculate that it might be relatively straightforward to measure CHF performance of a suitably modified bundle, and gain probably a rather good indication of this margin diminution.

There is some operational evidence (crud) that a little way downstream of this touching spacer grid nucleate boiling occurs (and which does not occur in the absence of such touching). The prediction of the occurrence very low quality sub-cooled nucleate boiling (and even more its relative propensity to occur, which is of most interest here) is arguably one of the more robust predictive capabilities associated with two phase flow. (Indeed, it is barely two-phase flow, after all). This suggests that it should be possible to gain some credible indications of the reduction in margin to bubble crowding CHF caused by the deformation of the fuel, relative to its initial geometry.

However, it is our understanding that the form of CHF that is most likely to be of concern here is the film dryout kind. Modelling of this using CFD depends upon adequate sub-models of droplet deposition, droplet entrainment, and of the flow of the liquid film. None of these are actually handled in a very 'physical' way in present approaches. Whilst it is the case that despite this results for smooth rod bundles, and even spacer grids, are actually rather good, it is hard to see how one could be confident in predictions for this rather difficult geometry. This is an area where we suspect good progress could be made, but only via a substantial research programme, and over a corresponding period. We are not certain, but assume that the timescale and associated resources in this present case would not permit this.

1 INTRODUCTION

Our instructions[1] with regards to this study were to discuss means to assess the "local heat transfer coefficient", or perhaps more generally the propensity to "critical heat flux" of the fuel rods in a PWR on the outer periphery of a subassembly, when that subassembly has bowed such that the outer face of its spacer grid comes into contact with the outer face of the spacer grid of the neighbouring assembly. The reason for the concern is that flow control tabs on these spacer grids are turned inwards on the outer rows of fuel rods, such that taken together the two spacer grids and their tabs could form a significant impediment to flow of coolant.

The structure of the report is as follows.

In Section 2 we present the geometry at issue, and expand upon the scope of the work and the questions to be addressed.

In Section 3 we discuss the background to the topic generally (albeit unfortunately) termed CHF, or 'Critical Heat Flux'. These are the circumstances when nuclear fuel that is intended to be cooled by liquid water becomes cooled, rather, by only steam.

In Section 4 we discuss the various essentially empirical methods that are available for the prediction of this CHF condition; gatherings of experimental measurements represented via algebraic correlations, and experimental measurements gathered to form 'Look up Tables'.

The use of computational fluid dynamics for the prediction of subcooled nucleate boiling is described in Section 5, as a precursor to a discussion of, in effect, how this is extended to permit to a degree the prediction of both bubble crowding CHF and film dryout CHF using both CFD, and more 'classical' phenomenological modelling, in Section 6 and Section 7 respectively.

All the above has related essentially to prismatic geometries. In Section 8 we assess the ability of modern CFD to predict flows in the complex geometries of rod bundles and spacer grids, and in Section 9 we review the state of the art in the prediction of boiling flows in these geometries.

A review of approaches to CHF measurement is presented in Section 10.

Drawing on all of the above, in Section 11 we discuss what options are in our view available for assessing the propensity to CHF in the fuel downstream of touching spacer grids.

2 THE PARTICULAR CIRCUMSTANCES OF CURRENT INTEREST

2.1 The 'touching spacer grid' geometry

Our understanding of the geometry is indicated schematically in Figure 1. This shows a plan section of part of two adjacent subassemblies, at a height that also shows a spacer grid. The solid grey portions are our attempt to indicate both the spacer grid outer wrapper, and in particular the approximately semicircular folded-over tabs that obstruct part of the flow passage between adjacent pins. Note in this figure the clear passage for the axial flow of coolant between the two spacer grid wrappers.

In Figure 2 we show the same assemblies, but after radiation-induced deformation has caused bowing, such that the lateral displacement of one or both subassemblies causes the outer faces of their wrappers to come into contact. The upward flow of coolant is impeded across probably the entire width of the space grid, by these wrappers, and in particular tabs, that are now in contact.

After these two rather idealised drawings, in Figure 3 we show a more realistic three-dimensional representation of an Areva spacer grid. Taken together it is hoped the geometrical issue under consideration is made clear by these figures.

2.2 Operational evidence

It is our understanding that evidence for this touching includes the observation of surface marking on the outer faces of adjacent spacer grids, presumably where they have been brought into contact by subassembly deformation, and either in-service fretting, or the process of fuel extraction, has caused visible marking.

One consequence (it is believed) of this touching, and postulated coolant flow reduction, is the observation of patches of crud about 10 hydraulic diameters downstream of the tabs. Crud is commonly observed to be formed preferentially at locations where there is some nucleate boiling on the surface, and the assumption is that nucleate boiling has occurred at this location because the reduced flow and possibly turbulence has allowed wall superheat to increase, to the point that such boiling can occur.

2.3 Thermal hydraulic consequences

2.3.1 Reduced margin to DNB

One consequence of the reduced flow and changed turbulence conditions downstream of this obstruction is that the ratio (margin) to the departure from nuclear boiling ("DNBR") might be reduced. Indeed, the presence of the crud, indicating nucleate boiling where it used not to occur, is good evidence of this.

Without passing any comment on its likelihood or degree, it is worth commenting that the circumstances and "phenomena" involved in this would be essentially that of normal DNB. It is just that the rate of flow of the coolant, and its turbulence characteristics, would be different from in a normal subchannel.

The circumstances under which all of this might arise one might generally expect to be characterised by normal (that is, high) pressure, normal (that is, high) flow rates, but with the thermal power generation within the pin increased significantly above its nominal intended

value. The occurrence of these circumstances, their causes and likelihood, is part of the normal safety case for the plant and so on, and we are not addressing that at all here.

2.3.2 Reduced margin to film dryout

As we discuss extensively elsewhere in this report, the other mechanism by which the metal cladding might become cooled only by vapour, rather than by liquid water, is the mechanism of "film dryout".

As is discussed as part of this, the occurrence of film dryout in a normal smooth tube depends upon the interaction of the phenomena of droplet deposition, droplet entrainment, and the rate of evaporation of the liquid film due to heating from the wall.

Whilst one might expect the rate of heating to be little changed, in other respects the mechanism for film dryout will be probably radically different.

The thin liquid film flowing up the fuel rod will encounter the wrapper itself, and as this wrapper is touching its neighbour, the film will presumably be forced to move inwards, into the subassembly, before carrying on vertically upwards on the inside of the wrapper, and on nearby fuel rods. Of itself, one might speculate that that would not degrade film dryout performance. Simple-mindedly, the liquid is actually being forced to flow in a more useful location, over fuel cladding, rather than over the outside of a spacer grid. However, at the downstream (vertically-upward) exit from the spacer grid, the folded-over tab would seem likely to disrupt the film, and could cause there to be a region in the downstream "wake" of the tab where the fuel surface was cooled only by vapour.

One generally expects concerns over film dryout to occur at low pressures and low flow rates, and indeed often at powers below nominal. As for the reduced margin to DNB, the likelihood and circumstances of such occurrences are part of the safety case of the plant, and are not something that we consider here.

2.3.3 Closing remarks

It is our understanding that of the two possible mechanisms by which the fuel might be threatened, DNB or dryout, that dry out is of greater concern. We will consider both, but the balance of emphasis will be on the dry out issue.

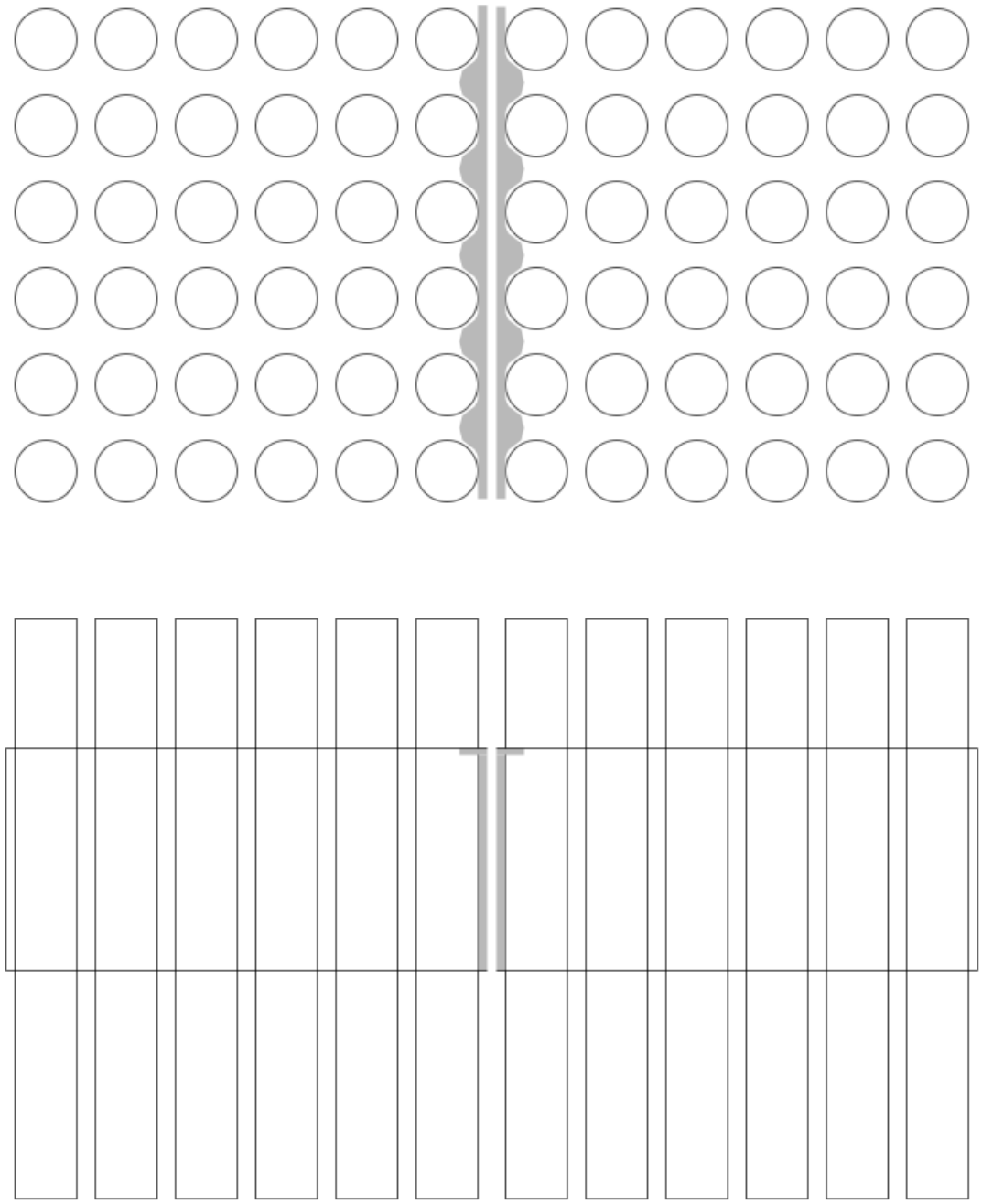

Figure 1
An idealized depiction of portions of two adjacent sub-assemblies in their normal, intended configuration. The upper part of the figure shows them in plan section, and the lower part in side elevation. The solid grey region is an attempt to indicate the space grid outer wrapper, and the folded-over tabs that close part of the flow passage between adjacent pins on the exterior of the subassembly. (NB: Indicative only, and not to scale.)

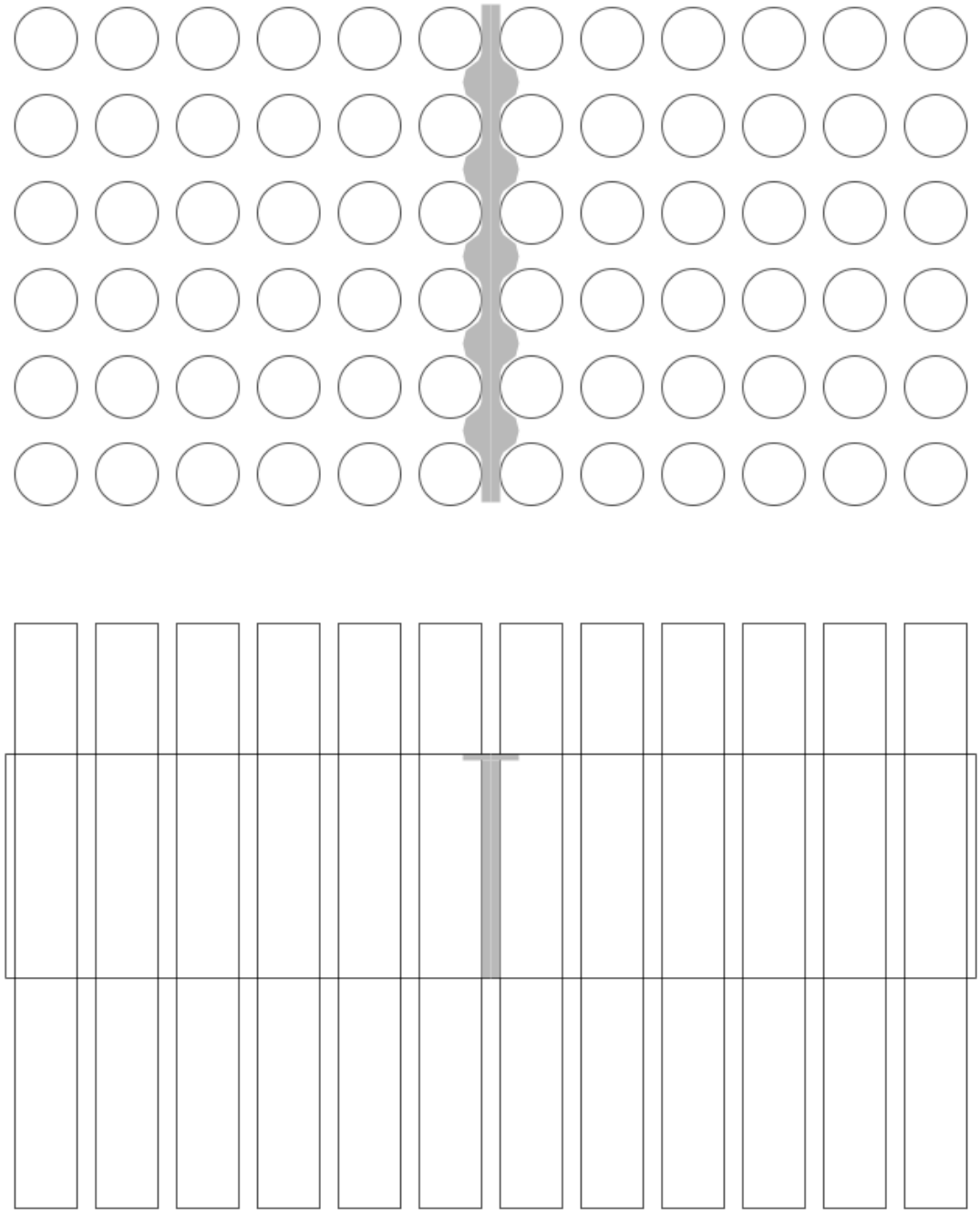

Figure 2
Portions of two adjacent subassemblies after deformation has caused them to move together and the outer faces of the two wrappers to touch. These touching wrappers, together with the folded over tabs, now form an impediment to the flow of coolant.

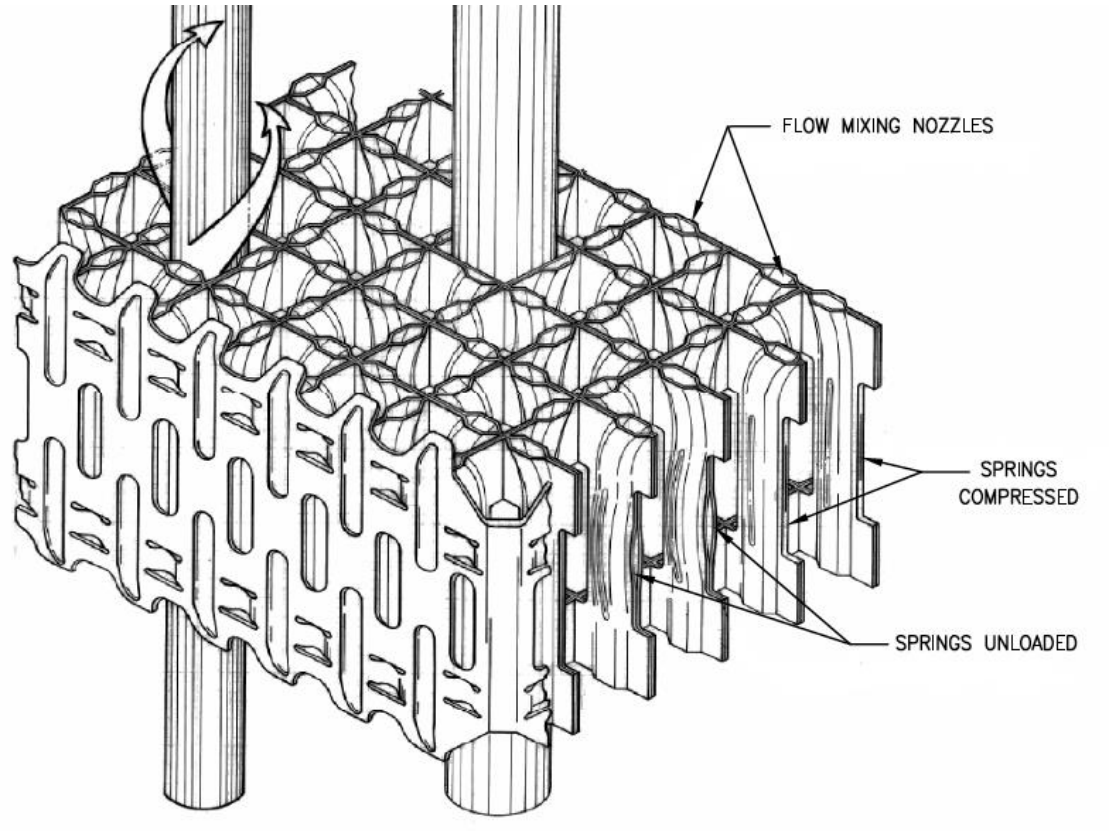

Figure 3
A typical Areva spacer grid. Note the inwards-folded tabs on the outside face of the assembly.

3 CHF: PHENOMENA, PHYSICS AND TERMINOLOGY

At low to medium heat fluxes, boiling heat transfer is an efficient means of transferring heat from a surface to a fluid flowing over it. The fluid can either be a sub-cooled liquid (in which case the boiling process is referred to as *sub-cooled boiling*) or a vapour-liquid mixture. However, under certain conditions, a transition can occur which leads to a less favourable heat transfer situation. This transition can be defined as follows

- For a *heat flux controlled surface* (e.g. one with electrical heating or nuclear heating), the transition corresponds to *an inordinate increase in surface temperature* following a small increase in surface heat flux, or a small decrease in fluid flow rate or a small increase in the fluid temperature entering the system.

- For a *surface temperature controlled surface* (e.g. one heated by condensing steam), the transition corresponds to *an inordinate decrease in the surface heat flux* following a small increase in surface temperature

In what follows, we shall be concerned principally with the first type of manifestation of the transition. Many names have been given to this transition and this has caused considerable confusion. Perhaps the most correct names are *boiling transition* or *boiling crisis* but these have not been widely adopted. All of the other names (*departure from nucleate boiling (DNB), burnout, dryout, critical heat flux (CHF)*) contain an implicit assumption of the mechanism of the transition and/or of its consequences. However, in what follows, we use the term CHF to describe the transition. This nomenclature is now widely adopted but it should not be taken to imply that the transition is governed specifically by heat flux.

CHF is of profound importance in water reactor design and analysis. Its significance spans from "normal operation", where boiling processes contribute to imposing limits on powers and power densities, to various aspects of postulated accidents, involving the drying-out and subsequent re-wetting of hot surfaces. The importance of the CHF phenomenon is reflected in the large literature on the subject. Extensive earlier reviews are given by Hewitt[2], Tong and Tang[3] and Hewitt[4].

A general representation of flow regimes and associated wall temperatures in vertical flow in a heated tube is given in Figure 4[5]. We will discuss below the main regions within this that 'critical heat flux' may occur.

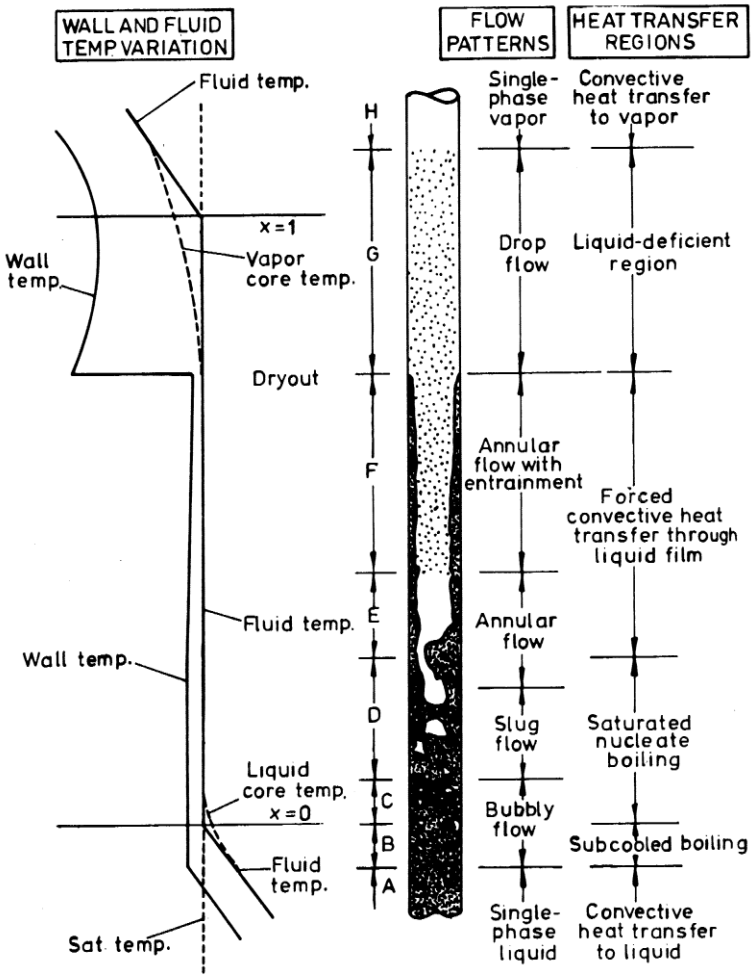

Figure 4
Regions of heat transfer in convective boiling (reproduced from Collier [5])

3.1 Regions of operation of CHF mechanisms

As a precursor to a phenomenological analysis, Le Corre[6] presented a description of the regions of applicability of the various CHF mechanisms in sub-cooled boiling. He distinguishes three types of CHF as follows:

Type 1: Bubbly flow. At high mass flux and subcooling, isolated bubbles may slide and detach but not coalesce. Wall-rooted bubbles are observed to coalesce with neighbouring bubbles. At CHF, a reduced boiling activity is seen.

Type 2: Vapour clots. This type of behaviour is usually observed under moderate subcooling. Bubbles detach from nucleation sites but remain within the bubbly layer, coalescing to form periodic vapour clots.

Type 3: Slug flow. Here, vapour slugs are observed with a thin film along the wall. Fluctuating wall temperatures can be measured with high temperatures corresponding to the vapour slugs.

In general, CHF corresponds to the local wall overheating, the prevention of rewetting and the subsequent spreading of the dry spot. In Type 1 CHF, the dry spot is controlled by the

wall nucleation cycle whereas in Type 2 and Type 3 CHF, the time of the dry spot formation is controlled by the passage of vapour clots and vapour slugs. Le Corre et al plotted the location of the three types of CHF in terms of quality and Weber number, defined via $We = G^2 D / r_f s$, where G is the mass flux, D the channel diameter, r_f the density of the saturated liquid and s the surface tension). The resultant plot is shown in Figure 5.

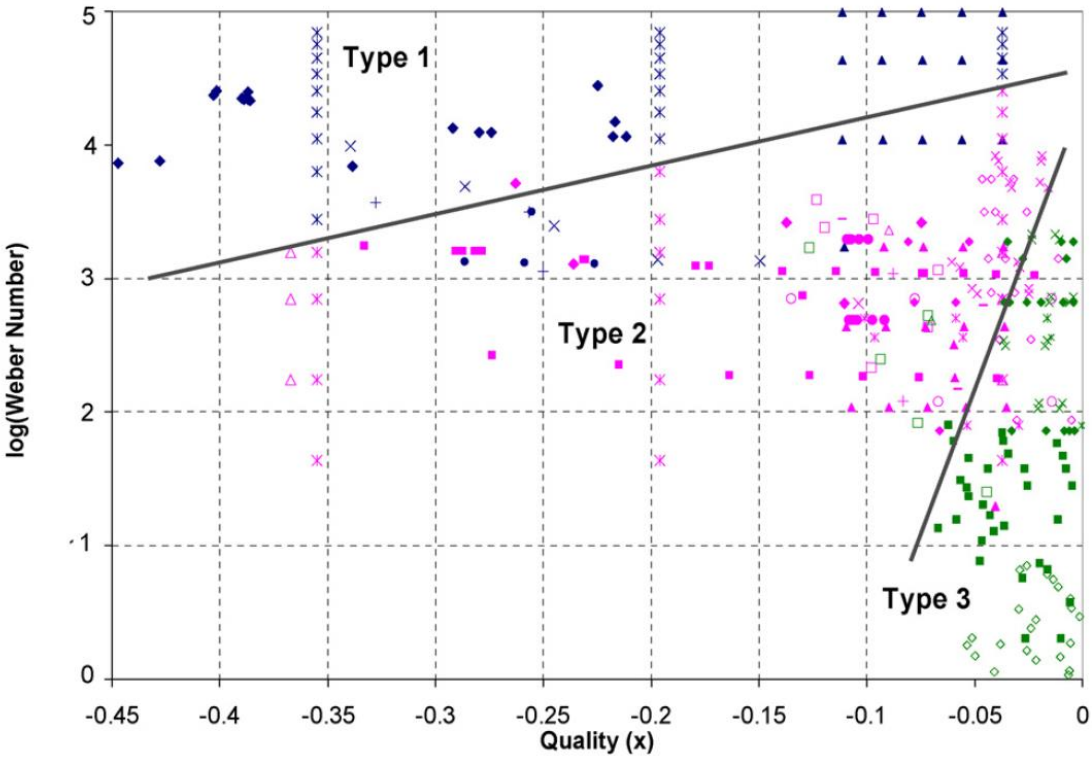

Figure 5
Sub-cooled boiling CHF Flow Regime Map, from Le Corre[6]

An alternative, complementary view of the regions of operation of CHF, which extends to the high-quality, film dryout case, is given in Figure 6, by Semeira & Hewitt, taken from Hestroni[7].

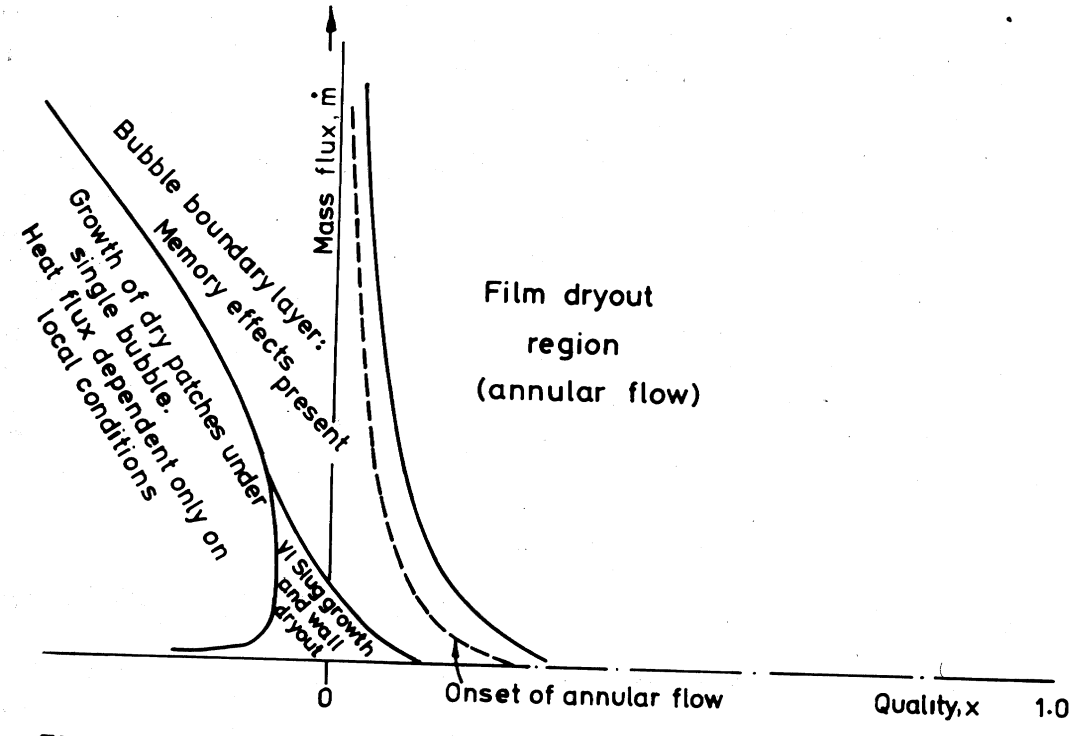

Figure 6
Indicative regions of operation of CHF mechanisms, from Hestroni (page 6.4.56) [7]

3.2 "Critical heat flux" mechanisms: Sub-cooled and low quality

In a regime commonly termed 'bubbly flow', during 'normal' nucleate boiling small vapour bubbles are formed at nucleation sites, and (assuming conditions permit) grow, and then lift off or are swept off into the flow. This is a very effective means of heat transfer, and wall temperatures very little above fluid temperatures are sufficient to remove large heat fluxes. As the heat flux through the surface is increased, the rate of formation of these bubbles, and their area density, increases. At some *critical heat flux* the high bubble density, and / or the inability of the fluid to re-wet the wall following their departure, results in the wall being blanketed with vapour. Heat transfer through this vapour layer is very poor, and with the postulated fixed heat flux, the surface temperature must rise greatly.

A common (and appropriate) term for this phenomenon is 'Departure from Nucleate Boiling', DNB. The heat flux at with it occurs is a function of the flow conditions generally, but the main dependencies are on

-the local degree of sub cooling of the bulk fluid

-the local turbulence intensity / Reynolds number.

3.3 "Critical heat flux" mechanisms: High quality film dryout

The other main physical circumstances under which a dramatic transition in surface heat transfer occurs is in the final drying out of the liquid film; the interface between regions F and G of Figure 4, and the end of 'annular flow'. Prior to this point the liquid film has been subject

to a loss of liquid both from entrainment of droplets from its surface, and by evaporation. It was also in receipt of liquid, by the deposition of droplets entrained in the vapour flow in the core. The balance of these effects is that the film thickness and mass flow rate reduce with height, up to the point where they both become zero, and film dryout occurs.

3.4 Visualisation of CHF data in the context of the mechanisms

We will discuss later how CHF experimental observations may be correlated and tabulated, but for the moment will just make use of a visual representation of this data to aid discussion of the mechanisms.

This visual representation was obtained by plotting tabulated values from the Look-up Tables of Groeneveld[8], but in principle identical (for present purposes) images would have been obtained by plotting evaluations of correlations.

The high mass flux – low quality values are associated with the move from sub-cooled nucleate boiling to vapour film generation, via bubble crowding or some similar mechanism. One striking feature of these regions is the strong dependence on pressure, with the CHF at 210bar being only about 1/5 of that at 70bar. This is in part of course a consequence of the great reduction of enthalpy of evaporation with pressure, here by a factor of about 3 ½.

The high quality CHF values are orders of magnitude lower, and generally are associated with the final drying out of a film of liquid flowing over the heated surface. All values are low, and there is not the opportunity for any marked effect of pressure to be apparent.

This clean separation into two regimes is in practice rather more nuanced, and actual behaviour depends of course on factors such as heat flux and flow rate. For example, it is possible for the heat flux to be such that nucleate boiling occurs at the interface of the film and the heated surface (where commonly conduction is sufficient to inhibit nucleation), and even for this rate of nucleate boiling to be such as to lead to a DNB-type CHF. However, as a means to identify the main characteristics of the two principal mechanisms, this should be a helpful characterisation.

There are a few general observations that can be made:-

As defined here, CHF of the 'low quality' kind will not necessarily occur at all during the change of the fluid from all liquid to all vapour.

Conversely (as long as conditions are such that film flow occurs at all) CHF will necessarily occur, as eventually the film will dry out. This could well be after a long length, if the applied heat flux is low, and be associated with a modest temperature rise in the tube wall (inter alia, making plain why the term 'burnout' is to be deprecated).

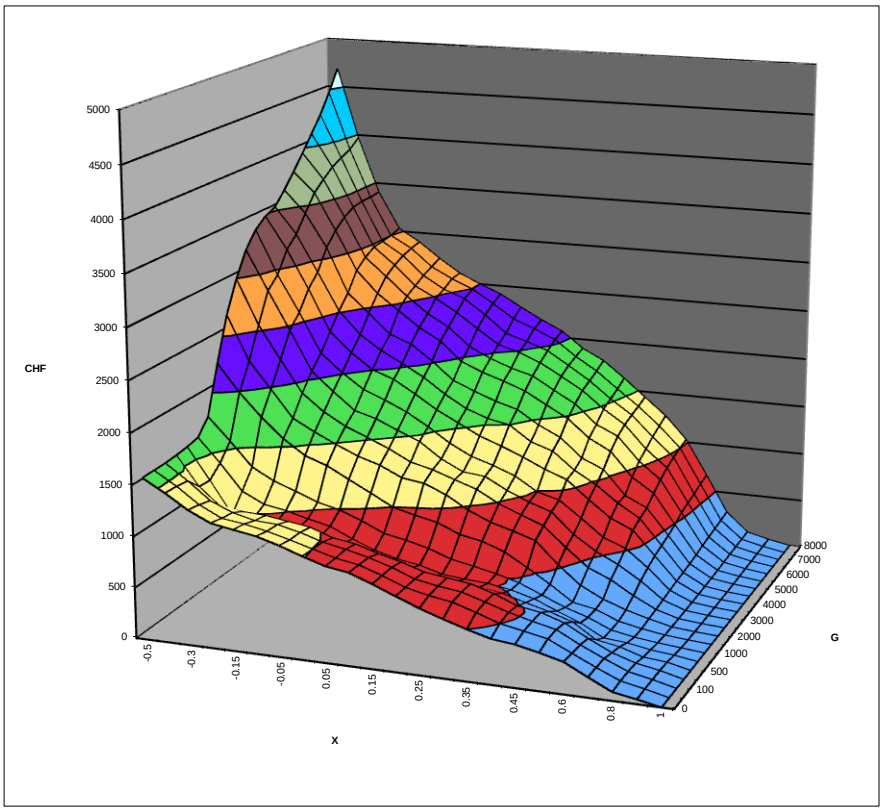

Figure 7
210 bar: Critical heat flux, CHF, (kW m^{-2}) dependence on mass flux (G, kg m^{-2} s^{-1}) and quality

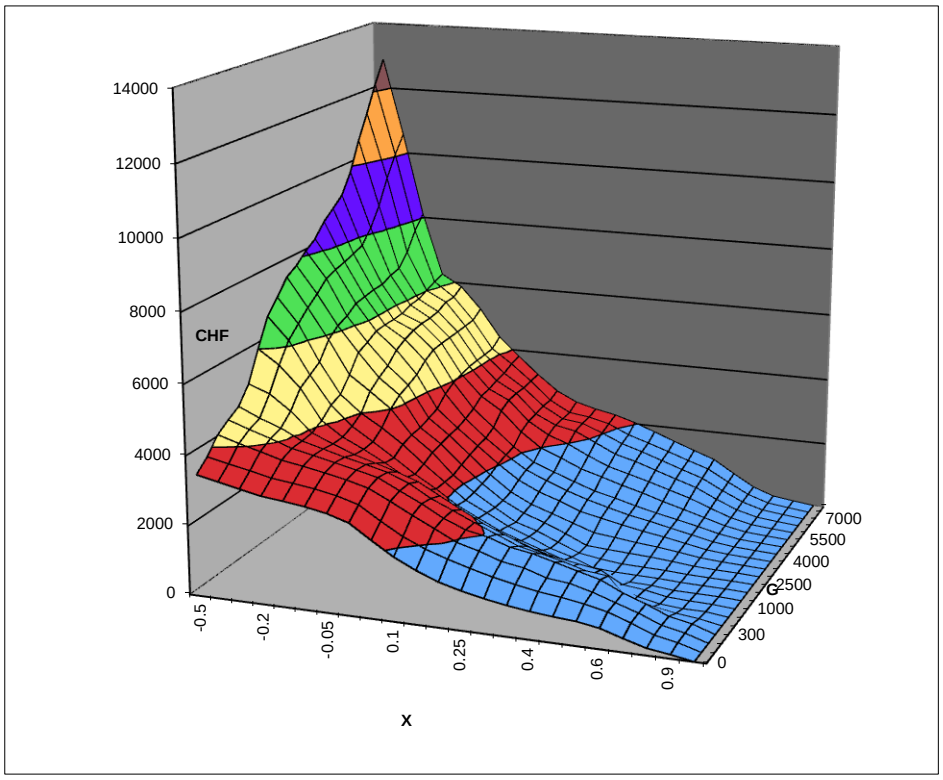

Figure 8
140 bar: Critical heat flux, (CHF, kW m^{-2}) dependence on mass flux (G, kg m^{-2} s^{-1}) and quality

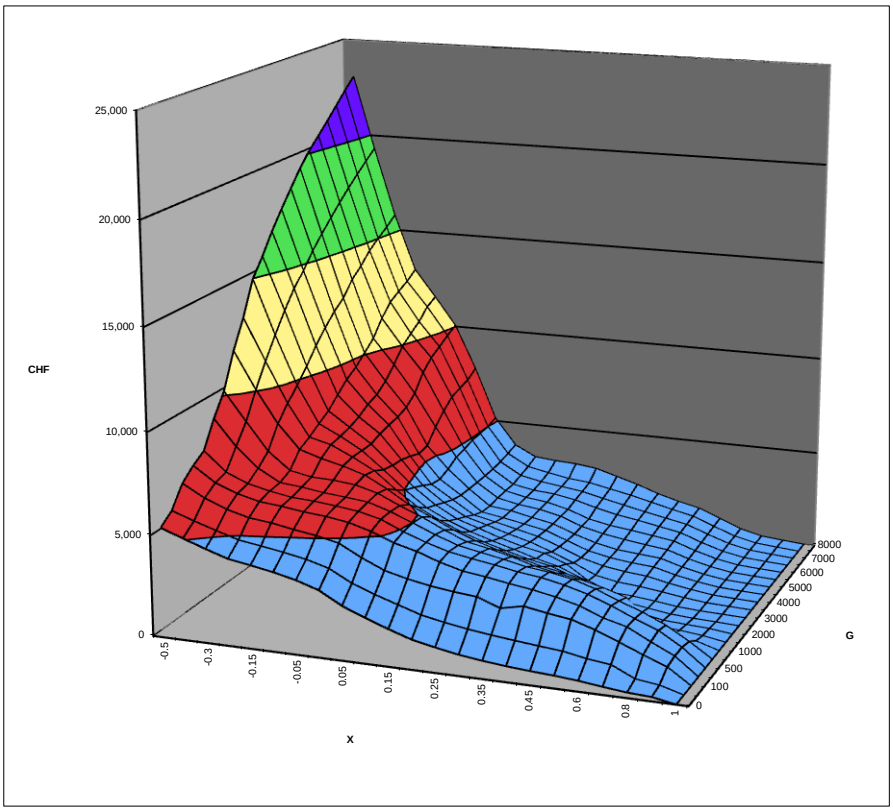

Figure 9
70 bar: Critical heat flux, (CHF, kW m^{-2}) dependence on mass flux (G, kg m^{-2} s^{-1}) and quality

4 CHF PREDICTION METHODS

To design, and to conduct safety assessments, it is plainly desirable to be able to predict whether or not, and which kind of, CHF will occur under any particular set of circumstances. In this section we will discuss what might loosely be termed "classical" prediction methods. We will divide these into three broad classes; simple(!) interpolation of data via look-up tables, "empirical correlations", and the third "phenomenological modelling". However, there is not a sharp distinction between these latter two. In particular phenomenological modelling necessarily employs empirical correlations anyway; the phenomena are too complex for true first-principles prediction.

4.1 Empirical algebraic correlating equations

4.1.1 Introductory remarks

Vast numbers of experimental measurement of CHF have been made, reflecting its wide industrial importance, in particular in the nuclear power area. As an indication, the latest set of 'Look Up Tables' (about which more below) are based on a collection of some 30,000 measurements[8]. These are commonly correlated to provide convenient tools to identify when CHF is to be expected, and a very large number of such correlations have been proposed.

As with correlating any set of experimental measurements, a degree of physical insight must be employed to identify the most significant independent variables, and (even more) the groupings into which these most naturally fall. Tong[3] gives a helpful description, which we will paraphrase here:

The system pressure determines the saturation temperature, and other related properties of the fluid, including the enthalpy of vaporisation, important for bubble formation. The viscosity and surface tension, evaluated again at the saturation temperature, control the bubble size, buoyancy, and the local void fraction distribution. The local enthalpy and mass flux affect bubbly-layer thickness, and liquid entrainment in annular flow.

Based on these arguments, correlations have been sought (eg the W-3 correlation) in the form of couplings of terms, which include functions of these groupings, viz:

$$q_{CHF} = F_1\left(X,p\right)F_2\left(X,G\right)F_3\left(D_e\right)F_4\left(H_{in}\right) \tag{15.1}$$

Nonetheless, the process is naturally still essentially empirical. It is also a very 'non-deterministic' one. As early as 1964 Milioti (in a Penn State University thesis) is reported by Collier[9] as having identified some 59 correlations.

4.1.2 The Macbeth correlation

An early correlation is that due to Macbeth[10], based on the hypothesis that the CHF is largely a function of the local mass quality. It is notable for its generality, and as an early version is worthy of a fuller discussion.

Before incorporating Macbeth's modelling approximations, it is helpful to establish some basic relationships.

In general CHF is a function of various physical quantities:

$$\dot{q}''_{CRIT} = f\left(G,D,p,X_{LOCAL}\right) \tag{15.2}$$

The enthalpy at any location z is (including the particular case when the applied heat flux is equal to some critical one):

$$h(z) = h_{INLET} + \frac{\dot{q}''_{CRIT}\pi Dz}{\dot{m}} \tag{15.3}$$

and the quality at any location z is in general

$$X(z) = \frac{h(z) - h_{lsat}}{h_{fg}} \tag{15.4}$$

or expressing the local enthalpy in terms of the inlet enthalpy and the applied heat flux:

$$\begin{aligned} X(z) &= \frac{\left(h_{INLET} + \frac{\dot{q}''_{CRIT}\pi Dz}{\dot{m}}\right) - h_{lsat}}{h_{fg}} \\ &= \frac{\left(h_{INLET} - h_{lsat}\right) + \frac{\dot{q}''_{CRIT}\pi Dz}{\dot{m}}}{h_{fg}} \end{aligned} \tag{15.5}$$

Note that the above statements are equally correct (and arguably more useful, and certainly more general) if the heat flux had not been denoted as the 'critical' value.

Macbeth starts from the hypothesis that the CHF is a function solely of the local thermodynamic quality; that is:-

$$\dot{q}''_{CRIT} = f\left(X_{LOCAL}\right) \tag{15.6}$$

That is, for any particular set of the many parameters on which the value of CHF does depend, there will be a single value of local quality at which it occurs.

According to Collier, Macbeth makes the additional assumption that the CHF is a ***linear*** function of inlet subcooling:

$$\dot{q}''_{CRIT} = A + B\left(h_{INLET} - h_{lsat}\right) \tag{15.7}$$

(This is a *really* tortured statement to make. It makes sense (it still may not be 'correct', but that is different!) ONLY if the unspoken restrictions are added that the tube is of a known, fixed length, and that that length is chosen so that CHF occurs at the tube exit. We will then require this.)

Using this assumption, we can eliminate $\left(h_{INLET} - h_{lsat}\right)$ between (15.5) and (15.7):

$$X(z) = \frac{\frac{\left(\dot{q}''_{CRIT} - A\right)}{B} + \frac{\dot{q}''_{CRIT}\pi Dz}{\dot{m}}}{h_{fg}} \tag{15.8}$$

This tidies up to:

$$X\left(z\right)=\frac{\dot{q}''_{CRIT}\left(\frac{1}{B}+\frac{\pi Dz}{\dot{m}}\right)-\frac{A}{B}}{h_{fg}}=\dot{q}''_{CRIT}\frac{1}{h_{fg}}\left(\frac{1}{B}+\frac{\pi Dz}{\dot{m}}\right)-\frac{A}{h_{fg}B} \tag{15.9}$$

or

$$\dot{q}''_{CRIT}=\frac{X\left(z\right)+\frac{A}{h_{fg}B}}{\frac{1}{h_{fg}}\left(\frac{1}{B}+\frac{\pi Dz}{\dot{m}}\right)}=X\left(z\right)\frac{h_{fg}}{\left(\frac{1}{B}+\frac{\pi Dz}{\dot{m}}\right)}+\frac{A}{B\left(\frac{1}{B}+\frac{\pi Dz}{\dot{m}}\right)} \tag{15.10}$$

or

$$\dot{q}''_{CRIT}=X\left(z\right)\frac{h_{fg}}{\left(\frac{1}{B}+\frac{\pi Dz}{\dot{m}}\right)}+\frac{A}{\left(1+\frac{\pi DzB}{\dot{m}}\right)} \tag{15.11}$$

or

$$\dot{q}''_{CRIT}=M+NX\left(z\right) \tag{15.12}$$

Equation (15.12) indicates that the assumption of a linear relationship between CHF and inlet subcooling (with its attendant qualifications) corresponds to a linear relationship between CHF and the local quality at which CHF occurs.

In essence, this has established that a consequence of Macbeth's postulate that 'CHF is a ***linear*** function of inlet subcooling' is that the functional relationship in (15.6) is itself the linear one

$$\dot{q}''_{CRIT}=f\left(X_{z=z_{CHF}}\right)=M+NX_{z=z_{CHF}} \tag{15.13}$$

where

$$N=\frac{h_{fg}}{\left(\frac{1}{B}+\frac{\pi Dz}{\dot{m}}\right)} \tag{15.14}$$

and

$$M=\frac{A}{\left(1+\frac{\pi DzB}{\dot{m}}\right)} \tag{15.15}$$

where in each of these definitions the z is the location at which CHF is observed.

(And so why not simply make this assertion up front? Anyway:-)

We can invert (15.14) to obtain

$$B = \frac{-N}{\left(\frac{N\pi Dz}{\dot{m}} - h_{fg}\right)} \tag{15.16}$$

and (15.15) to obtain

$$A = M\left(1 + \frac{\pi DzB}{\dot{m}}\right) \tag{15.17}$$

or

$$A = M\left(1 - \frac{\pi DzN}{\left(N\pi Dz - \dot{m}h_{fg}\right)}\right) = M\left(1 - \frac{1}{\left(1 - \frac{\dot{m}h_{fg}}{N\pi Dz}\right)}\right) \tag{15.18}$$

We can rewrite (15.7) using these to get

$$\dot{q}''_{CRIT} = M\left(1 - \frac{1}{\left(1 - \frac{\dot{m}h_{fg}}{N\pi Dz}\right)}\right) + \frac{-N}{\left(\frac{N\pi Dz}{\dot{m}} - h_{fg}\right)}\left(h_{INLET} - h_{lsat}\right) \tag{15.19}$$

This is in effect the Macbeth correlation. Values of the constants M and N are found by causing the straight line they generate to be the 'best' fit to the experimental observations.

4.1.3 Boiling length correlations

An alternative way of correlating is via boiling length, defined as the distance in the flow direction beyond the point at which the thermodynamic quality becomes zero.

In an 'inlet conditions' or boiling length-based representation, the CHF is modelled as being a function of the inlet quality and the distance along the tube till CHF is observed:

$$\dot{q}''_{CRIT} = f\left(G, D, p, L, x_{INLET}\right) \tag{15.20}$$

The quantities are

G	Mass flux
D	Tube diameter
p	Pressure
L	The tube length (see below)
X_{INLET}	The thermodynamic quality at inlet

In the above, L is the tube length, or, better, the distance from the inlet into the tube at which the CHF occurs. (Naturally, at a different value of imposed heat flux, this distance would be different.)

Here, x is the thermodynamic quality, which is directly related to enthalpy by

$$h = h_{l\_sat} + x h_{lg} \tag{15.21}$$

For a uniform heat flux, a correlation that involves these variables is found to be a reasonably good representation of what is observed.

The equivalence of inlet conditions and local conditions representations: The fact that both representations are reasonable is not surprising, as the representations are fundamentally the same. We will demonstrate this:

Since at any axial location L we have

$$h(L) = h_{INLET} + \int_{L'=0}^{L=L} \dot{q}''_{CRIT} \pi D \, dL' \tag{15.22}$$

we can use (15.22) and (15.21) to express

$$x_{LOCAL} = g\left(x_{INLET}, L, \dot{q}''_{CRIT}\right) \tag{15.23}$$

in effect recovering (15.20), as

$$\dot{q}''_{CRIT} = f\left(G, D, p, g\left(X_{INLET}, L, \dot{q}''_{CRIT}\right)\right) \tag{15.24}$$

albeit possibly requiring some iteration to evaluate numerically.

Note that whilst these approaches may be formally 'algebraically' equivalent, they do not in general give quite the same numerical values for predicted CHF. This is because they are anyway only approximate 'fits' to the observed actual heat flux, which is both a chaotic phenomenon, and is a function of more variables than those featuring in the expressions above. (In a similar vein, we will later see that the 'direct' and the 'heat balance' methods of using the look up tables do not lead to the same CHF values.)

A widely used boiling length correlation is that due to Biasi[11], and (despite its age!) it is the main correlation offered, for example, in the TRACE code[12].

4.1.4 Closing remarks

The generation of correlations has continued. In a recent review, Hall[13] identified over 100 correlations for sub-cooled flow in a uniformly heated round tube.

Moreover, having also gathered what they claim is the largest database of such measurements, some 32,000 data points[14], Hall used these to produce a further correlation. It is claimed to be more physically-based, employing only some ~1/10 of their database, but apparently is 'far more accurate' than others, and is 'more accurate' than the widely-used 'Look-Up Tables'[8].

A useful paper with various correlations quoted, and including a methodical comparison of their predictions, is produced by Ferrouk[15]. It covers the evaluation of the performance of twelve critical heat flux correlations. A review of critical heat flux models/correlations applicable to non-uniform axial heat profile is provided. Simulation results using prediction methods based on local conditions, the Tong F-factor and boiling length approaches were compared.

4.2 Data interpolation

4.2.1 Introduction

An alternative to, and indeed arguably a response to, the great proliferation of different correlations is simply a reversion to the raw data. In principle, this is what is done with "look up tables".

Early work began in parallel, both in the West and in the Soviet Union, with the Russian Academy of Sciences publishing tables in 1976. One of the main Western efforts was centred in Canada, and this work has become consolidated with the early Russian work, and has led to the now nearly ubiquitous Groeneveld Lookup Tables[8].

4.2.2 The construction and use of the tables

There is by now a simply vast collection of measurements of critical heat flux for water flowing inside pipes. (There is of course also a large set of data for other fluids and other configurations, but we will concentrate on water in pipes here.) For example, those in the database employed by Groeneveld [8] in his look-up table number some 33,000. They cover a range of conditions, including of different pipe diameters. In what follows we will concentrate on these 'Groeneveld' tables, as they are in by far the most widespread use.

4.2.2.1 Tube diameter

The tabulated data are all produced by reference to the critical heat flux in an 8mm tube. The scaling of critical heat fluxes measured in pipes different from 8 mm in diameter is achieved by using an empirical expression of the form[16]:

$$q''_C\left(8mm\right) \approx q''_C\left(D\right)\left(\frac{D}{8}\right)^{0.5}$$

All tabulated values are thus for 8mm tubes, and values for other diameters are then obtained by the user of these tables by the reverse of this process.

There is a considerable degree of 'data cleansing' undertaken as part of the process of compilation of these tables.

4.2.2.2 The basis of the tables

In the tables, the critical heat flux is, by construction, taken as a function only of local conditions. The CHF is considered to be a function of only:

(i) Pressure

(ii) Local bulk subcooling or quality

(iii) Mass velocity.

Values of CHF are tabulated with these as the independent variables.

An example of such a tabulation is given in Figure 10, which is extracted from the Russian table which are reprinted in the Heat Exchanger Design Handbook[5].

Table 4 U.S.S.R. Academy of Sciences [28] standard tables for CHF for water in upward flow with uniform heat flux[a]

	Local bulk mean water conditions																			
Mass velocity,	Subcooling, °C					Quality														
kg/m² s	75	50	25	10	0	0.05	0.1	0.15	0.2	0.25	0.3	0.35	0.4	0.45	0.5	0.55	0.6	0.65	0.7	0.75
						$p = 29.5$ bar														
750	–	–	–	–	–	7.95	7.50	7.10	6.75	6.45	6.15	5.80	5.50	5.25	5.00	4.80	4.20	3.75	3.20	–
1 000	–	–	8.80	8.40	8.20	7.70	7.25	6.75	6.35	5.95	5.60	5.25	4.95	4.65	4.30	4.00	3.70	3.35	–	–
1 500	–	9.50	8.75	8.20	8.00	7.25	6.55	6.00	5.40	4.90	4.60	4.15	3.80	3.40	3.00	2.60	–	–	–	–
2 000	10.53	9.65	8.60	8.00	7.75	6.70	5.90	5.55	4.75	4.25	3.80	3.35	2.90	2.50	–	–	–	–	–	–
2 500	10.80	9.90	8.65	7.90	7.60	6.35	5.50	4.80	4.25	3.70	3.25	2.80	2.35	–	–	–	–	–	–	–
3 000	11.25	10.05	8.65	7.85	7.40	6.05	5.20	4.55	3.95	3.25	3.05	2.65	–	–	–	–	–	–	–	–
4 000	12.10	10.35	8.75	7.75	7.20	5.75	4.80	4.05	3.50	3.05	2.65	–	–	–	–	–	–	–	–	–
5 000	12.60	10.65	8.85	7.70	7.05	5.25	4.30	3.80	3.30	2.90	2.50	–	–	–	–	–	–	–	–	–

Figure 10
An example of a Look up Table, here an extract from the Russian tables of 1976, reproduced in the Heat Exchanger Design Handbook[5].

4.2.2.3 Construction of the tables

Plainly, generating these tables from a rather disparate collection of some 30,000 sets of data is a major statistical exercise, involving first some fairly sophisticated data cleansing. There is then much data smoothing, averaging and interpolation, to generate actual table entries at the required discrete, uniformly spaced table locations. Some details are given by Groeneveld[8], and we will not reproduce this here. It is an effort which has spanned many years, involving many researchers, and it is probably true to say that subject to their underlying characteristics, the tables are now quite sophisticated and mature.

4.2.2.4 Extraction of CHF values from the tables

The normal use of the tables is simply to read a CHF value for the conditions of interest. If these conditions lie between the tabulated values, the user must simply interpolate, as he sees fit. If his diameter of interest is not 8mm, he scales to whatever it is using the equation above.

4.2.3 Assessment of the accuracy of the tables

There is no simple or single answer to the question of how accurate are values taken from the tables.

Firstly, two data values themselves might be for identical conditions when characterised by only the three (four, if we include the diameter) parameters retained as independent variables, but since the real-world CHF may well depend on other factors in addition, we should not expect the data to agree with each other anyway. (The extent to which they do not is of course an indication of the importance of variables in addition to those used to characterise the case.) Further, whilst there should be a considerable degree of averaging within the quantities actually measured in experiments, the processes themselves are intrinsically chaotic; a nominally identical experiment will not produce exactly the same results when repeated, except in some average sense.

Secondly, there are two ways to determine if a CHF value from the table 'retrospectively predicts' any of the data from which the table was derived.

The two approaches will give different values of CHF, both of which will in general be different from the raw data.

The first approach is the direct reading of a CHF value from the table. Given a mass flux and quality, what CHF does the table tell us should have been observed?

An alternative approach is what is known as the heat balance method. The data collected are for uniform heat fluxes, and include the location at which CHF was observed; the 'heated length'. (It is normally a consequence of the way in which it is convenient to conduct experiments that CHF is observed at the end of the heated length, but there is nothing fundamental or significant about this.) It is thus known how much enthalpy has been added to the fluid by the time (position) CHF is reached, and from this the local quality can be determined. This is illustrated via Figure 11.

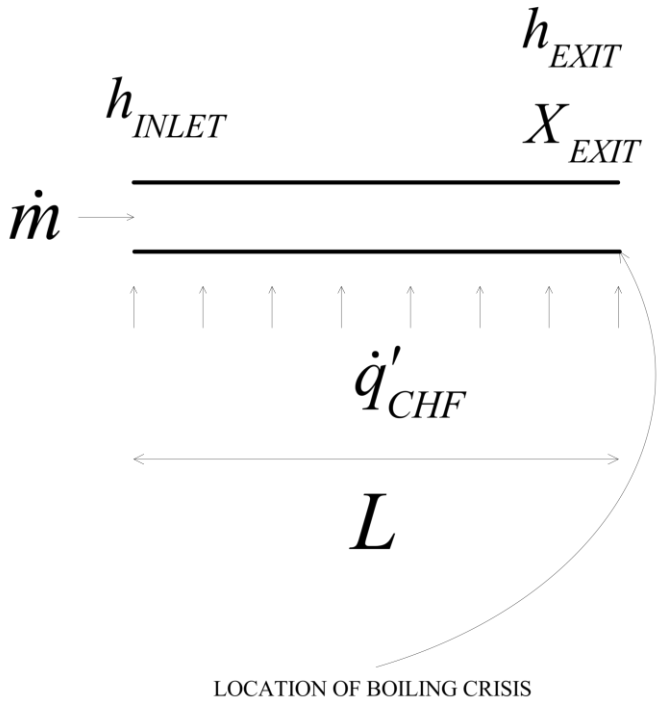

Figure 11
The quantities involved in measuring and characterising CHF

There is no 'heated length' that can be associated with a particular entry in the table, with this being the result of aggregation and interpolation over multiple data points. However, for a given experimental measurement, this is known. The approach is to determine, by trial and error, the linear heat input rate (what CHF value) results in the experimentally observed exit quality.

The producers of the tables have performed this evaluation, and present graphs that characterise the ability of their tables to back-predict the data from which they were derived. One such is reproduced here from Groeneveld[8].

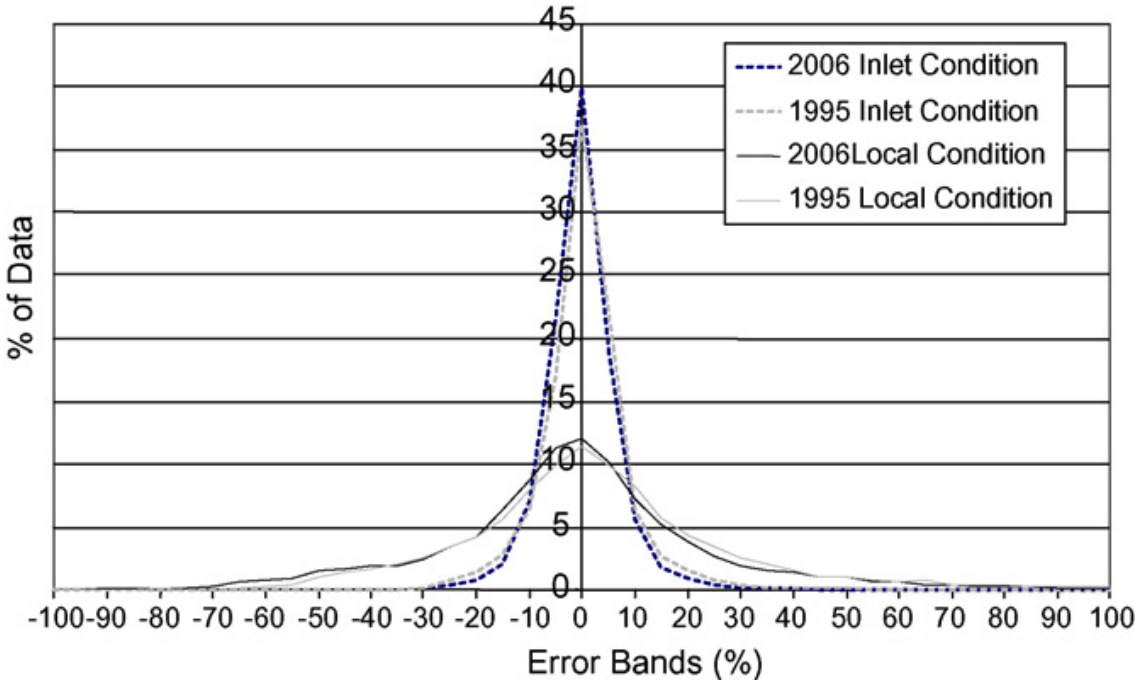

Figure 12
An assessment of the ability of the Look up Tables to back-predict the data from which they were derived, showing predictions based both on the local conditions, and on a heat balance / inlet condition basis. (Reproduced from Groenenveld[8].

With the experimental evidence itself very scattered when plotted as a function of only the (necessarily) limited number of variables able to be considered, and the difference between the Look up Table value and measurement thus varying erratically, the concept of comparing the accuracy of the Look up Table with any particular correlation has some philosophical difficulties. We will restrict ourselves here to a single comparison featuring in the TRACE system code Theory Manual[12].

In Figure 13 and Figure 14 are shown comparisons of the Look up Table predictions with those of the Biasi correlation. For high pressures and high flows, the agreement is fairly good. The correlation gives a smoother prediction, as would be expected. Note though that the graphs have logarithmic vertical axes; the differences in predicted CHF are not quite by 'multiples', but they are by significant fractions.

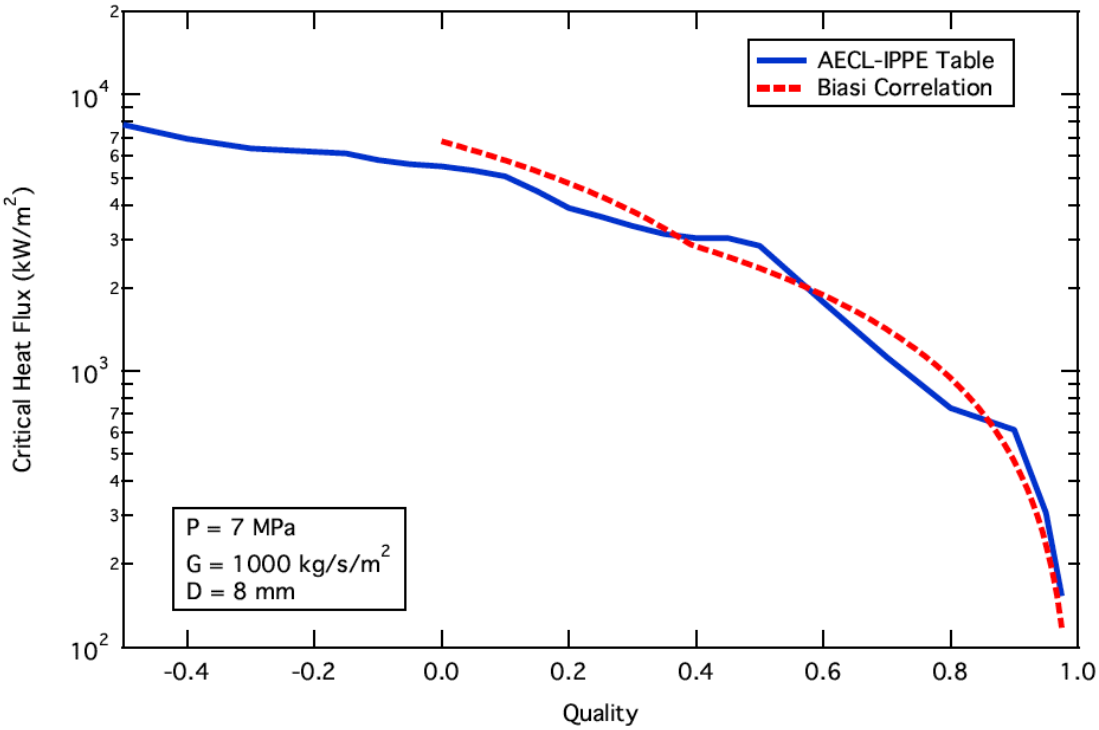

Figure 13
Comparison of the Look up Table and Biasi correlation prediction of CHF at high pressure, high flow conditions. From the TRACE theory manual[12].

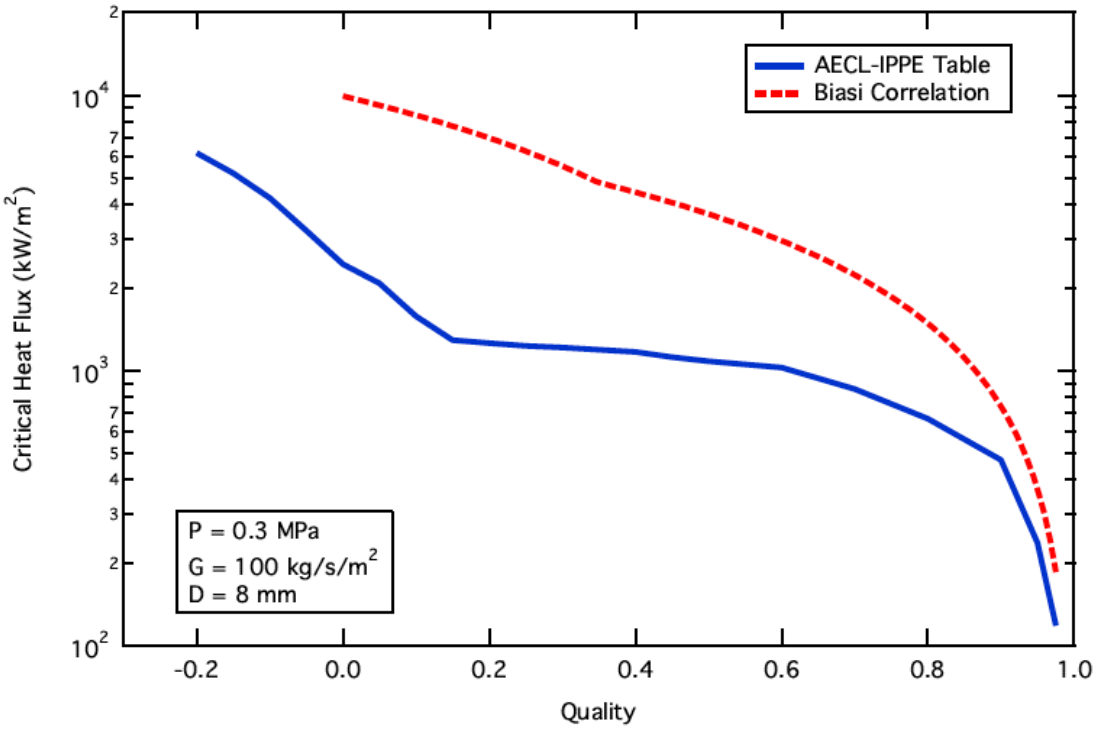

Figure 14
Comparison of the Look up Table and Biasi correlation prediction of CHF at low pressure, low flow conditions. From the TRACE theory manual[12]

4.3 The applicability of correlations and interpolation to cases with non-uniform axial heat flux profiles

4.3.1 Why should non-uniformity matter?

It is perhaps worth first discussing just why what has happened upstream should affect anything anyway, and why the local quality is not a sufficient indicator.

Consider the case of DNB (low quality bubble-crowding, or similar, CHF). The propensity for the formation of a vapour blanket at the wall will depend on the bubble density near the wall, and on the near-wall temperature, as well as on the local heat flux. These first two quantities will depend not only on the integral of the lineal power added to the flow up to this point, but on the recent rate of addition of heat. Consider the (extreme) case where, with uniform heating, DNB conditions had as good as been reached, and then there was a length of unheated tube. Bubble densities over the cross section would become more uniform, and may (depending on the enthalpy) reduce on average, and the near-wall temperatures would reduce as temperatures became more uniform over the cross section. If heating then resumed, DNB would not occur for some little distance, until a hot, bubbly near-wall region had been re-established. That is obviously an extreme case, but serves to illustrate the mechanism.

The sensitivity of the high quality, film dryout CHF to these 'history' effects is much greater still. Film dryout is a complex balance of evaporation, deposition and entrainment rates, with these latter two especially being sensitive to flow speed and distance traveled, as break-up

and coalescence occur. The flow regime as any particular local quality is reached, and the film thickness and droplet size distribution, will be sensitive to the rate at which heat has been added, making the local quality alone a poor indicator.

4.3.2 The similarity of the local and 'boiling Length' approaches

Data for uniformly heated tubes is often correlated using a relationship between critical heat flux $\dot{q}_{crit}$ and local quality *x*. A common alternative form of correlation is that relating quality at the point of occurrence of the CHF phenomenon to the *boiling length* L_B (i.e the distance between the point at which the fluid reaches the saturation temperature and the point at which the CHF phenomenon is observed). Correlations of these respective types are presented above. The two forms of relationship are sketched in Figure 15.

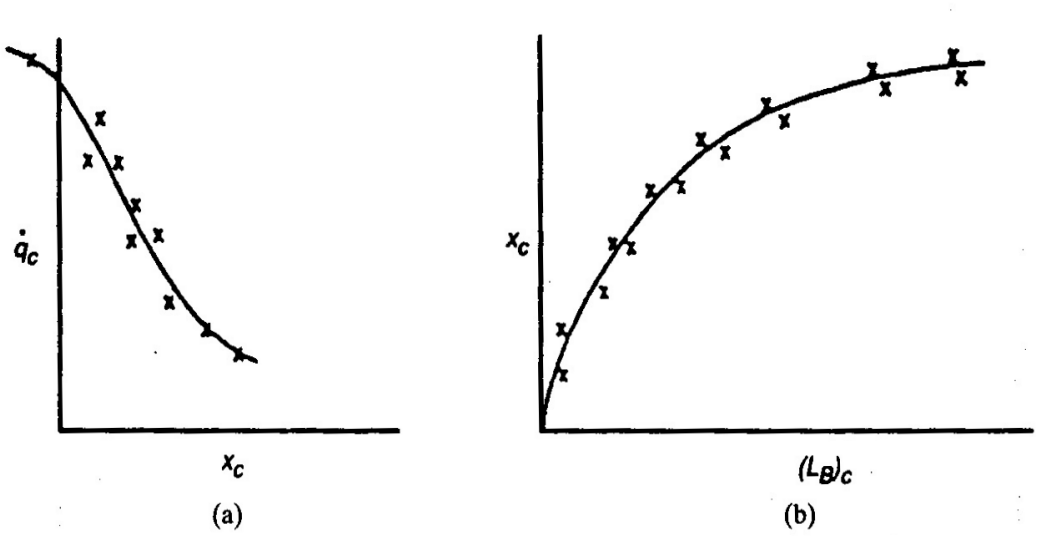

Figure 15
Flux/quality and quality/boiling length representations of CHF data

The $\dot{q}_{crit}/x$ form of relationship seems to indicate the existence of a phenomenon governed by *local conditions* and the x/L_B relationship appears to indicate an *integral* phenomenon, governed by events that have happened in the distance L_B upstream of the location of CHF. However, the local quality is itself a simple linear function of the boiling length, and thus too has just this 'integral' dependence.

A simple energy balance:

$$L_B q'' \pi D = \dot{m}'' \pi D^2 x h_{fg}$$

gives us the critical boiling length

$$L_B = \frac{\dot{m}'' D x_{LOCAL} h_{fg}}{q''} = f\left(x_{LOCAL}\right)$$

or

$$x_{LOCAL} = \frac{L_B q''}{\dot{m}'' D h_{fg}} = f\left(L_B\right)$$

Most data have been obtained with uniformly heated tubes, and it is readily shown that, for this case, the two relationships are equivalent and it is not possible to make a distinction between them.

4.3.3 Non-uniform heating

The difference is found when considering *non-uniformly heated tubes.* A typical non-uniform heat flux distribution is that of a cosine shape as found in many reactor situations. The way in which a cosine flux shape is related to the $\dot{q}_{crit}/x$ and x/L_B type of correlations is illustrated in Figure 16 and Figure 17 respectively. As the power input is increased, then the "operating lines" (i.e. the loci of flux/quality and quality/boiling length along the channel) shift until they ultimately touch the correlating line. Note that, for non-uniform heating, the location of CHF is not necessarily at the end of the channel.

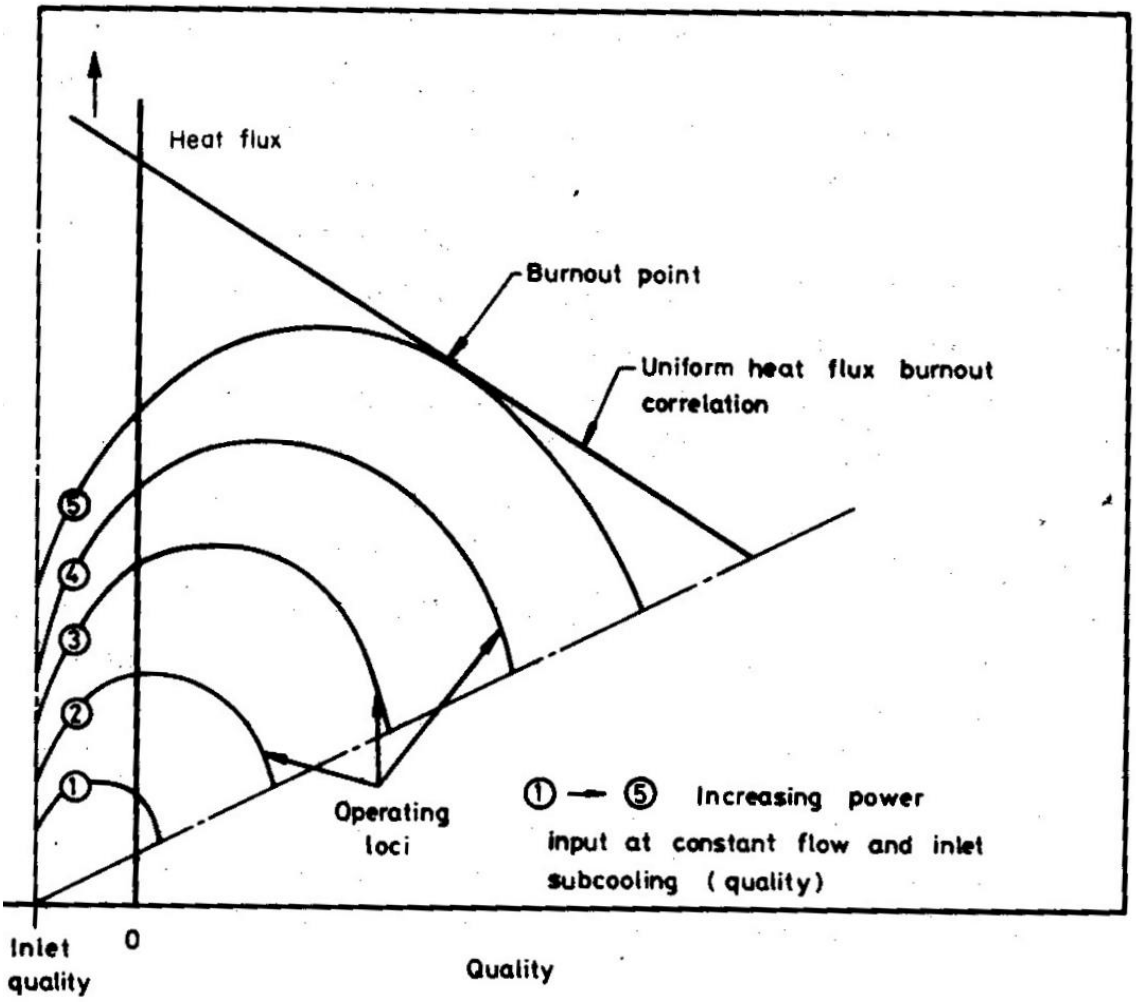

Figure 16
Application of flux/quality correlation obtained for uniform heat flux to prediction of CHF ("burnout") with a non-uniform (cosine) heat flux distribution

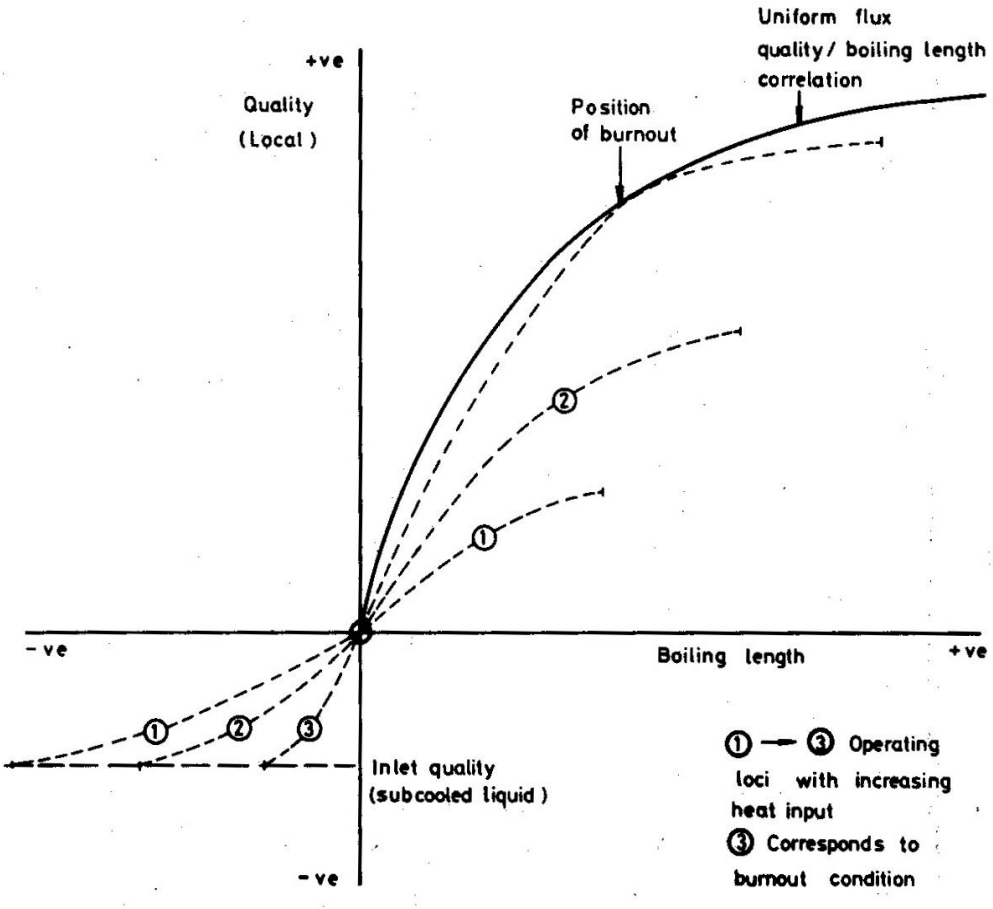

Figure 17
Application of quality/boiling length correlation obtained for uniform heat flux to prediction of CHF ("burnout") with a non-uniform (cosine) heat flux distribution

Data for non-uniformly heated tubes do not correlate in terms of flux and quality as is exemplified by the results shown in Figure 18. On the other hand, data for non-uniform heat flux are often much better correlated by the quality/ boiling length approach as is exemplified in Figure 19. However, it should be stressed that neither approach can be applied completely generally since both are essentially empirical. This lack of generality can be illustrated by considering the "cold patch" experiments described by Bennett et al[17]. A 61-cm unheated zone was present at various positions in a vertical tube tubular test section whose total length was 4.27m, as shown in Figure 20. With the unheated zone in certain positions, it was possible to obtain higher powers to CHF ("burnout") than for the case where the tube was uniformly heated. Of course, these results vitiate the flux/quality relationship, which is not unexpected considering the results shown in Figure 18. However, the results are clearly also contrary to there being a unique quality/boiling length relationship. To predict such results, it is necessary to invoke phenomenological models of the type described in Section 4.4.

The effects of non-uniform heating have been recognised in the past and an empirical method for estimating the effect (the Tong F-factor method) [18] has been quite widely applied. In this method, the following fluxes are defined:
-The actual heat flux at position z along the channel, $\dot{q}(z)$

-The CHF at distance *z* predicted from a flux/quality correlation for uniformly heated tubes, $\dot{q}_{crit}(z)_u$

-The actual CHF at distance *z* along the channel for the case of non-uniform heating, $\dot{q}_{crit}(z)_{nu}$

A margin to CHF may be defined at a position z_{crit} along the channel as:

$$\text{CHF margin} = \frac{\dot{q}_{crit}(z_{crit})_{nu}}{\dot{q}(z_{crit})} = \frac{\dot{q}_{crit}(z_{crit})_u}{F(z_{crit})\dot{q}(z_{crit})}$$

where the *F*-factor is defined as:

$$F(z_{crit}) = \frac{\dot{q}_{crit}(z_{crit})_u}{\dot{q}_{crit}(z_{crit})_{nu}}$$

Tong et al derived the following semi-empirical expression for *F(z)*:

$$F(z_{crit}) = \frac{C}{1-\exp(-Cz_{crit})}\int_0^{z_{crit}} \frac{\dot{q}(z)}{\dot{q}(z_{crit})}\exp[-C(z_{crit}-z)dz$$

where the distance along the channel *z* is given in meters and the parameter *C* is given by the following empirical expression:

$$C = \frac{7.01\times10^6[1-x(z)]^{7.9}}{\dot{m}^{1.72}}$$

where *x* (*z*) is the quality at distance *z* along the channel and $\dot{m}$is the mass flux in kg/m²s.

Hewitt[2]recommends that the flux/quality relationship be used for $x < -0.1$ and the quality/boiling length relationship for $x > 0.1$ and that the Tong F-factor method be used in the range $-0.1 < x < 0.1$. However, it should be stated that, for complex heat flux shapes, recourse should be made to a more phenomenological approach as discussed in Section 4.4.

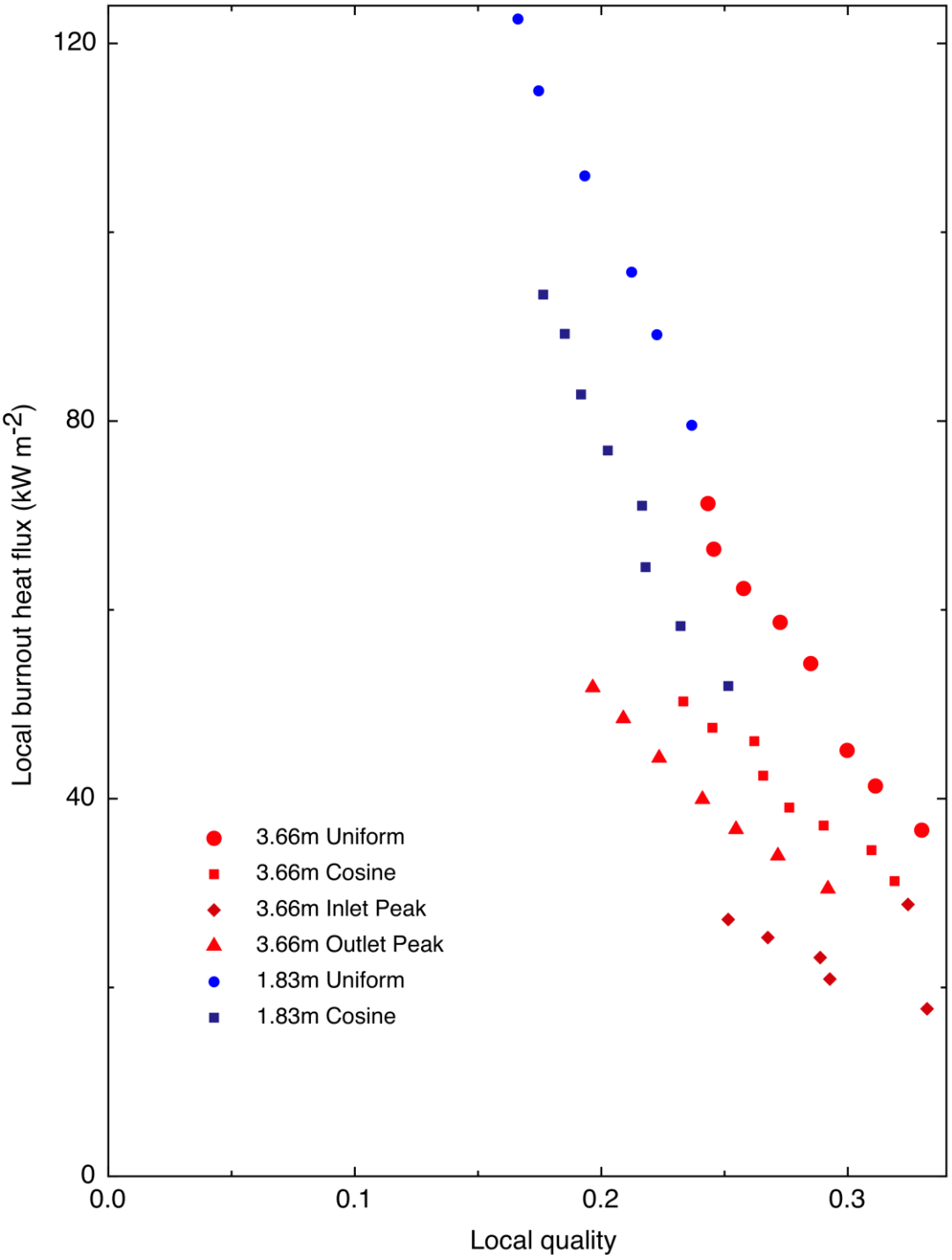

Figure 18
The effect of non-uniformity in the wall heat flux. Flux/quality plots for Refrigerant -114 CHF in an annulus with various axial heat flux distributions. Pressure 0.86 MPa, mass flux 760 kg/m²s, id 14.3 mm, od 22.2 mm. Re-plotted from Shiralkar [19]

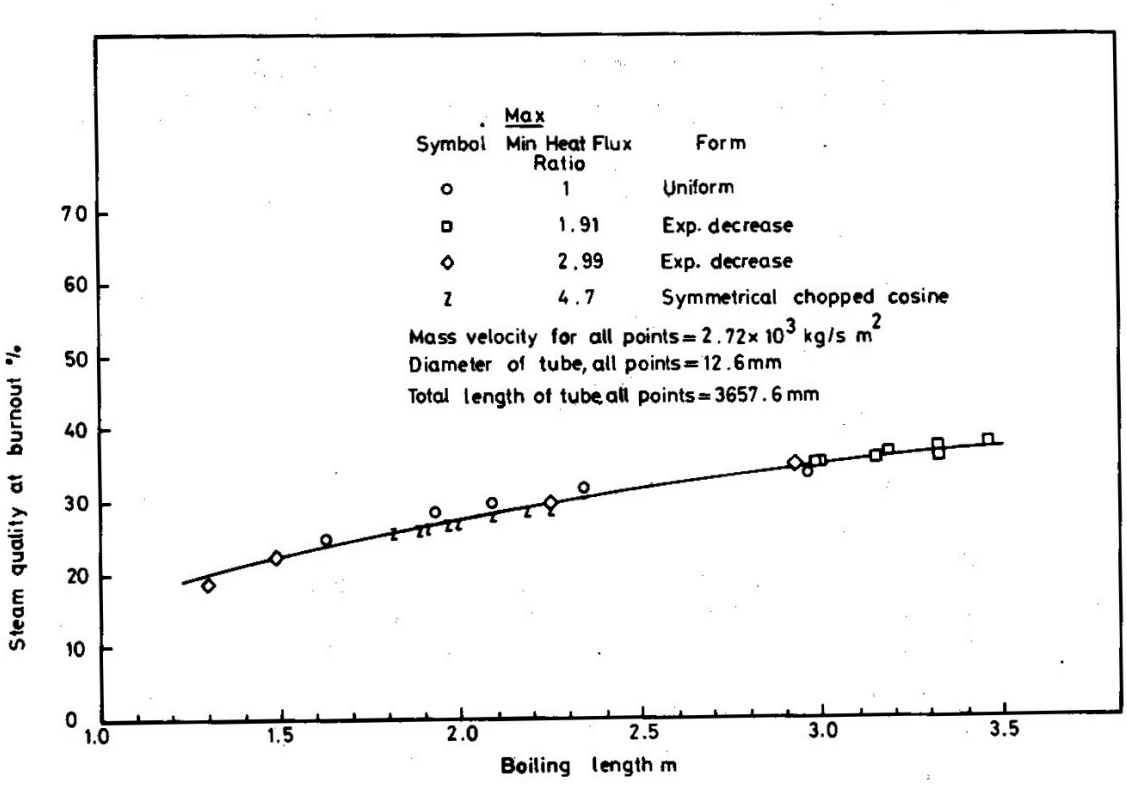

Figure 19
CHF with various heat flux distributions, plotted in the quality/boiling length form. Pressure 6.89 MPa [20]

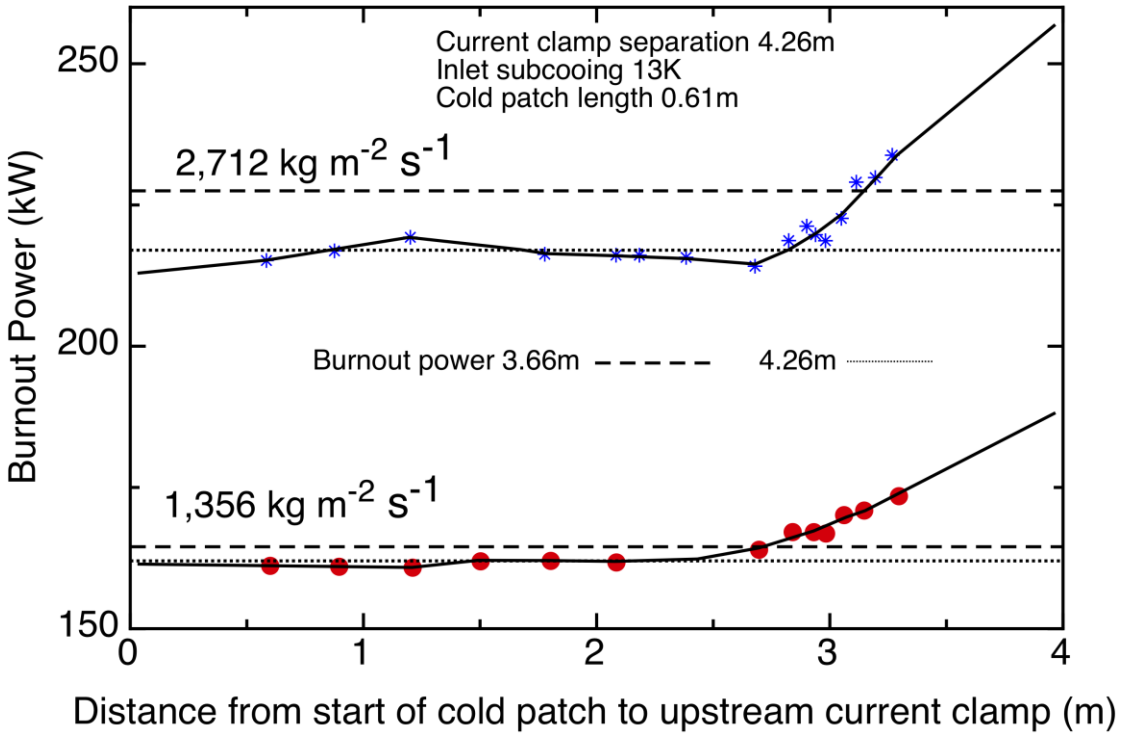

Figure 20
Power to CHF in a tube with an unheated zone ("cold patch"): Evaporation of water at 6.89MPa in a 12.6 mm diameter tube, re-plotted from Bennett[17].

4.4 Phenomenological modelling

Thus far we have described essentially 'thoughtless', empirical approaches; observe what happens and assume that observed behaviour (tuned / adjusted as needed) would obtain in the case under consideration.

An alternative approach is to attempt to analyse and model the physical phenomena underway. The modelling approach naturally depends on the phenomena.

As discussed the two main types of event which are both termed CHF are "departure from nucleate boiling", DNB, occurring with high heat fluxes and still predominantly liquid coolant, and the final drying out of a residual liquid film wetting the walls of a heated channel, leaving only a vapour flow with a population of entrained droplets.

We will discuss in later sections the phenomenological modelling of each of these phenomena.

In Section 6 we will consider low quality and sub-cooled boiling regions, and in Section 7 we will address film dryout in annular flow.

Clearly, the above two mechanisms are very different and the question naturally arises about when the transition occurs between one mechanism and the other. Hewitt and Govan[21] produced a modified version of the Weisman and Pei[22] model which applied in both the sub-cooled and quality regions (including in annular flow) and which better fitted the "look-up" tables of international data. They plotted this modified model together with their annular

flow model in terms of CHF quality as a function of quality and their graph is presented in Figure 21.

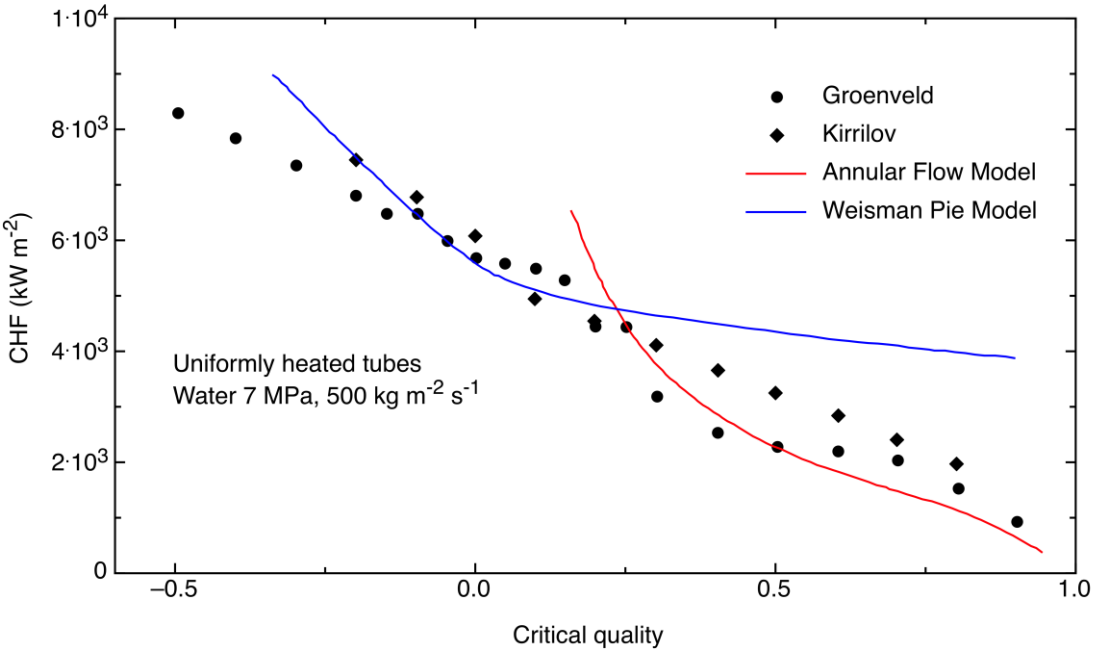

Figure 21
Comparison of international data sets[8] with the modified Weisman and Pei[22] (bubble crowding) model and the annular flow dryout model[21].

The graph also shows data from the both the Canadian and the Russian look-up tables (precursors of the modern ones[8]). The main points arising from this graph are as follows:-

•There is a relatively smooth transition from one mechanism to the other and it would be difficult to identify the change in mechanism within the data scatter.

•The mechanism of CHF applying in uniformly heated tubes is that which would give the *lowest* value of CHF – namely the bubble crowding model at low qualities and the film dryout model at high qualities.

•Even in annular flow, bubble crowding could occur if there was a local "hot spot" (i.e. a local spike in heat flux) that brought the *local* flux above that predicted from the Weisman and Pei model.

5 CFD PREDICTION OF COMPONENT-SCALE BOILING

5.1 Introduction

In the sections above we have been discussing "critical heat flux", in its bubble-crowding and film-dryout forms.

We will later be discussing the extent to which this can be modelled using CFD. However, a necessary precursor is to consider how CFD may be used to model less extreme sub-cooled nucleate boiling.

5.2 The physical processes of bubble nucleation and growth on a heated wall

The boiling process in a duct with a heated wall begins with the nucleation of a steam bubble, and indeed the physics of this nucleation process are still in truth a matter for research. (The general consensus is that nucleation sites are probably geometrical imperfections, associated with trapped pockets of non-condensable gas that has locally come out of solution, but there are many questions this simple explanation leaves unanswered. However, we will not pursue that here.)

Picking up the story when the bubble nucleus is perhaps a few tens of microns in size, growing in a superheated layer close to the heated wall, the bubble grows via the generation of vapour from this superheated liquid into the bubble cavity. This process itself is complex, with various mechanisms responsible for the very rapid flow of heat and vapour.

They include, inter alia, very short-term unsteady heat conduction within the heated solid; an individual bubble is largely formed from heat stored in the wall (cladding, in our case), which is replenished during a 'waiting period' before a subsequent bubble is formed. The 'flow' processes include the "leaving behind" of a very thin layer of liquid on the surface of the solid as the bubble grows from the generation of vapour. This thin layer of liquid, generally termed the 'microlayer' is itself very important in bubble growth, as it provides the mechanism for very rapid heat transfer from the wall and very rapid evolution of vapour.

Depending on the conditions, which for present purposes can range from perhaps 150 bar, ~300+ C, down to ~1 bar and ~100C, the bubble grows to a size where the combination of buoyancy and drag forces acting on it from the surrounding flow are able to cause it to detach from the wall, where surface tension forces were otherwise holding it.

This detaching from the wall might occur at the size of some millimetres at atmospheric pressure, and sub-millimetre at higher-pressure conditions. (Note of course that this factor of perhaps 10 or more in bubble departure diameter is associated with a factor of one or several thousand in bubble volume.)

The microscopic modelling all of these complex flow and heat transfer processes is a major (and fascinating) activity in its own right[†], and there is an associated large literature; see for example Figure 22, from Haensch, Walker et al[23] et al, and references therein.

[†] It forms a significant part, indeed, of the research of our group.

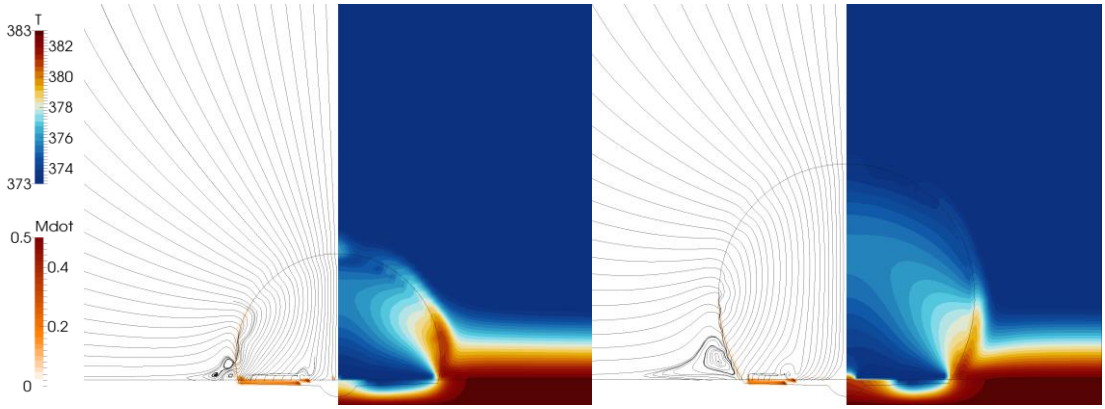

Figure 22
Streamline plots, mass transfer rates and temperature fields after 5ms and 15ms from Haensch, Walker et al [23].

Once detached from the wall, the bubble is acted upon by a variety of hydrodynamic and other forces. These can cause the bubble to break up, but they also can cause the bubble to coalesce with other bubbles.

They will cause the population of bubbles to drift away from the wall, or indeed can under some circumstances tend to cause the population of bubbles remain close to the wall.

Indeed, as we have seen above, it is the generation of a high population of bubbles close to the wall that is responsible for one of the two mechanisms for critical heat flux.

5.3 The development of boiling flow along a heated channel

This whole process begins initially when near-wall fluid first reaches sufficient superheat. With increased heating, there is increasing void (bubble population, quality) along the channel. In Figure 23 is shown a depiction of this, with some of the terminology typically adopted.

For idealized (bubbly) subcooled boiling flow, the boiling region can be divided into three sub-regions based on the macroscopically observable flow behaviour: an initial *partially developed boiling* (PDB) region, followed by a *fully developed boiling* (FDB) region and a region of so-called *significant void flow* (SVF). These regions are illustrated in Figure 23, along with the evolution of wall and bulk liquid temperature across the boiling region.

A point referred to as an *onset of nucleate boiling* (or ONB) marks the beginning of the PDB region. At this point, the wall temperature has risen sufficiently beyond the local saturation temperature so as to be able to activate nucleation cavities that can sustain bubble growth. Initially, the two-phase (or superheated) layer at the wall is thin and comprises a sparse population of small bubbles that remain attached to the wall. These bubbles are unable to depart due to strong local condensation effects that prevent them from growing into faster moving fluid. Large areas of the wall in this region do not undergo boiling and normal single-phase convection remains a significant wall heat transfer mechanism.

The remainder of the PDB region is associated with the development of this superheated layer and an accompanying increase in the density of active nucleation sites and bubble growth rates. This drives a transition from normal single-phase convection at the wall towards entirely boiling-driven evaporation and micro-convection at the end of the PDB region. Bubbles may grow sufficiently large closer to the end of PDB region and in the FDB region so as to now become able to depart from the wall. The bulk however remains

subcooled to the extent that any vapour swept away from the wall region is quickly condensed.

The FDB region is followed shortly thereafter by a so-called *onset of significant void* (or OSV). This marks a transitional point where the axial profile of void begins to rise steeply. In other words, where the two-phase region begins to extend into the bulk, as a significant volume of the vapour generated at the wall is able to penetrate into the subcooled core without being condensed away rapidly.

A host of inter-dependent factors, active across multiple length scales, govern the overall system behaviour and the locations of the relevant regional transitions. As fully developed boiling is achieved, the interplay between these factors becomes convoluted to the point of intractable. These include vigorous wall boiling that involves the explosive growth and coalescence of bubbles, turbulence-driven coalescence and break-up of bubbles that depart from the wall and a range of inhomogeneous interfacial forces that act upon this population of bubbles, determining the direction in which they are able to migrate and the regions in which they aggregate. Taken separately rather than in conjunction, each of these factors represent distinct (and as yet unresolved) fields of research in their own right. Clearly, the onset of DNB represents the most undesirable manifestation of this interplay. In this case, the existing complexity is further compounded by the need to consider the role of the micro-scale surface topography and the transient conjugate heat transfer associated with bubble growth.

Given current knowledge of boiling and turbulence, the cascade of length scales that must be dealt with here precludes any entirely first-principles or self-consistent modelling effort [24, 25], even for the case of low-quality boiling far from DNB. Neither is it computationally feasible at present to undertake a single high-resolution analysis that spans across all of these scales.

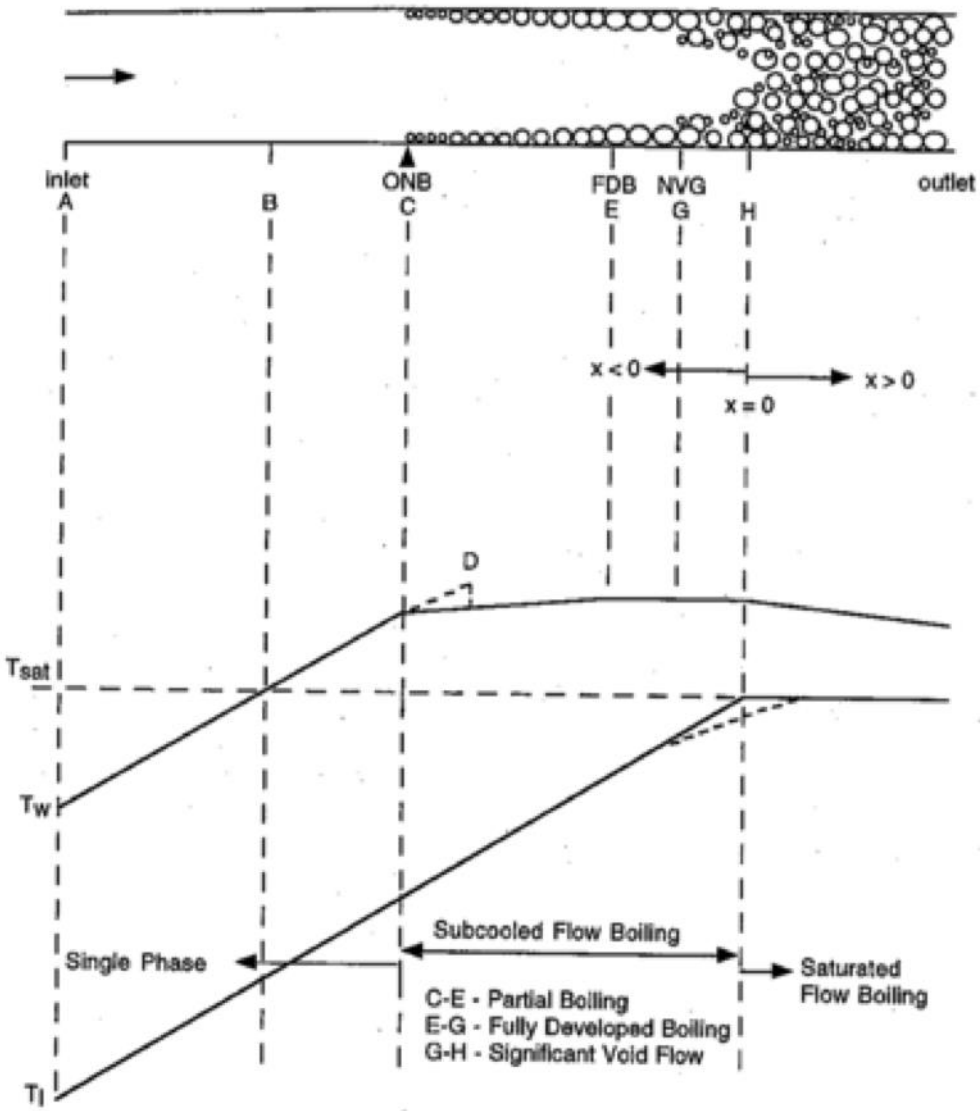

Figure 23
General schematic of sub-cooled boiling regions along a heated channel, adapted from Kandlikar [26]

5.4 Subsequent bubble motion

Once detached from the wall, the bubble is acted upon by a variety of hydrodynamic and other forces. These can cause the bubble to break up, but they also can cause the bubble to coalesce with other bubbles.

They will cause the population of bubbles to drift away from the wall, or indeed can under some circumstances tend to cause the population of bubbles remain close to the wall.

Indeed, as we have seen above, it is the generation of a high population of bubbles close to the wall that is responsible for one of the two mechanisms for critical heat flux.

5.5 Component-scale modelling; heat flux partitioning

Obviously it is not practicable to model the growth and subsequent motion of millions of individual bubbles as part of trying to understand conditions in a nuclear fuel channel undergoing some nucleate boiling. The approach taken is generally termed 'component scale' modelling, where spatial and temporal averaging is employed to keep costs tolerable.

The starting point is a normal Eulerian – Eulerian two phase flow CFD model, where, in essence, the normal conservation equations are solved for each phase, with inter-phase mass and momentum transfer terms incorporated via empirically-based models.

The principal additional need is some means to represent heat transfer and vapour generation at the wall. In essence, a closure relation is required that relates wall temperature and the 'local' fluid temperature to the heat flux from the wall. This is conceptually akin to a 'boiling heat transfer coefficient'.

In an approach generally attributed to Kurul and Podowski[27], and which is often known as the RPI heat flux partitioning approach, after the Rensselaer Polytechnic Institute, the heat is assumed to be removed from the wall via three mechanisms. These are sensible heat transport owing to single-phase convection q_{conv}, the latent heat transport due to evaporation q_{evap} and the sensible heat transport due to quenching q_{quench}.

The general form of the RPI model is as follows:

$$q_{total} = q_{conv} + q_{evap} + q_{quench} \tag{16.1}$$

The mechanisms are depicted in Figure 24.

5.5.1 Convective component

The convective part relates to the sensible heat transport to the liquid phase driven by normal convective cooling of the surface over the area unaffected by boiling; ie the pipe wall, minus that part of the pipe wall over which this does not occur because of the presence of bubbles. The convective heat flux component is calculated in much the same way as for normal single-phase diabatic flow, where the heat transfer coefficient is obtained using a characteristic temperature based on normal single-phase wall treatments.

5.5.2 Quenching

The so-called "quenching" component accounts for the additional sensible heat transport to the liquid phase in boiling-affected areas caused by the periodic surface rewetting associated with bubble departure, and more generally be the rush towards the hot wall of relatively cool liquid to fill the volume occupied by the departing bubble. It is worth remarking that the term quenching is associated normally with the rapid re-wetting of a hot surface with markedly cooler liquid. In this context, the use of this term is something of a misnomer as the heat transfer occurs over not only the small patch of surface surrounding the nucleation site that was previously dry, but over the much larger wetted (and cooler) region that was previously beneath or adjacent to the bubble. The temperature differences involved here are of the order of 1 to 10 K. The quenching heat flux component is modelled using the approach of Mikic and

Rohsenow [28], who represented the process as a transient conduction into a semi-infinite medium of fluid at a uniform initial temperature.[†]

5.5.3 Evaporation

The evaporative component is associated with the energy required to generate the vapour in each bubble, multiplied by the (average) bubble size, and the bubble departure frequency. That naturally requires knowledge of the bubble nucleation site density, the bubble departure frequency from each nucleation site, and the (average) diameter at which bubbles depart. None of this is in any sense "known" and the best that can be done is to use such experimental evidence as there is, gathered into appropriate correlations. All of these quantities vary markedly with pressure, and not surprisingly there is a great paucity of data of these rather detailed quantities at the 300 Celsius, 150 bar conditions that are probably of most interest.

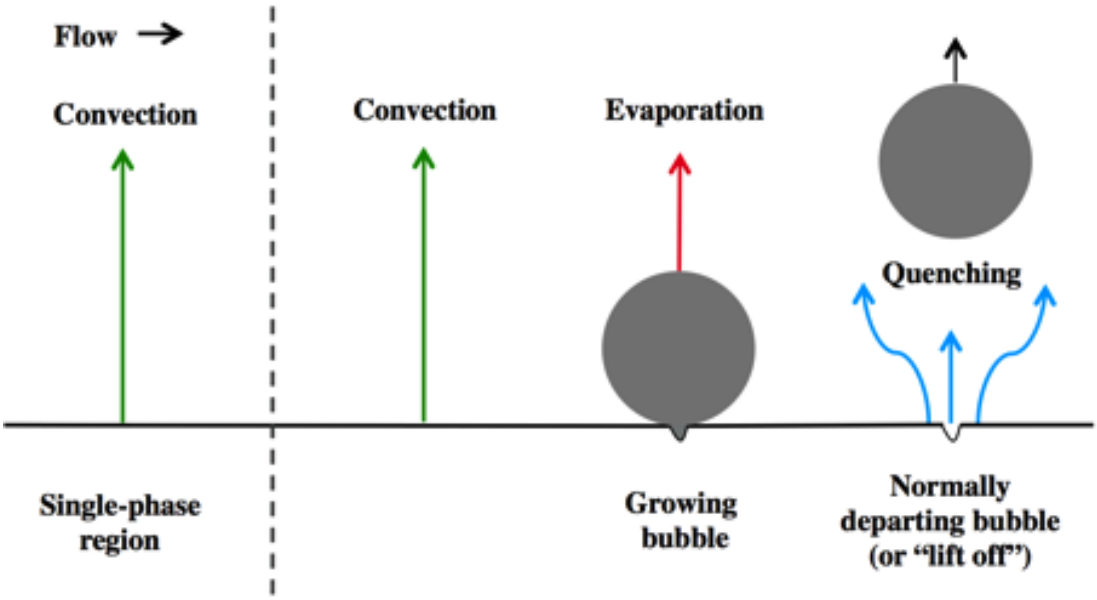

Figure 24
Heat transfer mechanisms considered in the heat flux partitioning approach.

Each of the components relies heavily on empirical information and correlations.

[†] We are actually ourselves just about to submit a paper investigating this. It is an example of the use of microscopic modelling to provide insights and quantification to support this semi-empirical component scale modelling. We have analysed in detail the single phase heat transfers occurring beneath a bubble during this "quench" process, and compared them to those predicted for that same bubble following the conventional Mikic and Rohsenow approach. It turns out that the more mechanistically-computed heat transfer is very much less.

5.5.4 Bubble transport

Once they have detached, there is a need for the subsequent motion, breakup, condensation and coalescence of the steam bubbles to be modelled. Once again, this is all based upon correlation-based implementation of observations from experiments, and again where the conditions arguably of most interest are probably those where the experimental evidence is most sparse.

5.6 The current status of component-scale wall boiling models

As one might expect, this area has developed a very large literature, of researchers proposing increasingly sophisticated and complex models and sub- models, and or slightly different correlations for the various physical phenomena needing to be incorporated.

There are various experimental benchmarks that have been used against which to test the predictions of these models, although frequently the quantities that one would most wish to compare predictions with, such as the spatial distribution of void, are not amongst those measured. (This is not a criticism of experimentalists; plainly measuring void distributions in a pipe at 300 Celsius and hundred 50 bar is a non-trivial activity.)

From a "purist" point of view there is relatively little published that could be described as a truly blind attempt to simulate a benchmark experiment. The complexity of the processes, and the number of correlations involved, make some degree of tuning almost inevitable.

However, viewed more pragmatically, there has been so much study of this area, and so much experienced gained of the tuning and the like that is required, that in practice the 'predictions' of this component scale modelling of boiling are often quite good. An indication of the state of the art is provided by the recent paper of Colombo and Fairweather[29]. The first two paragraphs of their conclusions, reproduced below, seem a fair summary:-

"An Eulerian–Eulerian two-fluid CFD model, including a Reynolds stress turbulence model, the method of moments-based S_C population balance approach and a boiling model derived from the RPI heat flux partitioning approach, was used to predict a large database of subcooled boiling flows. The database includes 20 experiments of subcooled boiling flows of water and refrigerants in vertical pipes and annular channels, and covers a wide range of conditions.

Overall, the model confirms the potential of CFD to provide detailed predictions of boiling flows and rather good agreement with data was found in some areas, but others still require significant improvements in model accuracy. At the present time, the general applicability of the model is not entirely satisfactory. Even if built in a mechanistic fashion, numerous empirical closure relations are required, not only for wall boiling, but also for the population balance and turbulence models. This clearly limits the overall model's general applicability and, therefore, the development of more mechanistic closures is highly desirable. A good example is provided by the bubble departure diameter that cannot be predicted with accuracy over extended ranges of conditions by the presently available correlations. The development of physically-based, more accurate closure models is challenging and may only be achieved with an increase in our knowledge of mechanisms that are as yet not completely understood, such as the growth and departure of bubbles, but also their breakup and coalescence and the interaction of turbulence with bubbles near the wall, amongst others."

6 THE PREDICTION OF BUBBLE CROWDING CHF

6.1 Introduction

During forced convection nucleate boiling, small bubbles are formed at the heated surface, and are swept away into the bulk of the flow. How deeply into the flow they travel before they condense, and how large a population density of bubbles exists, depends on how close to saturated is the bulk fluid, and, especially as regards the bubble density near the wall, on the magnitude of the heat flux.

If the surface heat flux is high enough, a bubble density close to the wall can be produced which is so high that the flow of further liquid to the wall, to keep it wetted, is inhibited by the bubbles themselves. This "bubble crowding" mechanism has been long identified as the principal phenomenon governing low-quality CHF (DNB), and a number of more or less physically based models have been proposed to describe it.

It is worth commenting that particularly early on, other mechanisms were proposed. The main one was associated with the reduced transport to the bubble layer associated with separation of the boundary layer from the wall, caused by the generation of vapour at the wall. However, the bubble-crowding mechanism does now seem to have majority support.

We will discuss in the following sections the development of a semi-analytical model of this, 'Weismann Pi', and then the use of CFD for this purpose.

6.2 Weismann – Pi

Whilst not perhaps absolutely the first, the most convincing work on the bubble crowding mechanism, and that now more or less taken to be synonymous with it, is that by Wiseman and Pei[22].

In Figure 25, reproduced from their paper, are shown schematically the conditions they modelled. The essence of the approach is to model the interchange of fluid between the bulk and the near-wall bubbly region, and to identify conditions under which insufficient liquid is able to reach the wall because bubble density is too high.

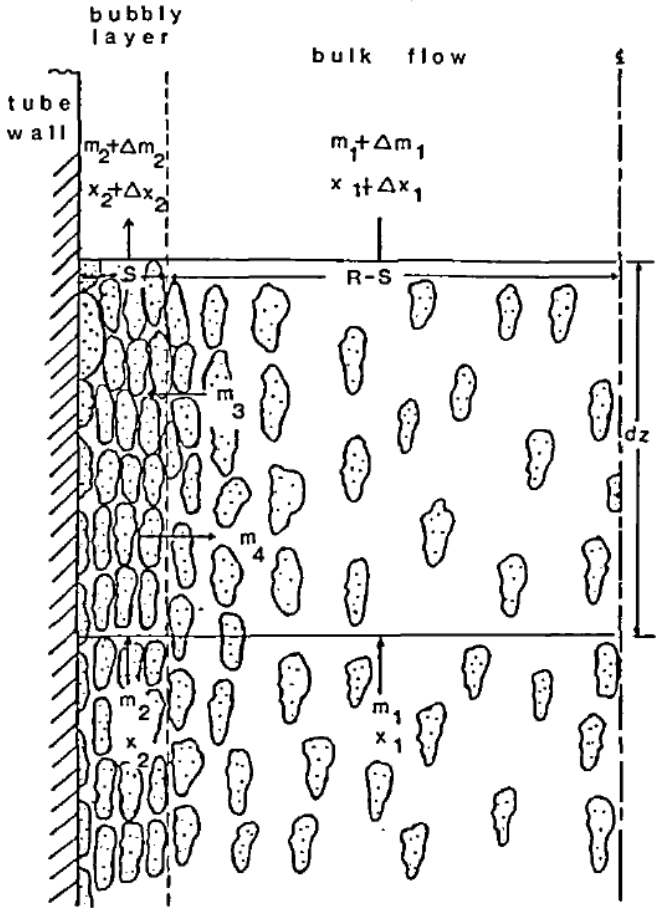

Figure 25
The flow conditions considered by Weisman and Pei[22], showing the division of the flow into a 'bubbly layer' and the bulk flow.

Their model postulated:

-The CHF is a local phenomenon, governed only by local flow conditions, and local quality and enthalpy.

-A high bubble density is developed in the region close to the wall where turbulent eddies are not large enough to transport the bubbles into the bulk flow.

-The CHF is considered to occur when this bubble population is large enough that 'significant' bubble-bubble contact occurs; a 'critical void fraction'.

-The vapour volume fraction in the bubbly layer is determined by what is needed to allow a balance between the towards-wall flow of liquid, and the flow of vapour towards the channel centre.

As will already be plain, this is of course not in any sense a first principles model, but perhaps better described as 'model-informed empiricism'.

The model is based on constructing a mass balance between the two (uniform) regions, of the core and the bubbly layer, where the net rate of liquid flow into the bubble layer balances the wall heat flux and the latent heat.

In a simpler (less precise) notation than theirs, but one which conveys the substance:

$$\dot{m}_{INTERCHANGE}\left(x_2 - x_1\right) = \frac{\dot{q}''}{h_{fg}} \tag{17.1}$$

The critical void fraction in the bubbly layer, x_2, was estimated by geometrical arguments. Experimental evidence is that boundary layer vapour bubbles are ellipsoidal, of aspect ratios about 3:1. For a population of equally sized such bubbles, it can be shown that the maximum void density before contact is ~0.82 . Making an assumption of minimal slip, this was taken as the critical quality.

It remains to estimate the turbulent transport between bubbly layer and core. This was done via a simplified algebraic representation of radial turbulent velocity components, modified to allow for the expected increased turbulent eddy diffusivity associated with a bubble – liquid mixture. *Inter alia*, this required an estimate of the bubbly layer thickness, which was made from the postulate that the eddy size is related to the Prandtyl mixing length.

The model construction is quite complex, and results in an equation with two empirical constants, values for which are selected so as to cause the model to 'predict' measured CHF conditions.

By selection of these constants, a good fit to measured CHF was achieved, as is indicated in Figure 26, reproduced from their paper.

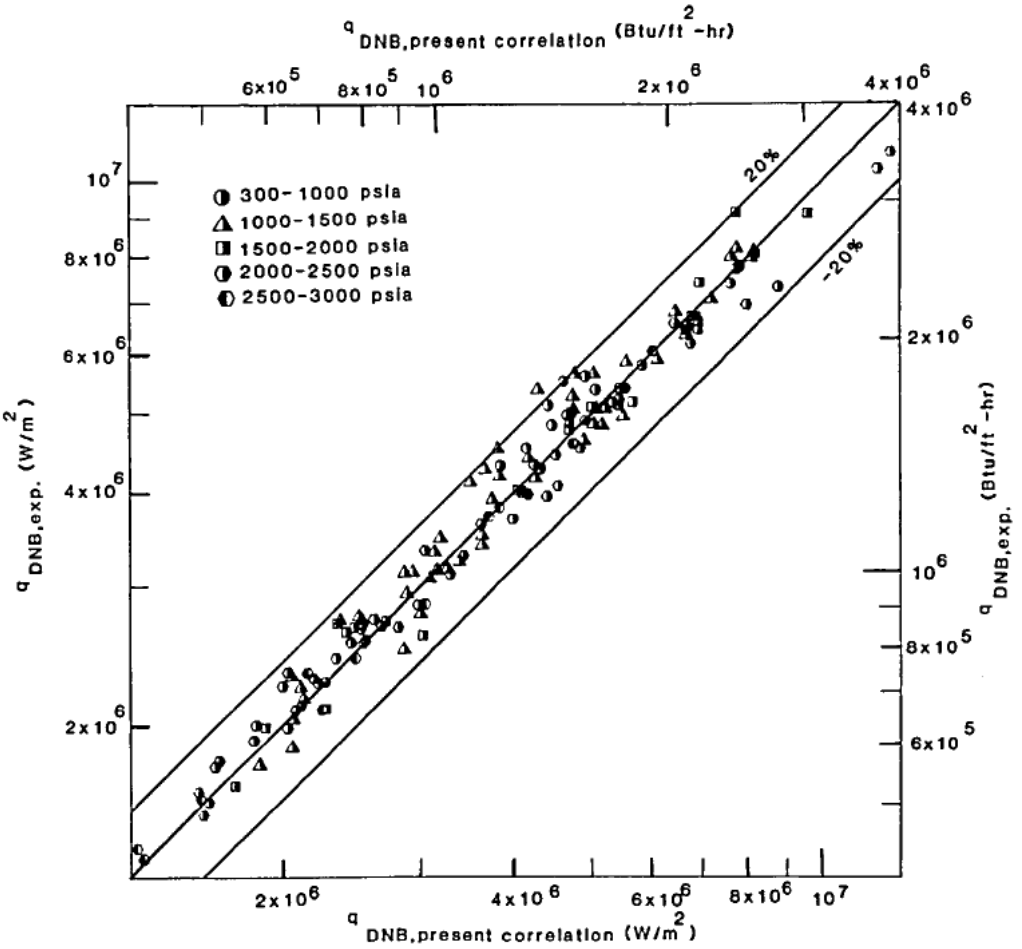

Figure 26
'Predictions' of the model, compared to experimental data; Figure 3 of Weisman[22].

Using the empirical constants found by the fitting to the experiments of Figure 26, this model was then applied to model non-uniformly heated tubes. This is reproduced and shown in Figure 27.

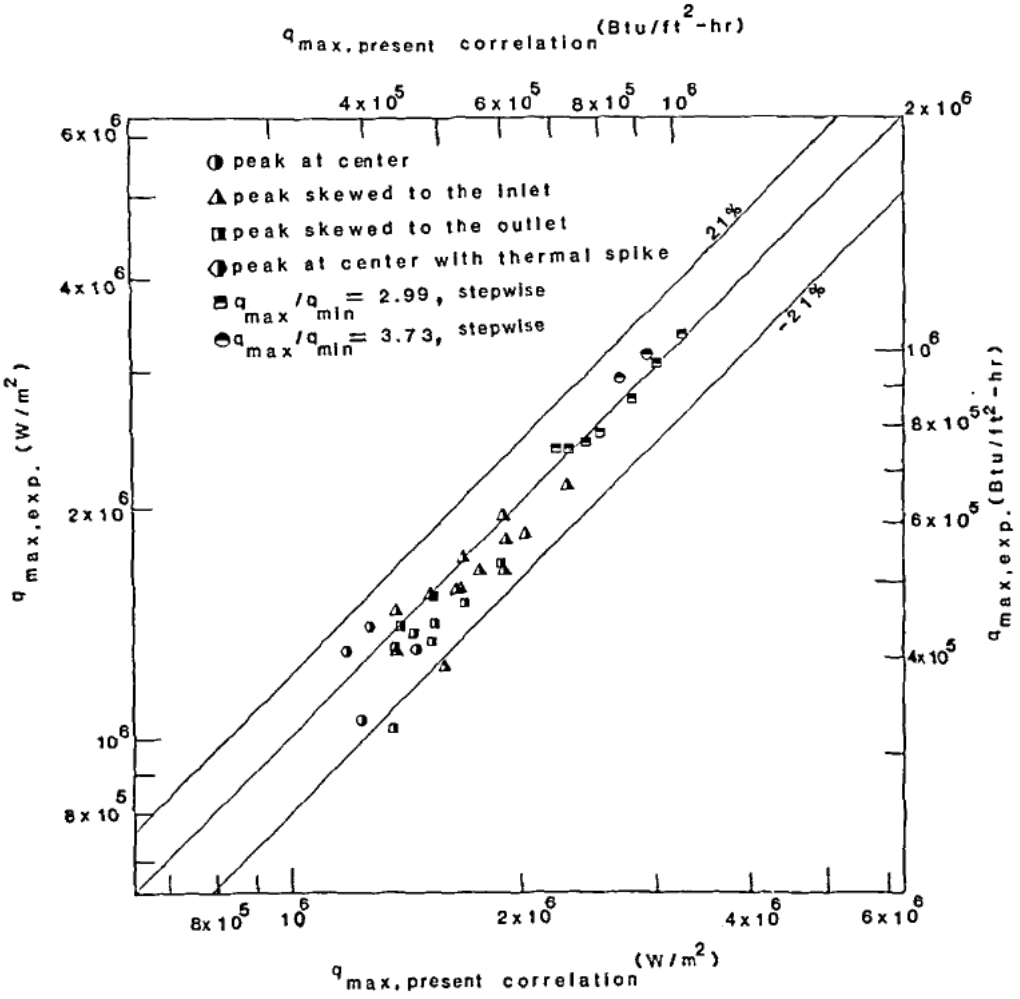

Figure 27
Comparison of model predictions with measured CHF in non-uniformly heated tubes. Figure 4 of Weisman[22].

Remarkably good agreement was obtained, lending support to the postulate that low quality CHF is largely a 'local conditions' phenomenon. As a further demonstration that their model captured the main phenomena well, its application to fluids other than water produced impressively close predictions. Predictions are essentially as good as the W-3[30] and CISE [31]correlations over the range of these correlations, and extend with little accuracy loss well outside the range of these correlations.

Whilst obviously still needing to be fitted to experimental results, the model overall provides a clear demonstration of the power of performing such fitting in the structure of a phenomenologically-based model.

6.3 CFD prediction of bubble crowding CHF

We have discussed above the use of CFD in component-scale modelling of boiling, and have noted that amongst the quantities that it predicts are the spatial distribution of void.

Implementation is naturally in practice a little more complex than this, but it is possible to use the value of near-wall void (vapour) predicted as an indicator of whether or not DNB is

taking place. As discussed above, in the Weissman - Pi approach a local void fraction of 0.8 was adopted, and indeed a value similar to this is frequently used as a criterion when using component scale CFD, with heat flux partitioning, to identify the occurrence of DNB.

A typical such paper is that of Lifante[32], who used an RPI treatments within Ansys-CFX, augmented to incorporate 'post-(local) dryout' heat transfer. We reproduce here, as Figure 28, a typical result from that paper (their figure 7), comparing predicted wall temperature with measured. Whilst it is hard to claim this as a pure prediction (one as good as never sees studies like this as *a priori* blind predictions) the approach plainly does have considerable capability and promise.

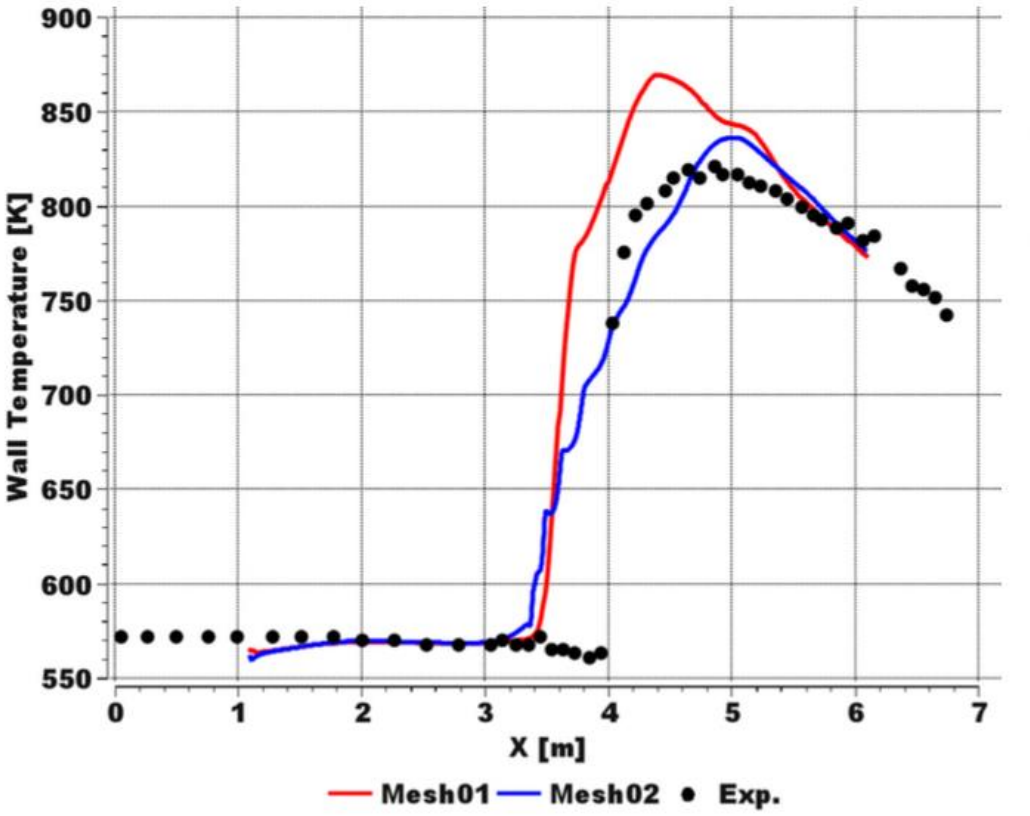

Figure 28
Reproduced from Lifante[32], where it is Figure 7: A comparison of predicted and measured wall temperature through the region of bubble-crowding CHF, for flow in a tube of water at 7 MPa, with a wall heat flux of 0.8 MW m^{-2}.

7 THE PREDICTION OF FILM-DRYOUT CHF

7.1 Introduction

In Section 7.2 we will present a brief description of the use of phenomenological modelling of dryout for the prediction of 'CHF', including a discussion of the 'state of the art' application in the nuclear industry. In Section 7.3 we discuss the (growing) ability to analyse broadly similar models of film dryout using CFD.

7.2 'Classic' phenomenological modelling

7.2.1 The basis of phenomenological modelling

In annular flow, there exists a liquid film on the channel wall and a gas (or vapour) core that carries a dispersion of liquid droplets. Figure 29 shows the nature of an annular flow.

It has been shown that, in annular flow, the CHF phenomenon corresponds to the drying out of the liquid film.

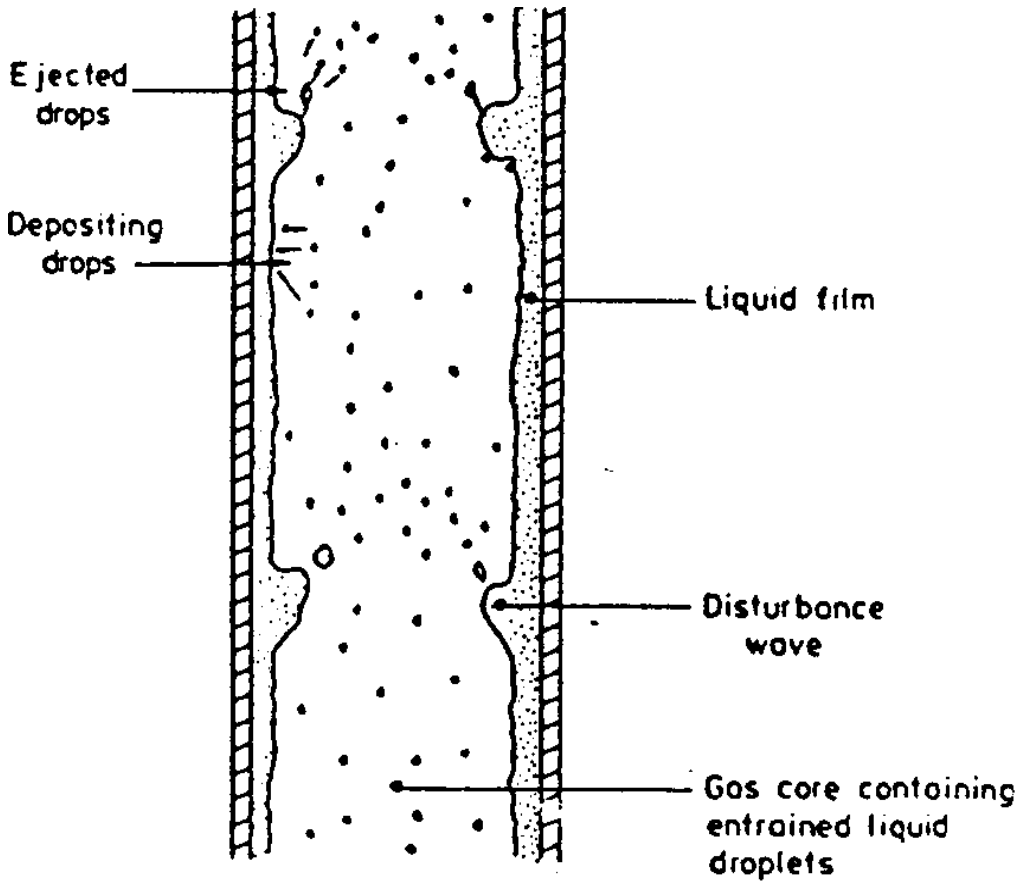

Figure 29
The nature of heated annular flow phenomena

Proof that CHF (dryout) occurs due to the disappearance of the liquid film was obtained in a number of experiments at the UKAEA Harwell Laboratory in the 1960's and 1970's. In these

experiments the liquid film flow rate was determined by removing the film through a porous wall section. The power input at which CHF occurred at the end of the channel corresponded closely with that at which the film flow rate went to zero. CHF in annular flow is therefore an *integral* phenomenon in which the processes of evaporation and droplet entrainment lead to the film drying out, despite the fact that these processes are partly offset by droplet re-deposition onto the film.

Film dryout occurs in annular flow where, over the entire upstream length, the integral of the rates of evaporation from the film, droplet entrainment from the film and droplet deposition onto the film are such that they lead to the film flow rate and film thickness becoming zero.

7.2.2 Algebraic development

The challenge of phenomenological modeling of dryout (CHF) in annular flow lies in being able to model these processes. Summaries of phenomenological models for dryout are presented by Hewitt[2, 4, 21]. Basically the models involve the estimation of the local value of the liquid film flow rate $\dot{M}_{LF}$ by integration of the following equation:

$$\frac{d\dot{M}_{LF}}{dz} = P(D - E - \dot{q} / h_{LG}) \tag{18.1}$$

where z is the axial distance, P the channel perimeter, D the deposition and E the entrainment rate (mass per unit channel surface area per unit time)), $\dot{q}$ the heat flux and h_{LG} the latent heat of vaporisation. This type of model has improved over the years, mainly reflecting the improved relationships for D and E.

$\dot{M}_{LF}$ is often expressed in terms of the *mass flux* corresponding to the film flowrate, namely $\dot{m}_{LF}$ which is simply $\dot{M}_{LF} / A$, where A is the channel cross sectional area. For a round tube of diameter d, the value of $\dot{m}_{LF}$ may be calculated by integration of the equation:

$$\frac{d\dot{m}_{LF}}{dz} = \frac{4}{d}(D - E - \dot{q} / h_{LG}) \tag{18.2}$$

Correlations for D and E are provided by Hewitt and Govan[21]. D is calculated from:

$$D = kC \tag{18.3}$$

where C is the concentration (mass per unit volume) of the droplets in the gas core calculated on a homogeneous basis as:

$$C = \frac{\dot{M}_{LE}}{\dot{M}_{LE} / \rho_L + \dot{M}_G / \rho_G} \tag{18.4}$$

where $\dot{M}_{LE}$ and $\dot{M}_G$ are the mass rates of flow of entrained droplets and vapour (kg/s). k is the deposition mass transfer coefficient (m/s) correlated as follows:

$$k\sqrt{\frac{r_G d}{s}} = 0.18 \qquad \text{for } C/r_G \le 0.3$$
$$k\sqrt{\frac{r_G d}{s}} = 0.83\left(C/r_G\right)^{-0.65} \qquad \text{for } C/r_G \ge 0.3 \tag{18.5}$$

where r_G is the gas density and s the surface tension. The entrainment rate E was correlated in the form:

$$E/\dot{m}_G = 5.75\times10^{-5}\left[\frac{d\rho_L}{\rho_G^2\sigma}(\dot{m}_{LF}-\dot{m}_{LFC})^2\right]^{0.316} \qquad \text{for} \qquad \dot{m}_{LF} \ge \dot{m}_{LFC} \tag{18.6}$$

where

$$\frac{\dot{m}_{LFC}d}{\eta_L} = Re_{LFC} = exp(5.8504 + 0.4249\frac{\eta_G}{\eta_L}\sqrt{\frac{\rho_L}{\rho_G}}) \tag{18.7}$$

Comparisons of these expressions with experimental data for D and E are shown in Figure 30 and Figure 31 respectively. Though the data are scattered around the correlating lines, and though this is an area for potential improvement in the future, the availability of these correlations makes possible the prediction of many situations of annular flow and CHF (dryout).

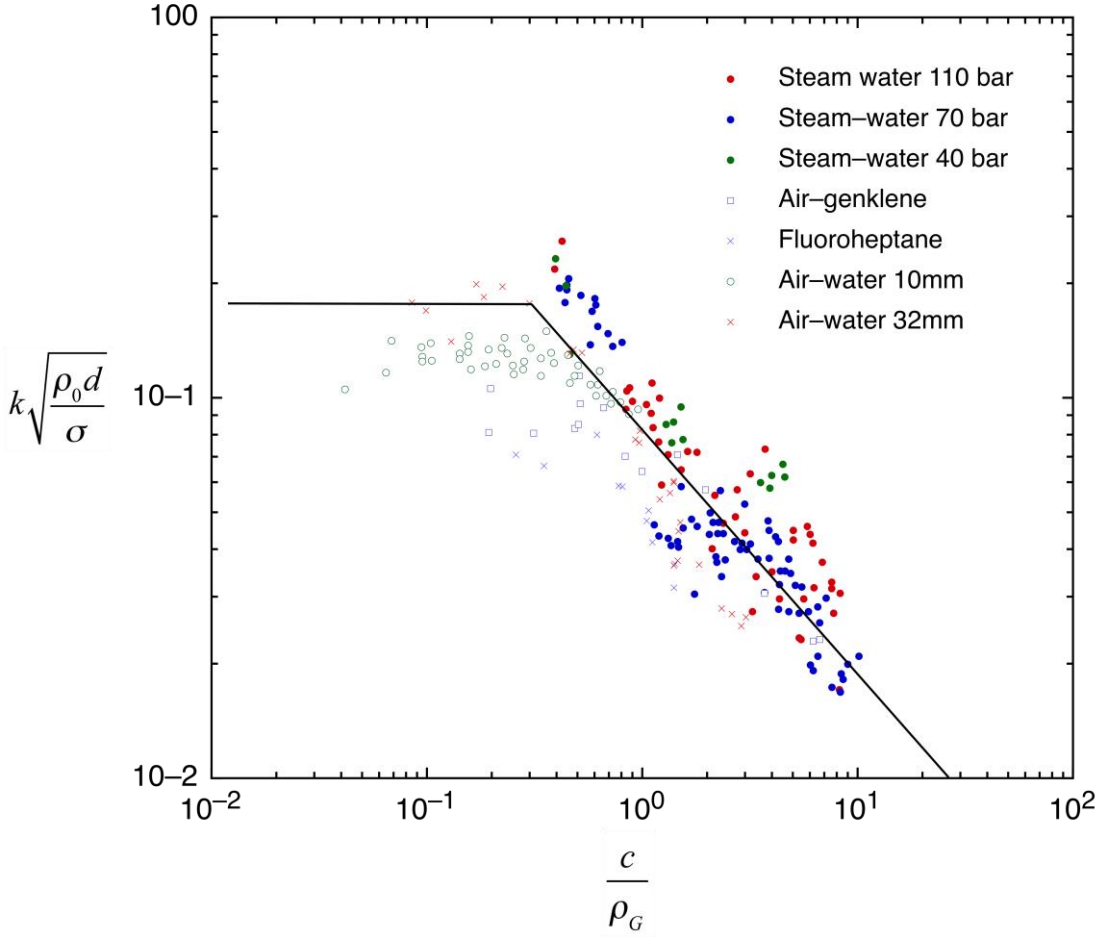

Figure 30
Comparison between the deposition prediction of the Hewitt & Govan model[21] and measurement

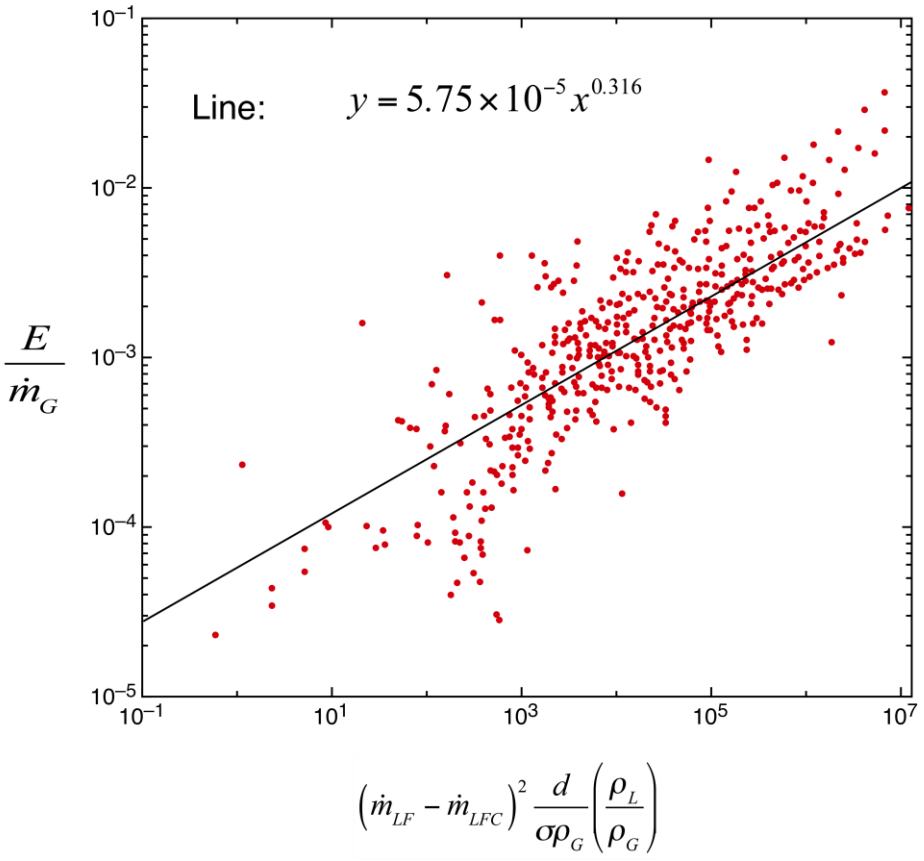

Figure 31
Comparison between the entrainment prediction of the Hewitt & Govan model[21] and measurement

Such models now give predictions which are at least as good as those obtained from empirical correlation methods (see Hewitt[4]). An example of predictions from the annular flow model is shown in Figure 32. Here, predictions and measurements are shown of entrained droplet flow mass flux $\dot{m}_{LE}$ where:

$$\dot{m}_{LE} = \dot{M}_{LE} / A = (\dot{M}_L - M_{LF}) / A \qquad (18.8)$$

where $\dot{M}_{LE}$ and $\dot{M}_{LF}$ are the mass rates of flow (kg/s) of the entrained drops and the film respectively, $\dot{M}_L$ is the total mass rate of flow of the liquid and A the channel cross sectional area. As will be seen, the model predicts well the variation of entrained flow rate with local quality as well as the position at which the entrained flow rate equals the total liquid flow rate – i.e. the position at which the film dries out leading to a dry wall condition and hence dryout or CHF. The soundness of this type of model is demonstrated by the fact that it can even predict dryout in channels in which part of the channel length is unheated. (Figure 32.)

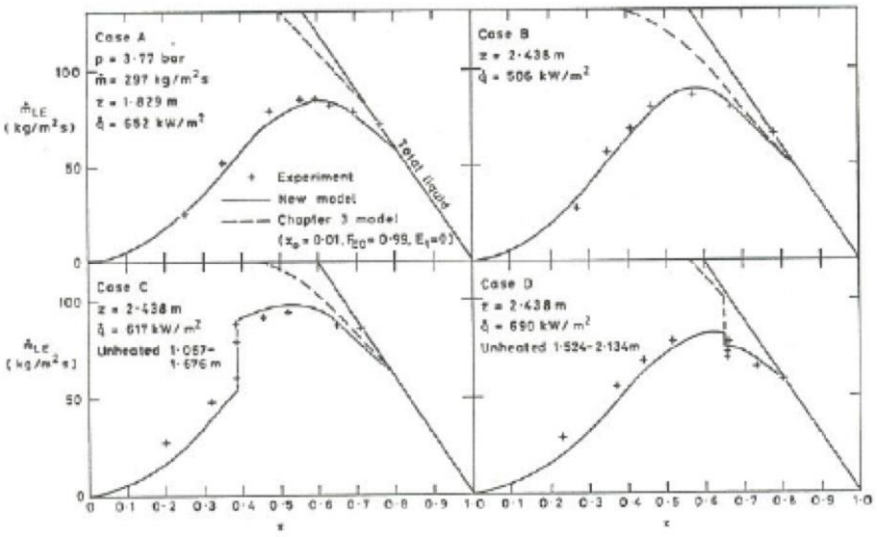

Figure 32
Prediction of entrained droplet flow rate in heated channel with and without unheated zones [21]

An obvious requirement in integrating the equation for film flowrate is that of having an initial value at the start of annular flow. This is not a significant difficulty in the prediction of dryout with long channels, where the result is only weakly affected by the initial condition. Measurements of the entrained fraction at the boundary between churn flow and annular flow are reported by Barbosa et al[33] who give a correlation which can be used to establish a boundary condition for the integration of the equation. However, the difficulty of using this approach is that the entrained fraction at the churn-annular boundary will itself be affected by *non-equilibrium* effects in the churn flow region itself. Thus, a non-equilibrium model that includes both churn flow and annular flow is required. Such a model is reported by Ahmad et al[34] . The approach used was to modify the correlation for local entrainment rate in annular flow to account for the enhanced entrainment rate in churn flows. Thus

$$\frac{E_{CHURN}}{E_{ANNULAR\_LOCAL}} = -8.73U_G^* + 9.73 \tag{18.9}$$

where U_G^* is the dimensionless gas velocity given by:

$$U_G^* = U_G\sqrt{\frac{r_G}{gd(r_L - r_G)}} \tag{18.10}$$

The transition to annular flow is assumed to occur when $U_G^* = 1$. Figure 33 and Figure 34 show the effect of entrained fraction at the onset of annular flow for a low mass flux and for a high mass flux respectively. For a low mass flux, the initial entrainment has little effect on the quality at dryout whereas it has a considerable effect at high mass flux.

There is some controversy about whether heat flux has a significant effect on entrainment rate. Milashenko et al[35] made measurements which implied that there was a significant heat flux effect which they correlated as an additional entrainment due to heat flux as follows:

$$E_t = 5.53\times10^{-7}\,\dot{m}_{LF}\left[\frac{\dot{q}\rho_G}{\rho_L}\right]^{1.3} \tag{18.11}$$

The component E_t was measured by determining the change in film flowrate occurring over a heated tube length. However, this kind of experiment can give misleading results since there is a change of quality, leading to a shift in the equilibrium value of film flow.

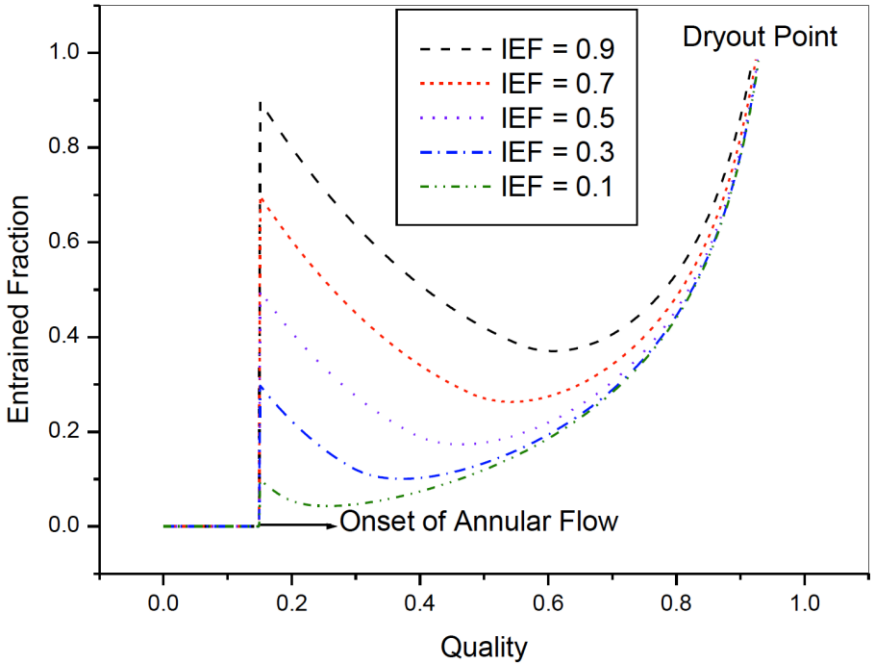

Figure 33
Effect of entrained fraction at the onset of annular flow on dryout quality for a mass flux of 380 kg/m²s [34]

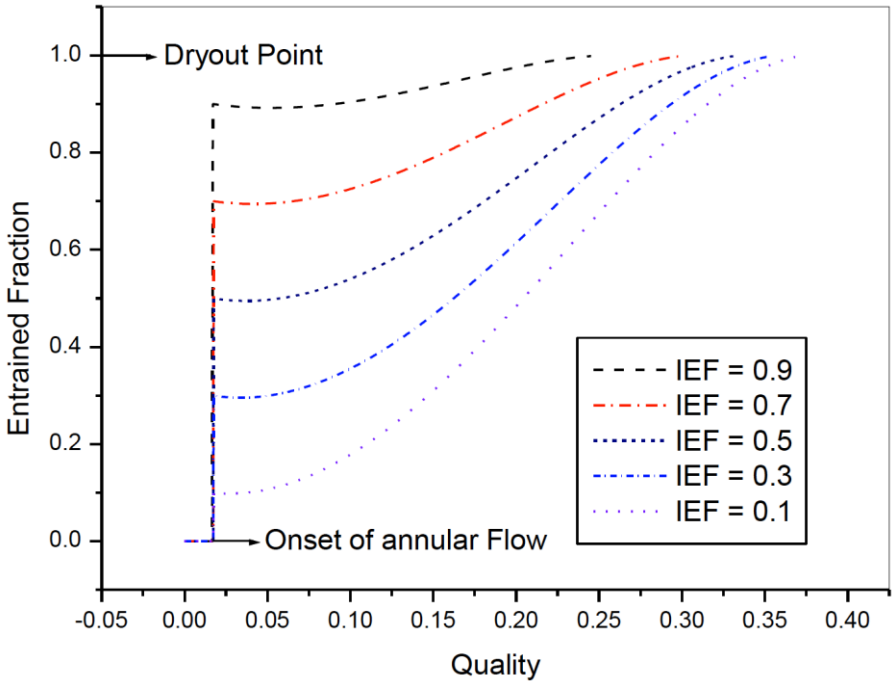

Figure 34
Effect of entrained fraction at the onset of annular flow on dryout quality for a mass flux of 3850 kg/m²s [34]

Clearly, bubble crowding models (such as that of Weisman and Pei [22], as described above) are very different from those for annular film dryout and the question naturally arises about when the transition occurs between one mechanism and the other. Hewitt and Govan[21] produced a modified version of the Weisman and Pei[22] model which applied in both the sub-cooled and quality regions (including in annular flow) and which better fitted the "look-up" tables of international data. They plotted this modified model together with their annular flow model in terms of CHF quality as a function of quality and their graph is presented in Figure 21; the graph also shows data from the both the Canadian and the Russian look-up tables (now merged into the Groeneveld Look up Tables[8]). The main points arising from this graph are as follows:

- There is a relatively smooth transition from one mechanism to the other and it would be clearly difficult to identify the change in mechanism within the data scatter.
- The mechanism of CHF applying in uniformly heated tubes is that which would give the *lowest* value of CHF – namely the bubble crowding model at low qualities and the film dryout model at high qualities.
- Even in annular flow, bubble crowding could occur if there was a local "hot spot" (i.e. a local spike in heat flux) that brought the *local* flux above that predicted from the Weisman and Pei model.

7.2.3 The performance of classical phenomenological modelling

There is a large literature on this, and we will just cite one or two recent papers, and show a few extracted results.

In 2013 Ahmad (PIEAS, Islamabad) [36] described the Imperial College GRAMP code, a typical classical phenomenological code, and investigated the performance of against recent CHF data from BARC, India. Taking just one typical set of results, in Table 1 are listed the

characteristics of a set of BARC measurements, and in Figure 35 are shown the predictions of these by GRAMP.

Pressure	29-71 bar
Mass Flux	820-1700 kg m^{-2} sec^{-1}
Diameter	8.8 mm
Length	3.5 m
Inlet sub-cooling	10 – 45 K
Heat Flux	832-1220 kW m^{-2}
Exit Quality	0.57-0.93
Boiling Length	2.9 - 3.4 m

Table 1
(Some of) the BARC measured cases against which the GRAMP code was tested.

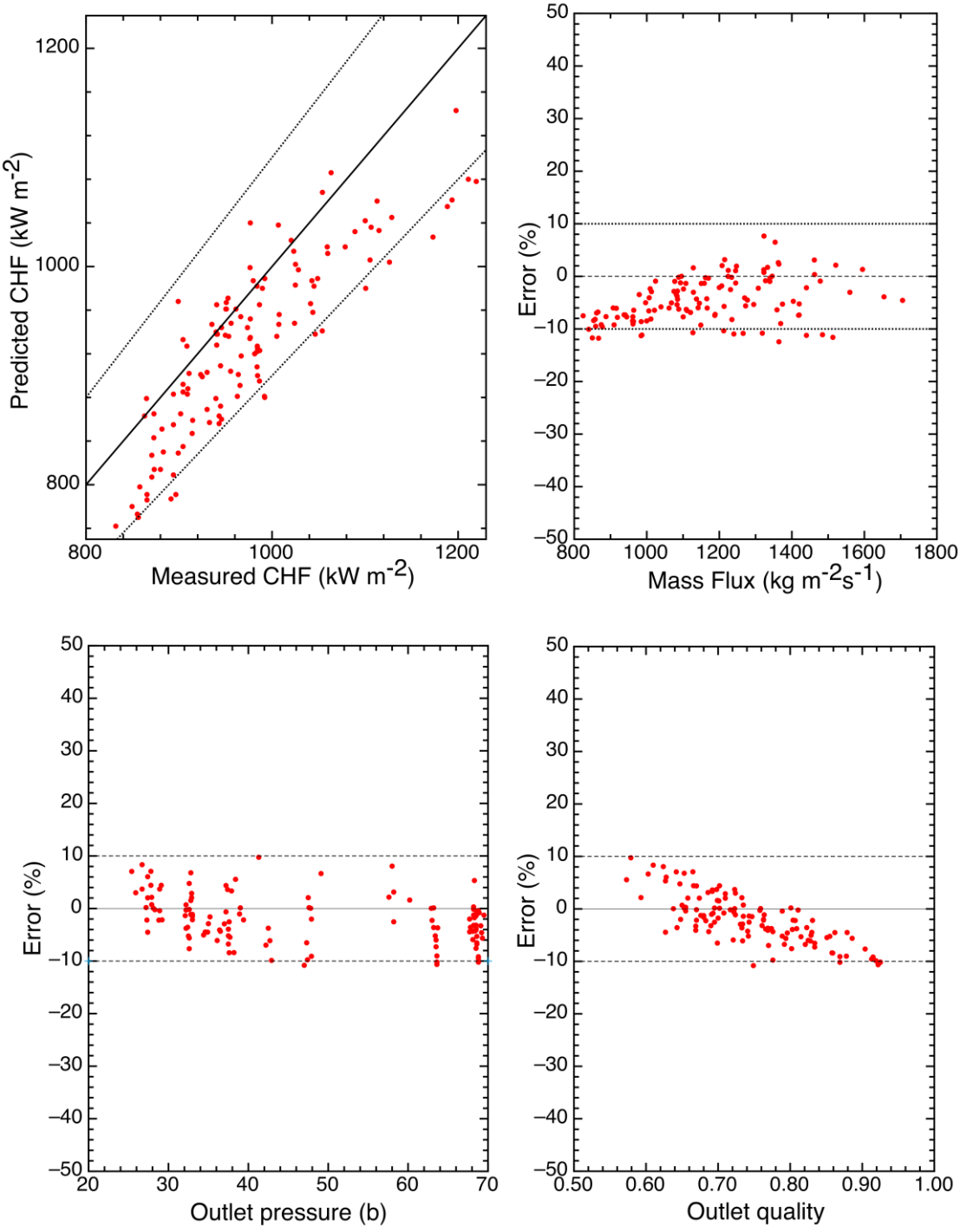

Figure 35
Data from BARC compared to the prediction by GRAMP. The dotted lines indicate a difference of 10% between measurement and prediction. (Taken from Ahmad[36])

Chandraker[37] similarly presents a study of the Indian (BARC) code FIDOM, and Sanmiguel Gimeno[38] presents a cross-comparison of FIDOM, BARC and the Westinghouse code MEFISTO.

7.2.4 Closing remarks

This area, of phenomenologically-based modelling of film dryout is an active field of research[39, 40], and it does seem to offer the most effective way to cope, in particular, with this issue of non-uniform heat flux. An example of a recent study in this area is the work of Adamsson [41], who coupled a film dryout model to a version of the VIPRE code, and produced quite encouraging agreement with measurements.

Despite the necessarily uncertain correlations on which they are based, it is fair to say that these classical phenomenological modelling methods provide a surprisingly accurate and flexible means to predict film dryout CHF.

Versions are readily developed to handle rod bundles.

'State of the art' industrial versions have further enhancements. The following comments are based on a particular industrial code:

A multiplier is applied to the deposition rate downstream of spacer grids. The "shape", that is, the downstream variation, of this multiplier is obtained from previous CFD studies of single phase flows with entrained particle tracking, to gain some knowledge of particle trajectories and consequent deposition rates. The magnitude of the multiplier (i.e. enhanced deposition) is a left as a free, essentially tunable parameter; the only free tunable parameter in the particular code at issue).

There is no disruption to the liquid film assumed to occur because of a spacer grid. The argument is made that probably the effects of additional entrainment because of the geometric disruption are counterbalanced by the effects of additional deposition due to the disruption to the vapour flow. The effect of possible enhanced entrainment due to the spacer grid, the multiplier mentioned above, is based on the net effect of enhanced deposition & entrainment.

As will be seen, CFD is beginning to be used to augment and refine the classical phenomenological modelling, and we now turn to this more generally.

7.3 Film dryout prediction using CFD

7.3.1 Introduction

In many respects building upon the general spirit of the phenomenological modelling discussed above, there has been a fairly steady effort over the last decade or so to build CFD-based models of the flow regime characterised by entrained droplets and a very thin liquid film. There are various publications that show reasonable agreement between predicted film dry out location and that observed in experiments. However, it is almost invariably case that the modelling involved is relatively obscurely presented. The general approach is that of the two fluid Eularian - Eularian treatment, with various flow regimes identified, and used to determine the set of closure relations used for the inter-phase transfers.

None of these approaches offer the fidelity or the flexibility for film dry out prediction under the circumstances of interest for the present work.

In the following sections we will very briefly identify and show some results from some of a selection of these attempts, and will then discuss what are the challenges involved in modelling for the issue of current interest, and what possible approaches might meet these. We will focus on approaches using the 'Extended Boiling Framework, 'EBF', being developed for Star CCM+ (and other codes; see later), and which probably represents the most sophisticated attempt to model film dryout.

7.3.2 CFD-based film dryout publications

7.3.2.1 Ioilev et al 2007[42]

An inter-phase topology map is employed, to select the closure relations employed. For present purposes, it is the 'liquid film, vapour core' regime that is of most interest, and within that the modelling of the liquid film. This remains rather empirical. The film is treated as being in the 'bubbly topology' flow regime as long as the film is one cell or more thick. Once it becomes thinner than that film flow equations are replaced by wall functions. 'Thick' film boiling is modelled using a modified version of the heat flux partitioning approach discussed above. Thin film boiling is modelled wholly empirically. The modelling of film to droplet exchange of mass, by entrainment and deposition, is not included.

Two experiments in a vertical channel 0.01 m in diameter and 7 m in length, at a pressure of 7 MPa (~BWR conditions), with a uniformly heated wall were used as verification test-cases. They differed in wall heat flux and inlet mass flux: 0.35MW/m2 and 497 kg/m2 s, and 0.8MW/m2 and 1,495 kg/m2 s.

Results for Experiment 1 are shown here, extracted from their paper, as Figure 36 and Figure 37. As will be observed, agreement is remarkably good.

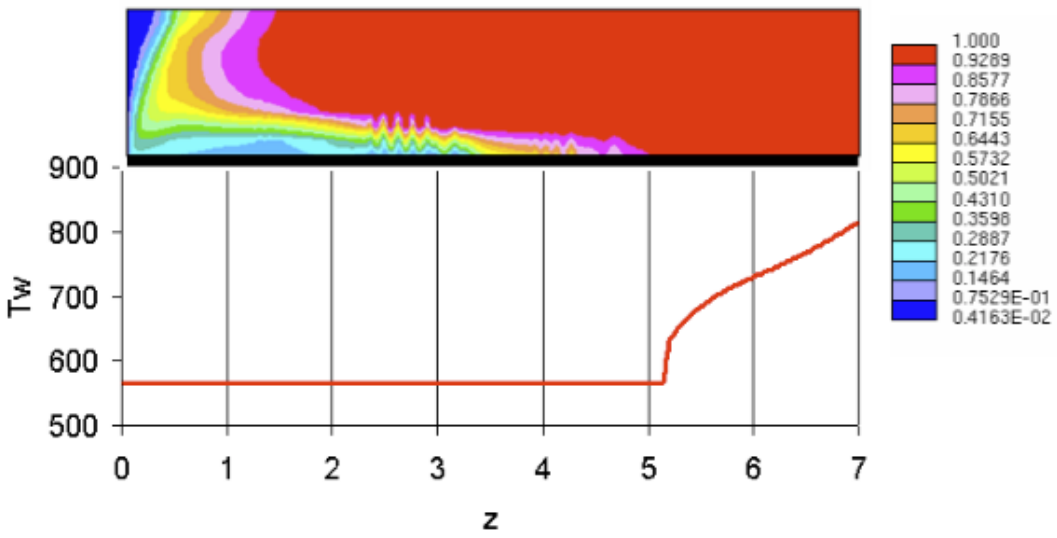

Figure 36
Predicted void fraction distribution and wall temperature; Experiment 1 (extracted from [42])

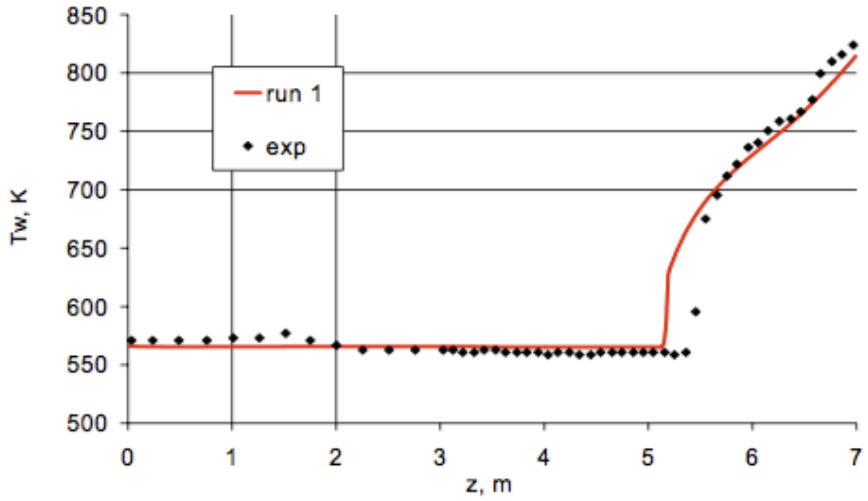

Figure 37
Measured and predicted wall temperature; Experiment 11 (extracted from [42])

7.3.2.2 Tentner et al[43]

A more developed version of this code is reported in 2014. Again, the treatment is based on an empirical topology map, but with a more sophisticated treatment of those wall cells that contain a thin liquid film, and identified as such by reference to the local void fraction and void fraction gradient. Again, droplet entrainment and deposition are not modelled. We will show here just one or two results from the paper.

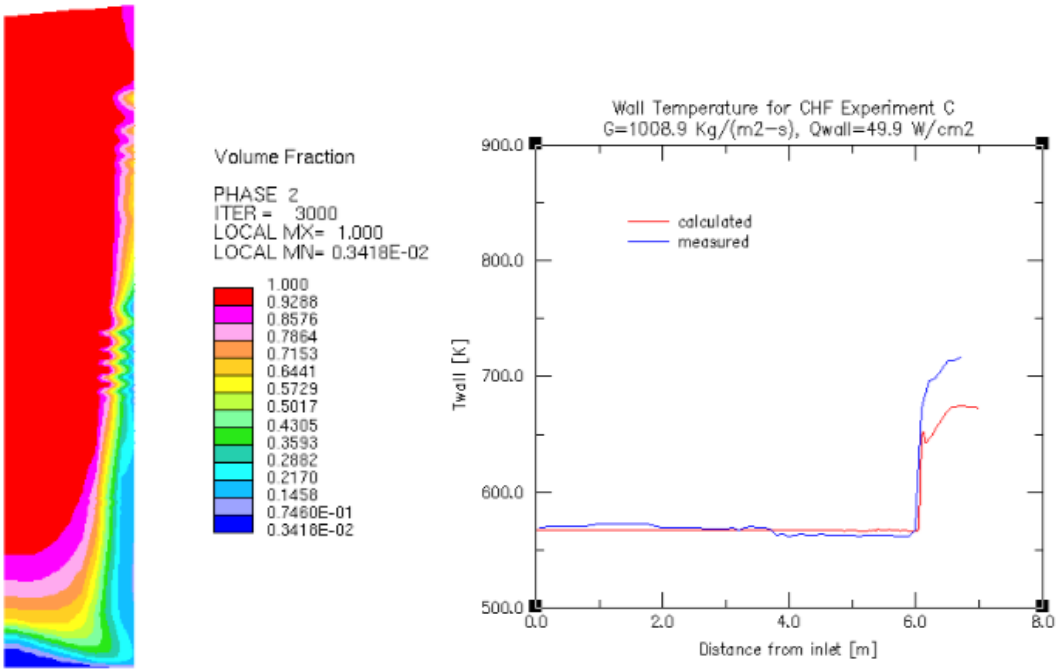

Figure 38
Experiment C (Figure 6c and Figure 7c) of Tentner et al[43]; Computed void fraction, and computed and measured wall temperature.

7.3.2.3 Tentner et al[44]

This paper reports further development of the Extended Boiling Model. However, the most noteworthy feature for present purposes is that the EBM is being ported to a different CFD code; NEK5000[45], a 'highly-parallel' code being developed at ANL for very large-scale simulations.

7.3.3 Issues in CFD modelling of film dryout

They are of course to a degree coupled, but it is helpful to separate the issues in CFD modelling of film dry out to droplet deposition, droplet entrainment, and the modelling of the flow of the film.

Droplet entrainment and deposition, the core part of 'classical' phenomenological modelling, is treated very sketchily in the CFD analyses published to date. There is much scope to improve this. For deposition this could be either via incorporation of the same forms of empirical quantification as are used in phenomenological codes, or via some form of Lagrangian modelling (or a combination of these approaches.) Entrainment probably needs to be empirical. Mechanistic entrainment would, *inter alia*, require some form of interface tracking for the film, well enough resolved to capture the generation of wave crests from which entrainment typically takes place. This would be challenging[†].

[†] In the interest of completeness:- We are currently setting up a research project (with a UK industrial sponsor) to attempt the first part of this; empirical droplet models, coupled to a suitable sub-grid film model. Discussions are less advanced, but with our Indian collaborators we are exploring the possibility of a new project combining interface tracking of film flow specifically over geometrical disturbances (notional 'grids') with measurements of film flow rates, film thicknesses, and high speed filming. However, this will be a very focussed study, over a single 'disturbance', to establish a

The second broad issue is how the film is modelled. The starting point is the 'normal' Eularian – Eularian approach, but this copes poorly as the film becomes ~one, and then less than one cell thick. One could envisage a refined discretisation, so that the film always remained several cells thick, but this, for the sub-millimetre films of interest would be expensive, and remove only some of the modelling problems. The correlations on which inter-phase mass transfer is based would really be being used outside their region of experimental support.

The alternative is the use of semi-empirical approaches and sub-models, and these are being added actively to those codes tackling this problem.

The 'exact' approach, of a film resolved well enough for flows within it, and entrainment from it, to be modelled, using some form of interface tracking technique (VOF or level set) would be prohibitively expensive for whole channel analyses.

There is perhaps more scope for a piecemeal approach, where expensive but "exact" CFD treatments could be used as *a priori* calculations, from the results of which semi-mechanistic, semi-empirical models could be derived. These could then be incorporated into a simpler but practicable CFD scheme. This is a very interesting area, and actually is one that we are actively considering undertaking work. We understand that work along these lines, albeit perhaps not quite this fundamental, is currently planned by one major North American BWR vendor, and the other major BWR vendor commented to us during a recent visit to them that entrainment from and disruption of films by spacer grids was one area where they felt advances were needed.

validated capability, and gain insights. We do not envisage this being a 'whole bundle', or anything like it, capability.

8 CFD PREDICTION OF SINGLE PHASE FLOWS IN ROD BUNDLES WITH SPACER GRIDS

Any use of CFD to predict the behaviour of ultimate interest in this present study, bubble crowding or film dryout downstream of a spacer grid, must rest initially upon the ability of the CFD treatment to model single phase flows such geometries. Plainly, if it cannot do that, there is little point in attempting to use it to model two-phase flows.

In this section we give a brief review of the current state-of-the-art of the application of CFD to flows in rod bundles and their associated spacer grids.

8.1 Introduction

Current Pressure Water Reactor (PWR) fuel assembly thermal-hydraulic analyses are mostly performed on a subchannel basis that neglects detailed heat transfer and flow distributions surrounding fuel rods. Subchannel codes require input of thermal mixing and hydraulic loss coefficients that are obtained from costly experiments.

Prediction of Critical Heat Flux (CHF), both due to dryout and departure from nucleate boiling (DNB), without relying on empirical correlations derived from rod bundle geometries has been one of the foci of research in nuclear engineering. The main motivation driving this area of research is to reduce the number of costly experiments required for licensing of advanced fuel bundle types.

This section reviews the current status of CFD analyses of PWR rod bundles modelling single-phase flows. Key areas and parameters that affect the quality of the CFD results are discussed. (This is a precursor to two-phase boiling flows, which are covered in Section 9.)

8.2 Single-phase modelling of fuel bundles

8.2.1 CFD prediction of pressure drop in fuel bundles at Mitsubishi and Westinghouse

Ikeda et al[46, 47] of Mitsubshi Heavy Industries examined the applicability of CFD for thermal hydraulic design of spacer grids. PWR spacer grids have mixing vanes on them to promote mixing of the coolant around the fuel rods. A well-designed spacer grid should give a small pressure drop, combined with good thermal mixing which lowers the coolant temperature and therefore gives better DNB performance.

DNB is of course a two-phase flow phenomenon, so it cannot be analysed directly in a single-phase flow analysis, i.e. without considering boiling. Ikeda et al judged DNB benefit based on the reduction of the single-phase peak spot temperature around fuel rods produced by the different grid designs. Effectively, it is a measure of the mixing ability of the mixing vanes.

Pressure loss measurements on 5x5 bundles were made at the Mitsubshi Fuel Research and Development Hydraulic Facility located at the Nuclear Development Corporation (NDC) and the DNB tests using Freon (two-phase flow tests) on a 3x3 bundle were conducted at the Columbia University Heat Transfer Research Facility.

Ikeda's CFD model[47] consists of only one span of a 5x5 rod bundle with a spacer grid. The grid structures include straps, springs, dimples, mixing vanes and welding nuggets. The commercial CFD code STAR-CD was used with 2 million trimmed cells. A single-phase flow model with the k-epsilon turbulence model was used. In later work Ikeda considered [46] two spans of a 5x5 bundle with 2 spacer grids. Again STAR-CD was used with 7 million trimmed cells.

Ikeda[47] reported the following results. For pressure loss, their CFD predictions are within 5% of measured data. Cross-flows generated by the mixing vanes were measured by "rod-type" Laser Doppler Velocitometry (LDV), which was designed to measure flows in the narrow gaps between the rods. CFD results are within 1 standard deviation of the measured data. The comparison between CFD 'hot spots' and measured DNB position shows good correlation. Ikeda concluded the paper with the confirmation of the applicability of CFD evaluation method for thermal hydraulic design of spacer grids.

Ikeda et al[46] later examined the effects of the turbulence model and discretization scheme used in their CFD model. Two sets of models were considered: Case A uses the standard k-epsilon turbulence model and first-order upwind scheme. Case B uses an anisotropic k-epsilon (with quadratic algebraic correlation terms) and a second-order scheme.

Ikeda found pressure loss over one grid span can be predicted within 5% using standard k-epsilon model and the first-order discretisation scheme (Case A) and within 2% using an anisotropic k-epsilon model and second-order scheme (Case B); see Figure 39.

Near the spacer grid where the swirling flow is strong the anisotropic k-epsilon model, together with the second-order scheme, give a better prediction of the pressure loss, to within 4%, whereas predictions by Case A range from 7% to 11%, as seen in Figure 40.

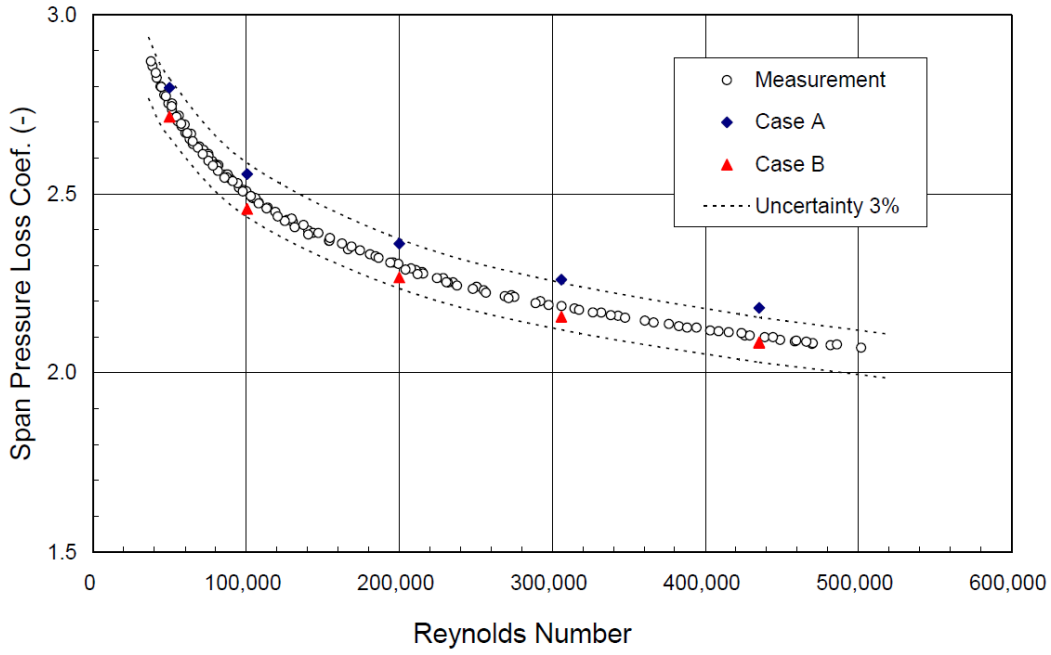

Figure 39
Comparison of pressure loss over one grid span (Extracted from Ikeda et al[46])

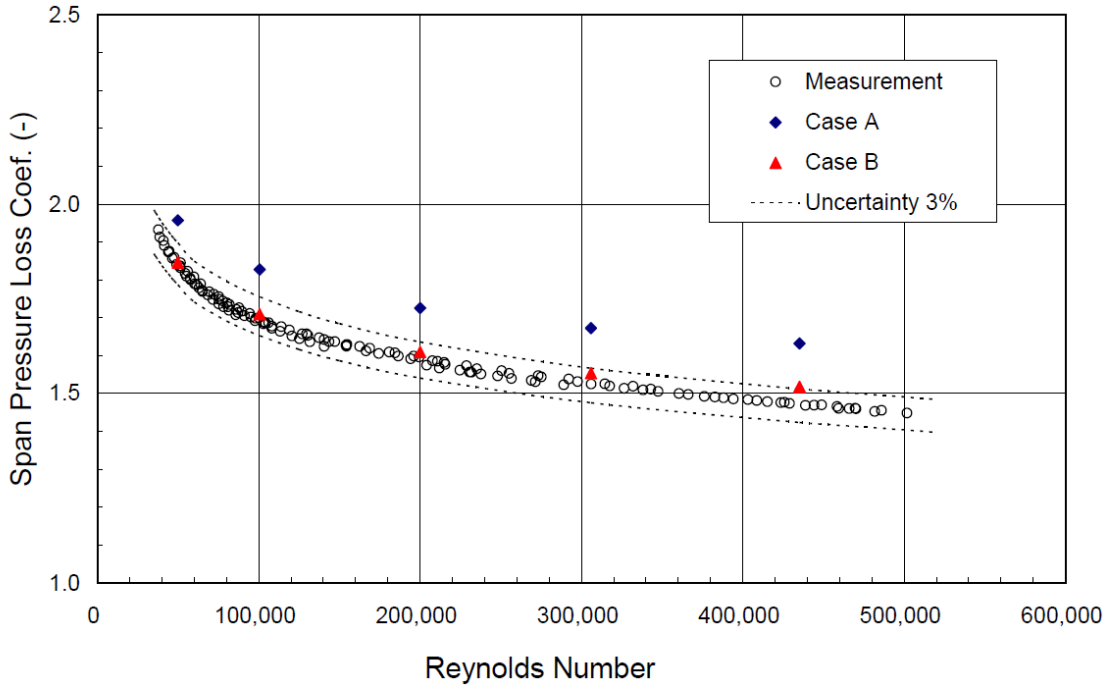

Figure 40
Comparison of pressure loss across a spacer grid (Extracted from Ikeda et al [2.2]).

Sugrue et al[48] presented very similar experimental and CFD modelling, work carried out at Westinghouse, and reached a similar conclusion, namely that single-phase modelling of a 5x5 rod bundle with spacer grids using the quadratic k-epsilon turbulence predicted a pressure drop over a grid span to within 3% of the measured value. Sugrue also used a trimmed mesh in the STAR-CCM+ code.

8.3 The EPRI NESTOR 5x5 rod bundle benchmark exercise

In order to address industry concerns related to the application of CFD to PWR cores, EPRI convened a CFD 'Round Robin' (RR)[49] benchmarking exercise in 2009. This group included participants from fuel suppliers, CFD software developers, universities, research organizations, and utilities. The RR participants volunteered to model a selection of experimental runs from the NESTOR (New Experimental Studies of Thermal-Hydraulics of Rod Bundles) program.

The NESTOR program involved an extensive testing on identical 5x5 full-length rod bundles mimicking a PWR fuel sub-assembly geometry that included (i) hydraulic isothermal experiments in the EDF-Chatou MANIVEL facility, and (ii) heated experiments in the CEA-Grenoble OMEGA facility. NESTOR provides a comprehensive set of high fidelity data for validating CFD calculations.

Apart from elucidating the current status of CFD analyses of PWR rod bundles, the goal of the benchmark exercise was

(i) to identify the key areas and parameters that can affect the quality of the CFD results and

(ii) to provide Best Practice recommendations for such CFD simulations.

The CFD results from the Round Robin exercise are well reflected in the papers by Martin et al of Areva[50] and Conner et al of Westinghouse[51]. A brief summary of their results is given below.

8.3.1 Brief summary of Round Robin results from Areva

Areva participated in the Round Robin benchmark and reported[50] their CFD results. The average deviation between predicted and measured pressure drop across spacer grids is typically in the order of +/- 3% [2.5]. Figure 41 and Figure 42 below show their comparison of predicted and measured the axial velocity and inner-wall temperature profiles.

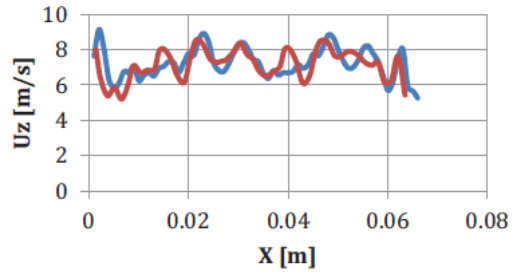

Figure 5: Axial velocity at z= 0.025m

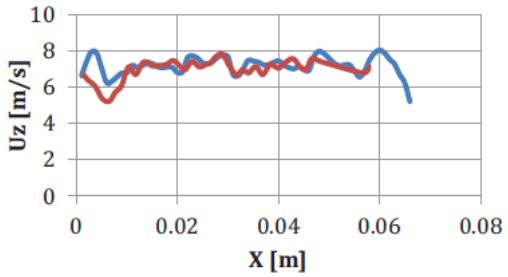

Figure 6: Axial velocity at z= 0.05m

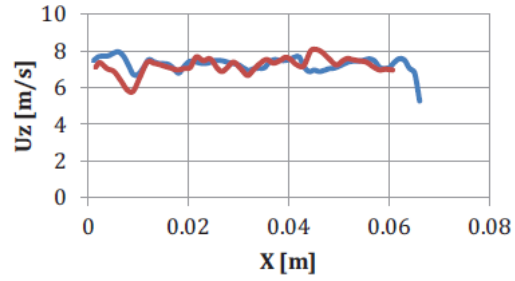

Figure 7: Axial velocity at z= 0.075m

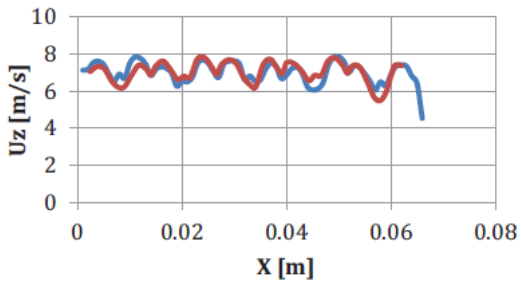

Figure 8: Axial velocity at z= 0.304m

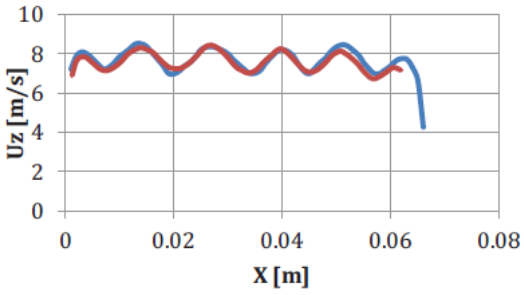

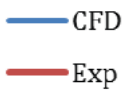

Figure 9: Axial velocity at z= 0.514m

Figure 41
Areva's comparison results of axial velocity (Extracted from Martin et al [2.5])

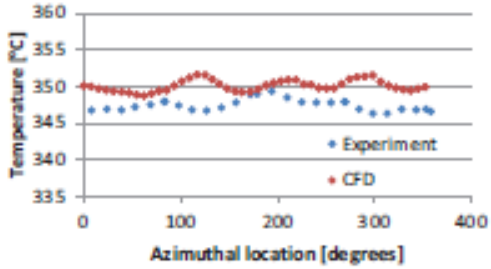

Figure 16: Circumferential inner-wall temperature for Rod 5 at Z_0=-1150mm

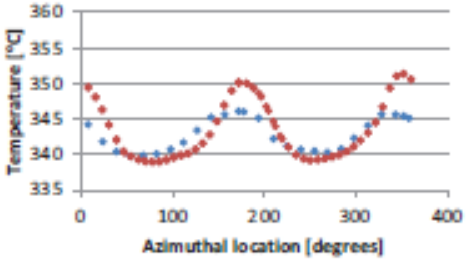

Figure 17: Circumferential inner-wall temperature for Rod 5 at z_0=-1030mm

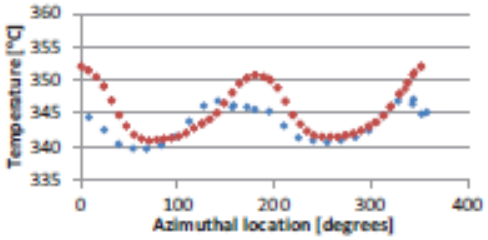

Figure 18: Circumferential inner-wall temperature for Rod 5 at z_0=-1000mm

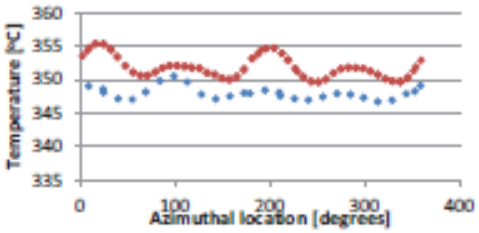

Figure 19: Circumferential inner-wall temperature for Rod 5 at z_0=-790mm

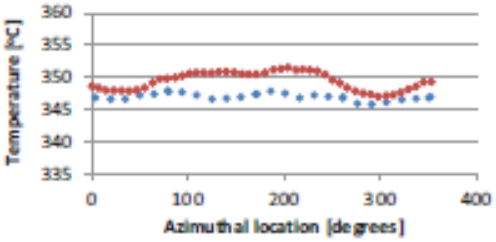

Figure 20: Circumferential inner-wall temperature for Rod 1 at Z_0=-1150mm

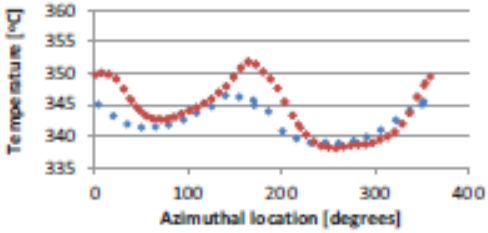

Figure 21: Circumferential inner-wall temperature for Rod 1 at Z_0=-1030mm

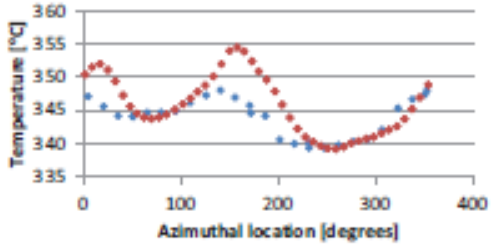

Figure 22: Circumferential inner-wall temperature for Rod 1 at Z_0=-970mm

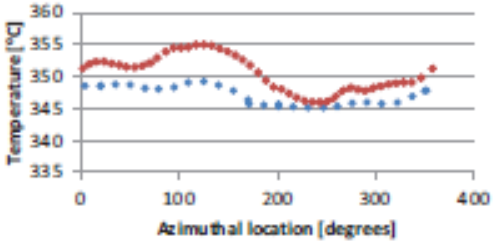

Figure 23: Circumferential inner-wall temperature for Rod 1 at Z_0=-790mm

Figure 42
Areva's comparison results of inner-wall temperature (Extracted from Martin et al [2.5]).

8.3.2 Brief summary of Round Robin results from Westinghouse

Westinghouse used a similar CFD model to that used by Areva and reported[51] the span pressure drop of the bundle with mixing vane grid to be predicted within 2% of measured values. Axial velocity and inner-wall temperature comparisons are shown in Figure 43 and Figure 44.

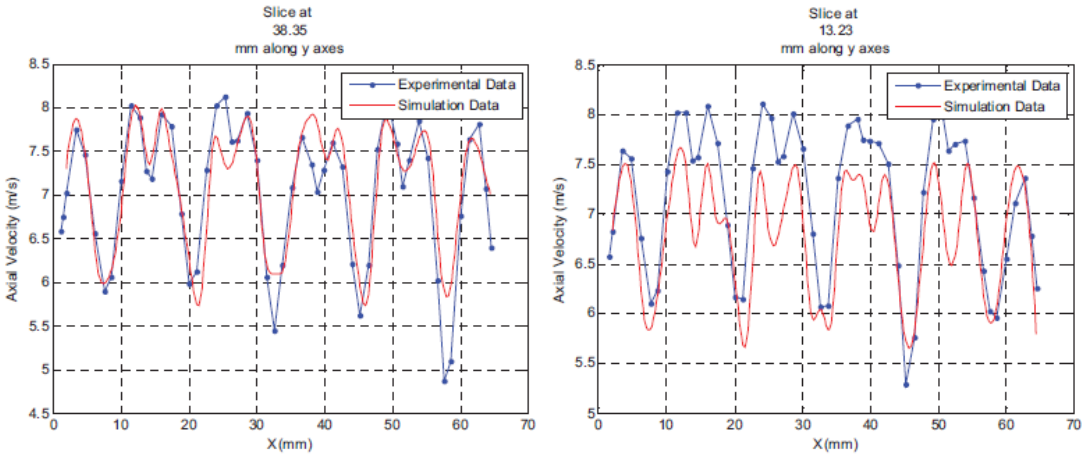

Figure 43
Comparison of axial velocity (Extracted from Conner et al[51]).

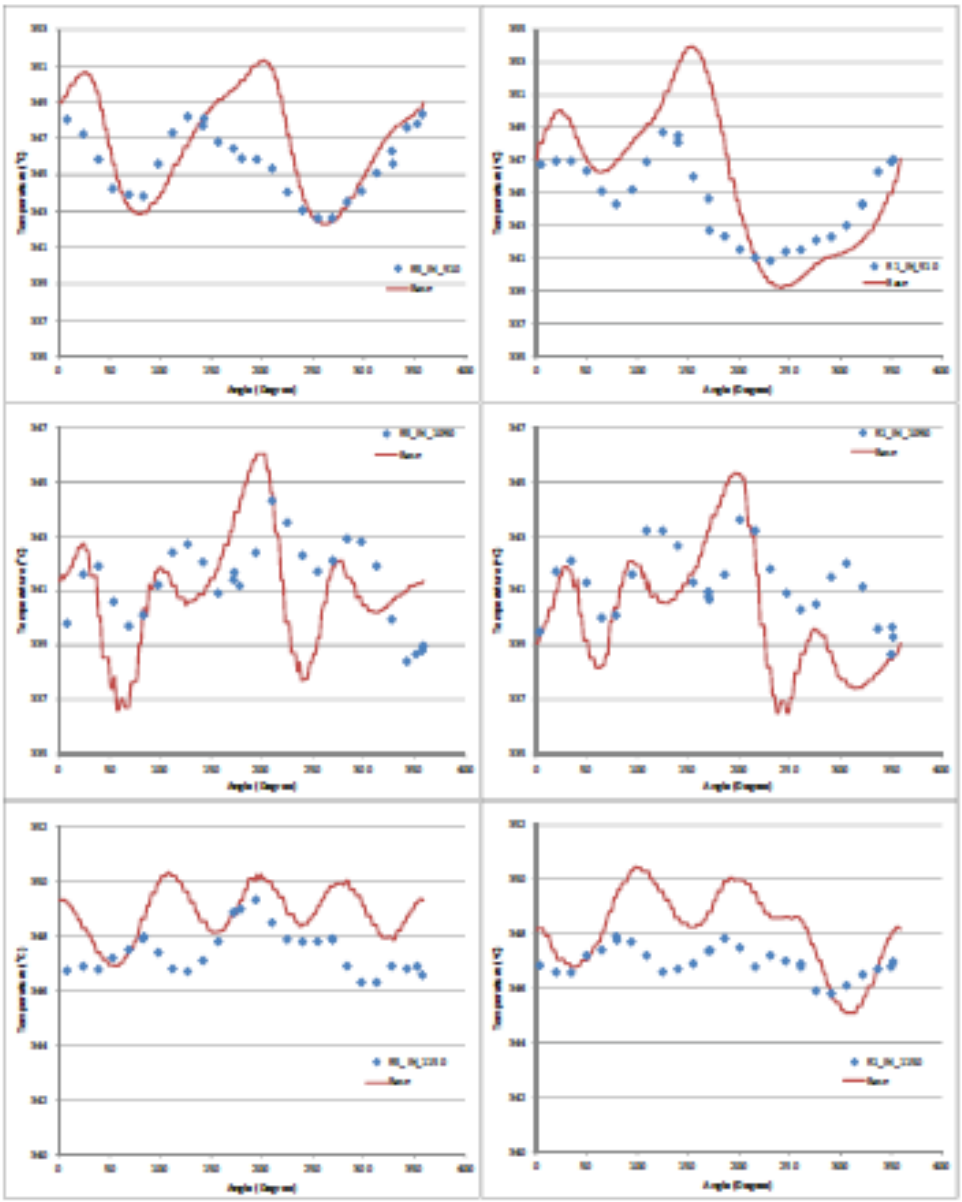

Figure 44
Comparison of inner-wall temperature (Extracted from Conner et al[51]).

8.4 Key areas and parameters affecting CFD results

The EPRI NESTOR Round Robin benchmark exercise examined the key areas and parameters that can affect the quality of the CFD results. In brief the key areas identified are

(i) -boundary conditions need to be appropriate

(ii) -use conjugate heat transfer (CHT) and volumetric heat source in the cladding to model fuel rod-to-flow heat transfer,

(iii) -near-wall treatment needs to be consistent with the turbulence model used (for example the y+ value in the near wall cells should be larger than 30 when the high Reynolds number k-epsilon model was used), and

(iv) -a trimmed hexahedral mesh with extrusion layers of mesh next to solid surfaces is preferred.

A Best Practices Guide is being prepared by EPRI. When available this Best Practices Guide would be a key reference document for CFD modelling of PWR fuel bundles.

8.5 Closing remarks

In essence, the ability of modern CFD codes to model single phase flows in rod bundles with spacer grids is really rather good. This extends to the modelling of single-phase heat transfer, which is a necessary prerequisite for the ability to model boiling flows.

9 CFD PREDICTION OF BOILING AND BUBBLE-CROWDING CHF IN ROD BUNDLES

9.1 Introduction

We have discussed in Section 5 above how sub-models can be introduced into two phase CFD treatments to allow a reasonable representation of wall boiling, and how this combined with the "normal" representations in such Eularian - Eularian codes of inter-phase forces, and bubble coalescence, breakup and condensation, can allow reasonable predictions of the spatial variation of void to be made. This is an active and current area of study, with various industrial and academic / laboratory groups involved[52-58]

We will now discuss a few examples of the use of this capability for the prediction of flows and heat transfer within nuclear rod bundles, including its use up to the levels of near-wall void at which bubble crowding CHF becomes probable.

9.2 Lo et al, PSBT 5x5 bundle

Lo and Osman[55] used the Eulerian multiphase boiling model in STAR-CCM+ to simulate the boiling flow in a one of the PSBT 5x5 rod bundle tests. PSBT is the well known NUPEC PWR Subchannel and Bundle Test International Benchmark exercise[59]. At one of the measuring planes Lo et al obtained an average void of 0.16, about 12% lower than the measured value of 0.18.

This same CFD calculation method is being used at both Westinghouse and Areva in analysing spacer grid designs and CHF performance of fuel bundles. A brief review of this work is provided below

9.3 CFD prediction of CHF in fuel bundles at Westinghouse

Yan et al of Westinghouse reported[56-58] use of the same STAR-CCM+ boiling model as described by Lo et al[55] to simulate boiling flows in a range of 5x5 rod bundle tests carried out in their ODEN CHF test facility.

The DNB detection method used in Westinghouse's CFD simulations[56-58] is analogous to the experimental method. In the CFD model, the power level was increased gradually while monitoring the calculated maximum wall temperature. When a sudden large jump in the monitoring temperature was detected, that point was identified as the DNB point and the power level as the DNB power. An example of the temperature-monitoring plot is shown in Figure 45[57].

In the CFD model reported there,[57] Yan et al only modelled the upper section of the 5x5 bundle where the flow is two-phase. The location of the starting point of two-phase flow comes from analysis using their sub-channel code. A trimmed mesh was used in the CFD model, with a total number of cells of around 292 million.

Figure 46 shows that the steam volume fraction on the surface of one of the high power rods approaches unity upstream of the grid spacer (the second grid from the top) at 100% DNB power. According to Yan et al[57] this is also the location where DNB was observed in their tests.

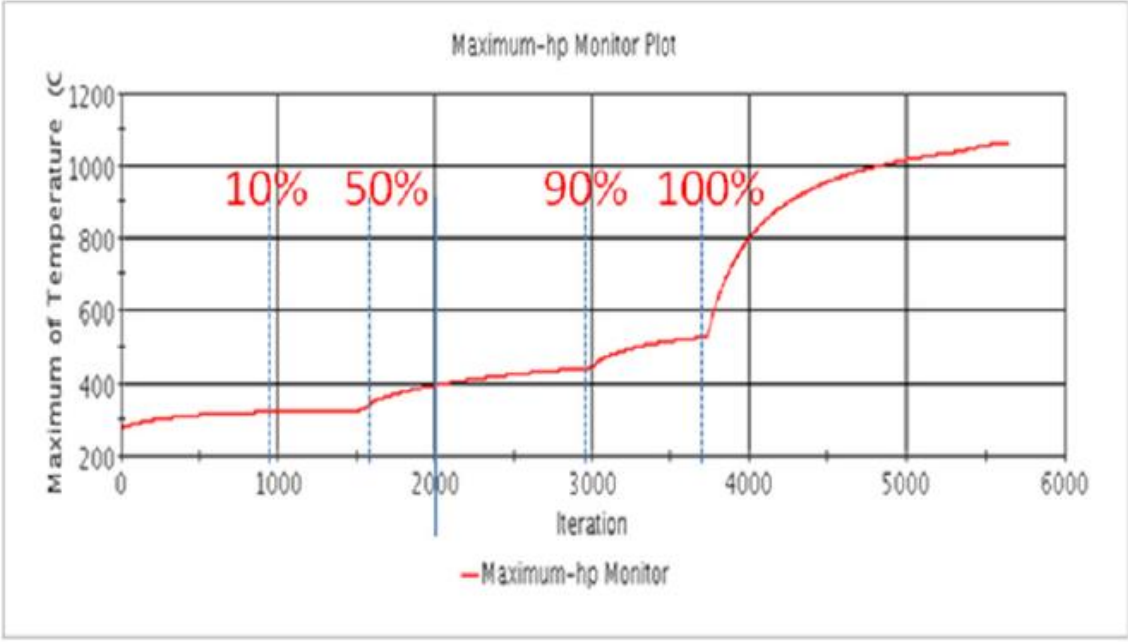

Figure 45
Maximum temperature rise with increase in heat flux. (Extracted from Yan et al[57]). The plot shows the maximum surface temperature calculated against iteration number (i.e. solution step). The blue dotted lines mark the iteration when the power was increased and the value of the power is given, in red, as percentage of DNB power.

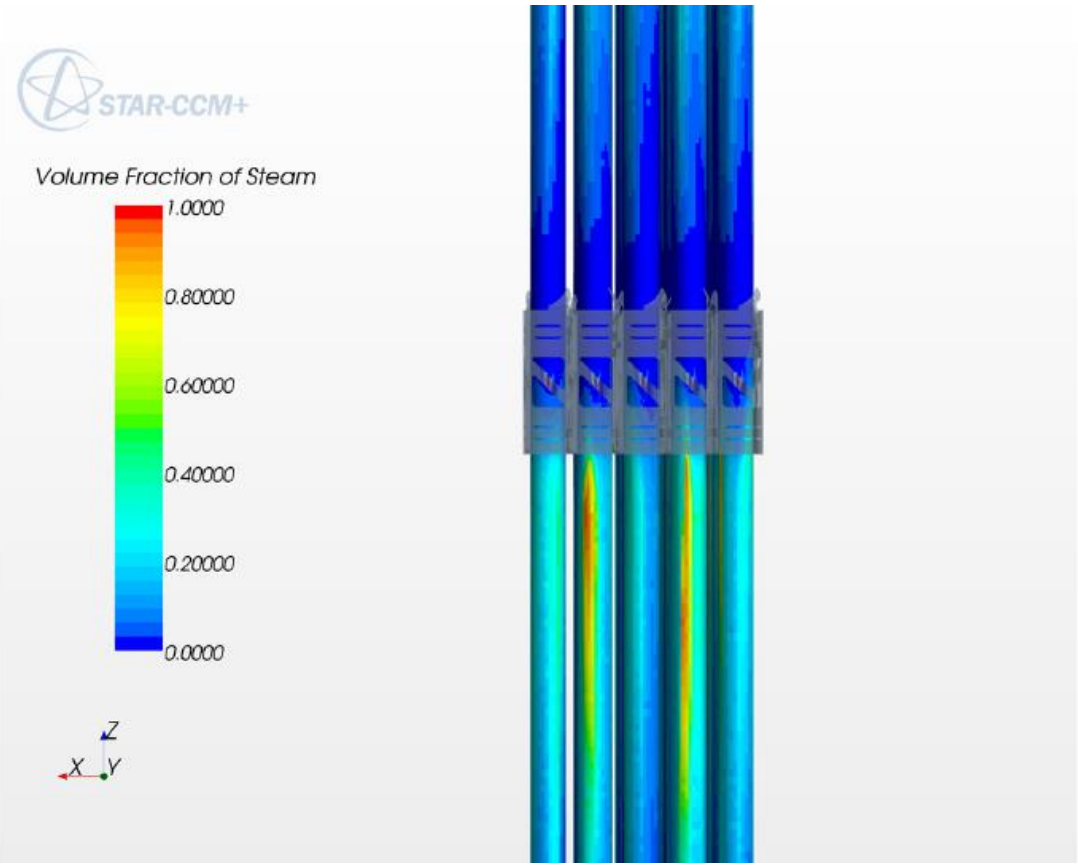

Figure 46
Steam distribution on the rod surface (Extracted from Yan et al[57].) The plot shows extremely high (near unity) void on the surfaces of the 2nd and 4th rods from the left just below the spacer grid, indicating the code predicted bubble crowding type DNB at those locations

In another study[58] Yan et al used a similar CFD model to determine the DNB power in 5x5 bundles with different spacer grid designs. The model size was reduced, with the total number of cells used this time around 145 million. Six test cases were considered, three with mixing vane grids and three with non-mixing vane grids. For all six cases studied, the DNB power obtained by CFD is ~85% of the measured value; see Figure 47. That is, the CFD-predicted DNB power is within 15% of (below) the measured DNB power. They also noted the location of DNB predicted by CFD to be consistent with their experimental observation.

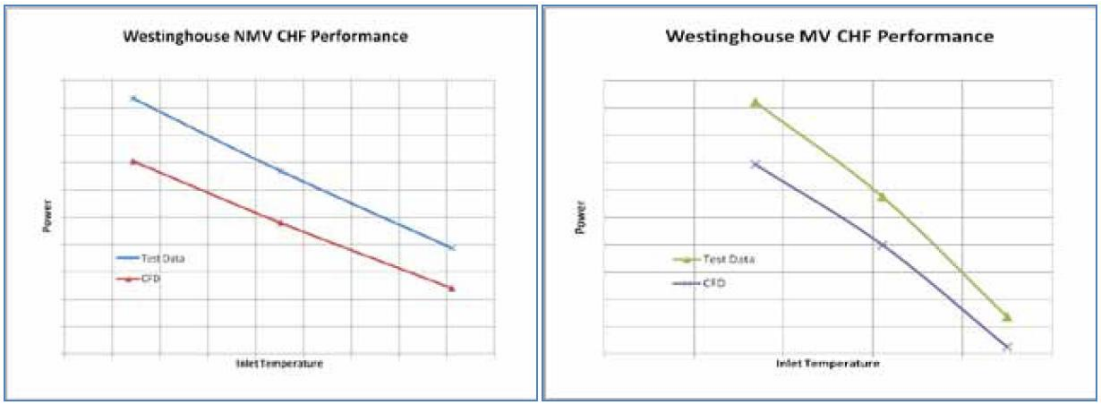

Figure 47
CFD predicted and Test CHF comparisons (Extracted from Yan et al[58].)

Yan et al also considered three different designs of spacer grids: a grid with mixing vanes (split vane grid), without mixing vanes (vaneless grid) and a Helically Fluted Tubular Grid (HFT)[56]; see Figure 48. They reported that in all cases predicted CHF was within 10% of that measured.

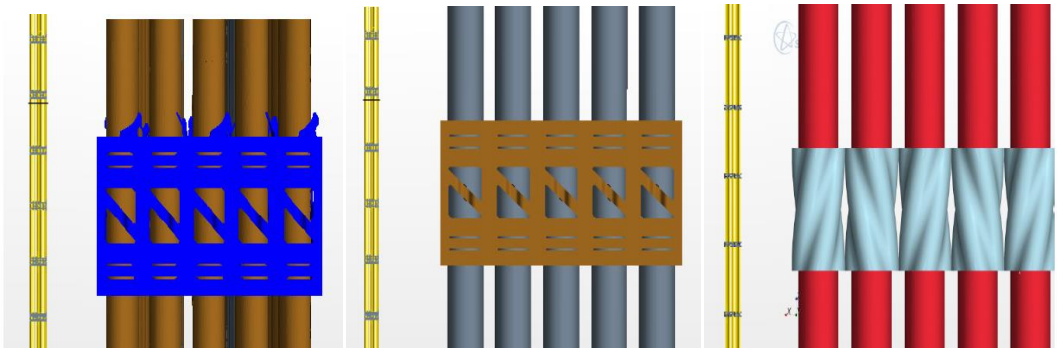

Figure 48
Three different designs of spacer grid (Extracted from Yan et al[56]).

The CFD results of Yan et al[56] predict that at 90% of the CHF power level there is no dryout area in the case with the split vane grid. However, with the vaneless grid there is a small dryout area predicted, and with the HFT grid there are large areas of dryout predicted. This is shown in Figure 48. These results indicate that the vaneless and HFT grids have a lower CHF value than the split vane grid. The better CHF performance of the split vane grid is presumably due to its ability to generate flow across the subchannels, as will be explained further below. These results correspond well with the test data.

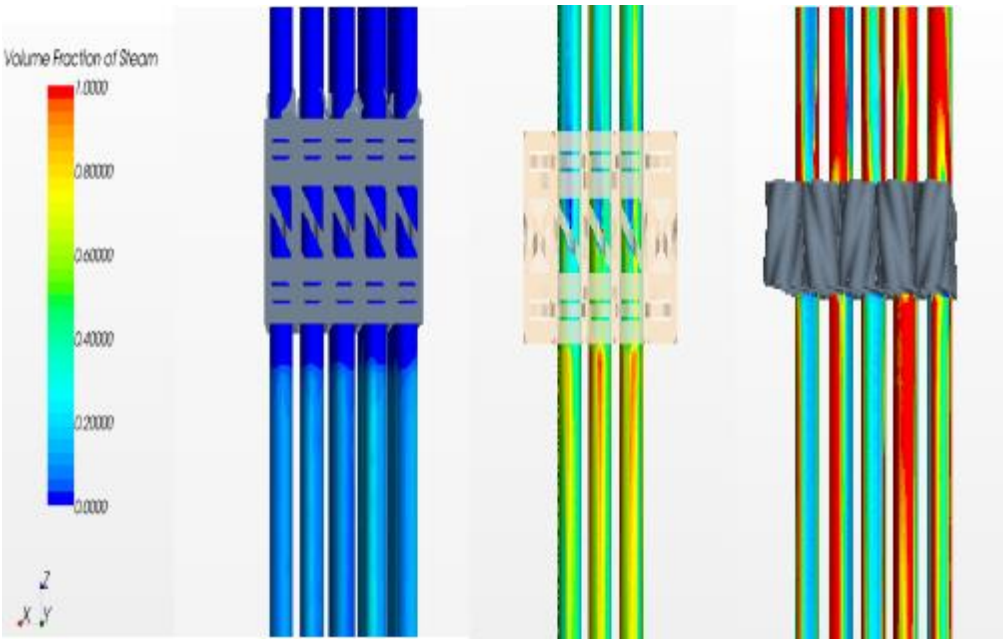

Figure 49
Vapour volume fraction on rod surfaces for the three spacer grid types. Red shows the dryout area. (Extracted from Yan et al[56].)

A more detailed examination of the calculated flow patterns shows the split vane grid creates a large amount of tangential flow and swirl inside the sub-channel. This flow pattern causes exchanges between the cooler fluid in the centre of the sub-channel and the hotter fluid near the rod surfaces. The resulting thermal mixing reduces the rod temperature and the amount of steam in the coolant; see Figure 50.

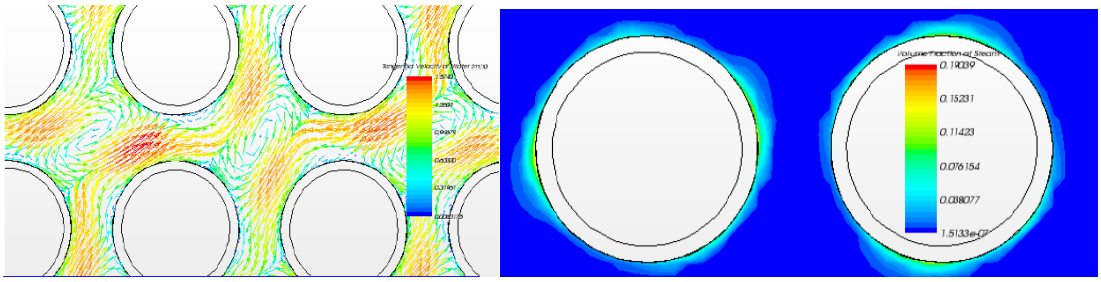

Figure 50
Tangential flow and void distribution at 0.017m above the split vane grid (Extracted from Yan et al[56].)

With the vaneless grid, the lateral flow inside the sub-channel is very small. Without the cross channel mixing flow, a higher concentration of vapour is allowed to build up around the rods; see Figure 51.

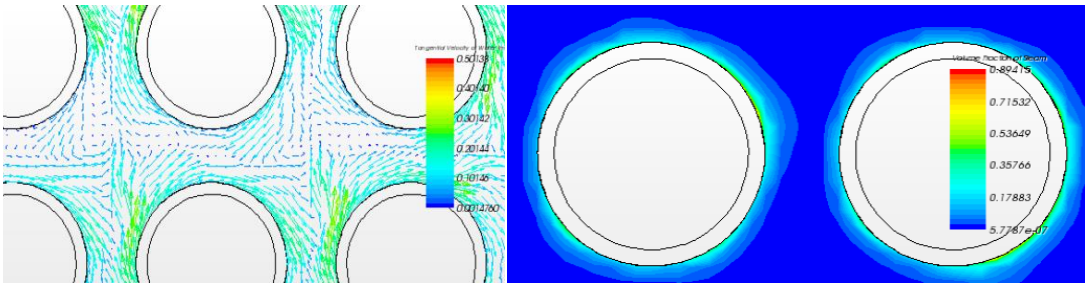

Figure 51
Tangential flow and void distribution at 0.017m above a vaneless grid. This contrasts with the performance of the split vane grid, shown in Figure 50. (Extracted from Yan et al[56].)

The HFT grid generates a strong swirling flow around the rod. The swirling flow carries the stream of vapour around the rod instead of carrying the vapour into the centre of the sub-channel. As a result the concentration of steam around the rods increases leading to dryout and CHF. See Figure 52.

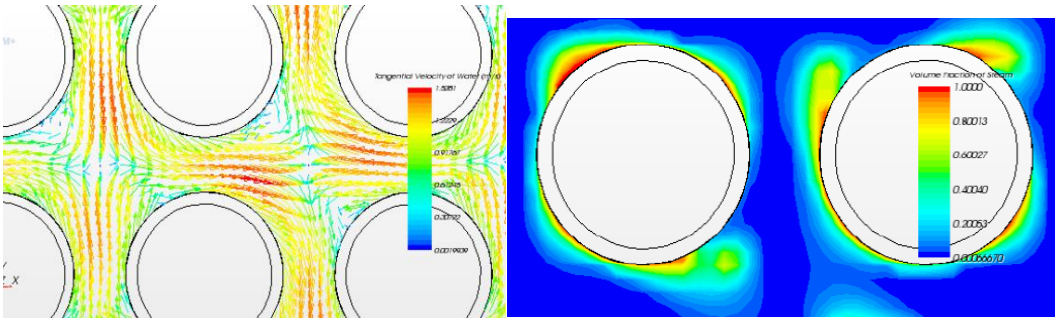

Figure 52
Tangential flow and void distribution at 0.017m above a HFT grid (Extracted from Yan et al[56].)

9.4 CFD prediction of CHF in fuel bundles at Areva

Areva has carried out very similar work to that of Westinghouse. Alleborn et al[60] used the Eulerian multiphase boiling model in STAR-CD to predict CHF in fuel subchannels. They used the heated pipe experiments of Weatherhead[61] for validation of their CHF predictions. The computed CHF heat flux shows a consistent under-prediction by a fixed margin, of around 25-30%. They used the same model to study effects of mixing vanes in a sub-channel, and found spacer grids with mixing vanes to be predicted to increase the CHF value by about 15%, which is in the range observed by measurements.

Goodheart et al[62] used the Eulerian multiphase boiling model in STAR-CCM+ to simulate five test cases of the OECD/PSBT Benchmark[59]. As did those of Westinghouse, their CFD models used trimmed cells, with ~121 million cells. The average void predicted at the three measurement planes in all 5 test cases fell within the uncertainty of the experimental values; see Figure 53.

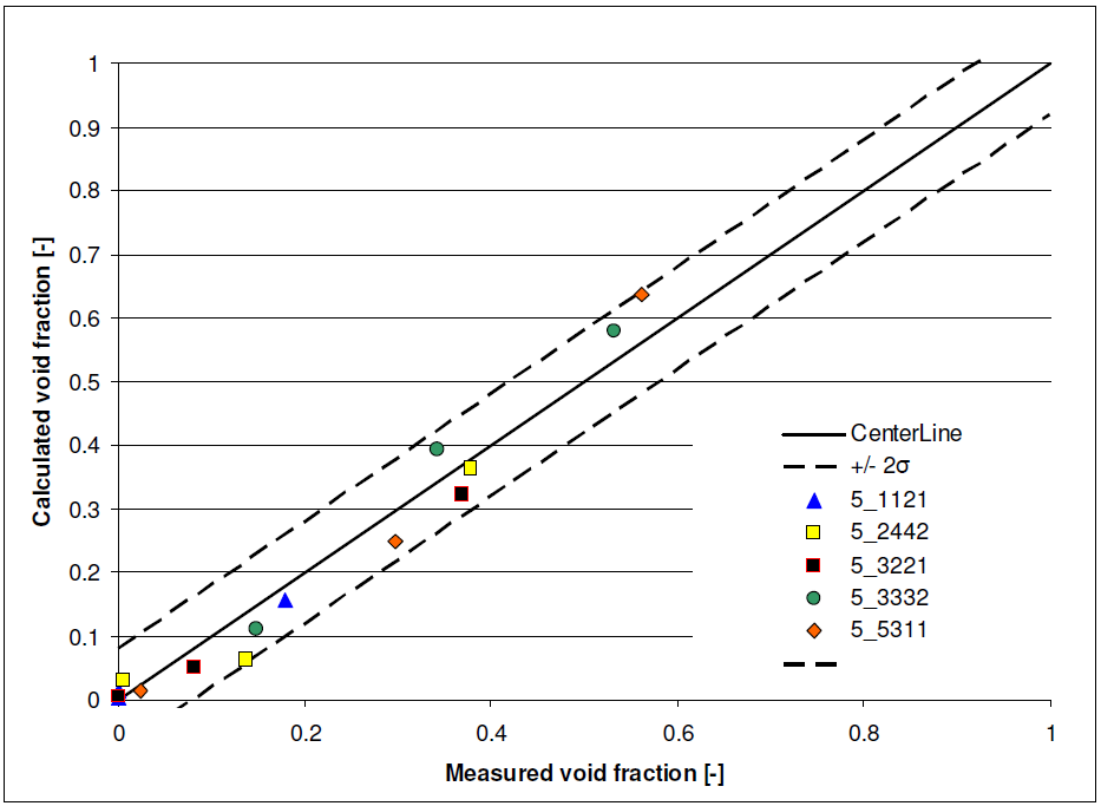

Figure 53
Comparison of averaged void between CFD and experiment for 5 PSBT test cases, extracted from Goodheart et al[62].

9.5 Closing remarks

Westinghouse and Areva are major vendors of nuclear fuel. Both companies are using the Eulerian multiphase boiling model in a commercial CFD code (STAR-CCM+) to analyse the design of their fuel bundles. In particular, it is being used to examine effects of spacer grids with mixing vanes on CHF performance. Such predictions have the same requirements as the single phase modelling discussed earlier, but add to this the use of the boiling models. These are undeniably complex, and prone to 'user effects'. It requires skilled and knowledgeable analysts to construct and interpret these models; this is well beyond generic 'black box' CFD (if indeed there is such).

Subject to that, the methods seem very powerful. The evidence from the published results of Westinghouse[56-58] is that CFD can be used to predict CHF (DNB) in fuel bundles. Predicted DNB power is within ~15% of the measured DNB power. Further, the approach can be used to study geometrical effects caused by the spacer grids.

Areva's studies[60, 62] came to broadly similar conclusions.

So far as DNB goes, two-phase boiling CFD has now reached a level of maturity where it is truly a valuable and reliable complement to measurements.

10 CHF MEASUREMENT FACILITIES

We present here a fairly short discussion of categories and kinds, rather than an exhaustive listing.

10.1 Introduction

It is not a hard and fast distinction, but it is convenient to divide CHF measurement facilities into two broad categories.

Some, generally smaller, are designed as "scientific" measuring facilities, typically allowing detailed particular phenomena to be investigated, or maybe incorporating particular kinds of instrumentation. There is not surprisingly quite large number of these, for a rather large variety of purposes.

Simply because it is one about which we happen to have the most direct knowledge, rather than because we are at all suggesting it is particularly important, we will give some information below about a rig which we are involved with designing and commissioning in India, aimed at investigating various aspects of film dryout CHF.

Given the enormous importance of CHF, and (perhaps in the light of the kinds of issues mentioned in the rest of this report!) it is generally thought necessary to rely upon very direct measurement of CHF performance, rather than to leave predictions. To that end all major vendors, and some associated national laboratories, maintain essentially full-scale, reactor condition facilities in which CHF can be measured. We were here simply mention briefly, and give references to, some of the main ones of these.

10.2 Film dryout CHF measurement at the Bhabha Atomic Research Centre (BARC), Mumbai

As has been discussed above, the dryout of the thin film of liquid on the heated wall depends, inter alia, on the rate at which droplets are entrained from this thin-film by the high-speed vapour flow over it.

There is a long-standing disagreement in the literature over whether or not the rate of entrainment of droplets is sensitive to the heat flux being applied to the film. Amongst other consequences, if it is found to be, is that entrainment rates measured in much simpler and cheaper air-water experiments will be seen to be less applicable. The most likely suggested mechanism if there is a dependence would be associated with the nucleation of bubbles of vapour within the film, and their ejection of droplets into the vapour flow as they rise through the film and burst at its surface.

The experimental details are rather complex, but in essence it requires being able to measure the flow rate of liquid in the film itself at the 100 bar, 300C operating conditions. . This is achieved by extracting all the liquid flowing in the film by making parts of the wall from a porous material, through which the liquid film is allowed to escape, and its flow rate measured.

The figures below show the overall facility, the flow / piping / instrumentation diagram, and a close-up of one of two sinter film extraction devices.

(In passing we would comment that this is of course only a very small and minor facility amongst those operated by BARC and, more broadly, by the Indian Department of Atomic

Energy. They operate in aggregate a comprehensive suite of CHF test facilities, covering a range of reactor types.)

Figure 54
The High Pressure (100 bar, 300 C) CHF film flow rate facility

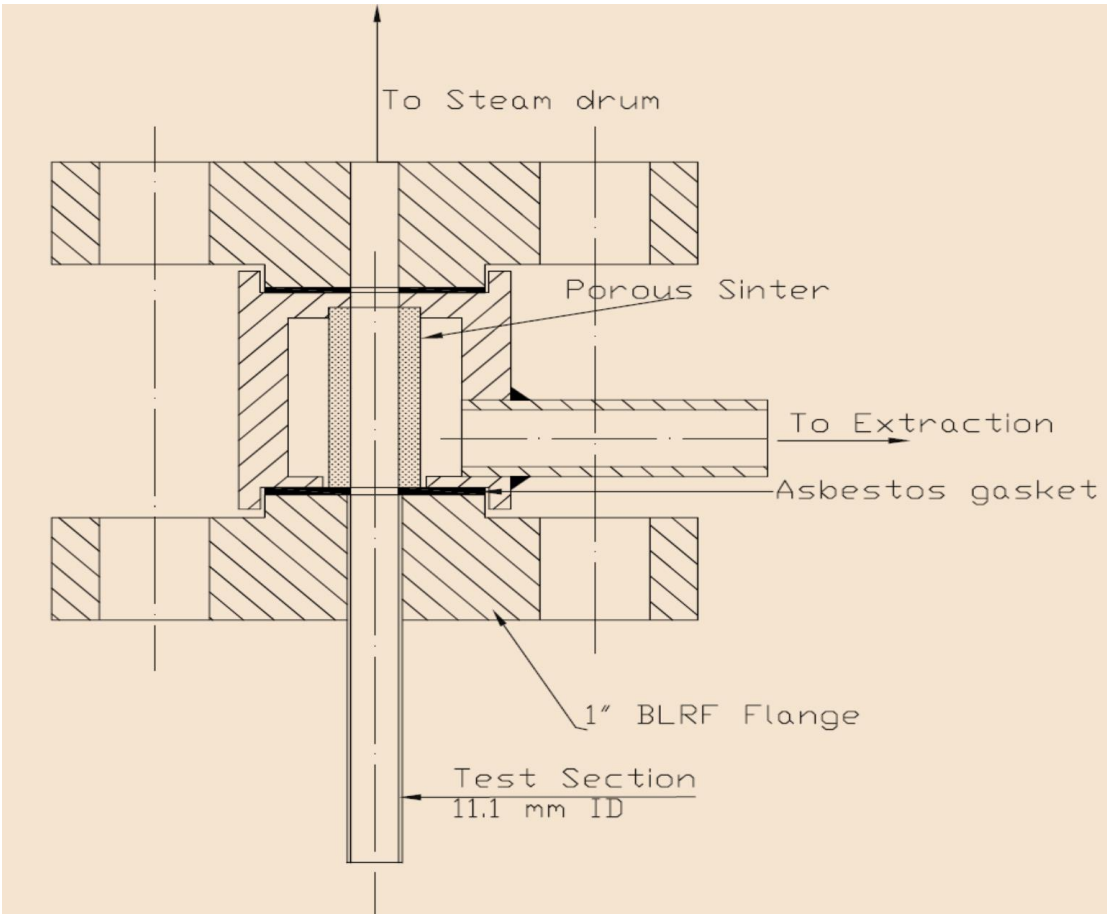

Figure 55
A detail of the sinter section, forming one of two film extraction devices

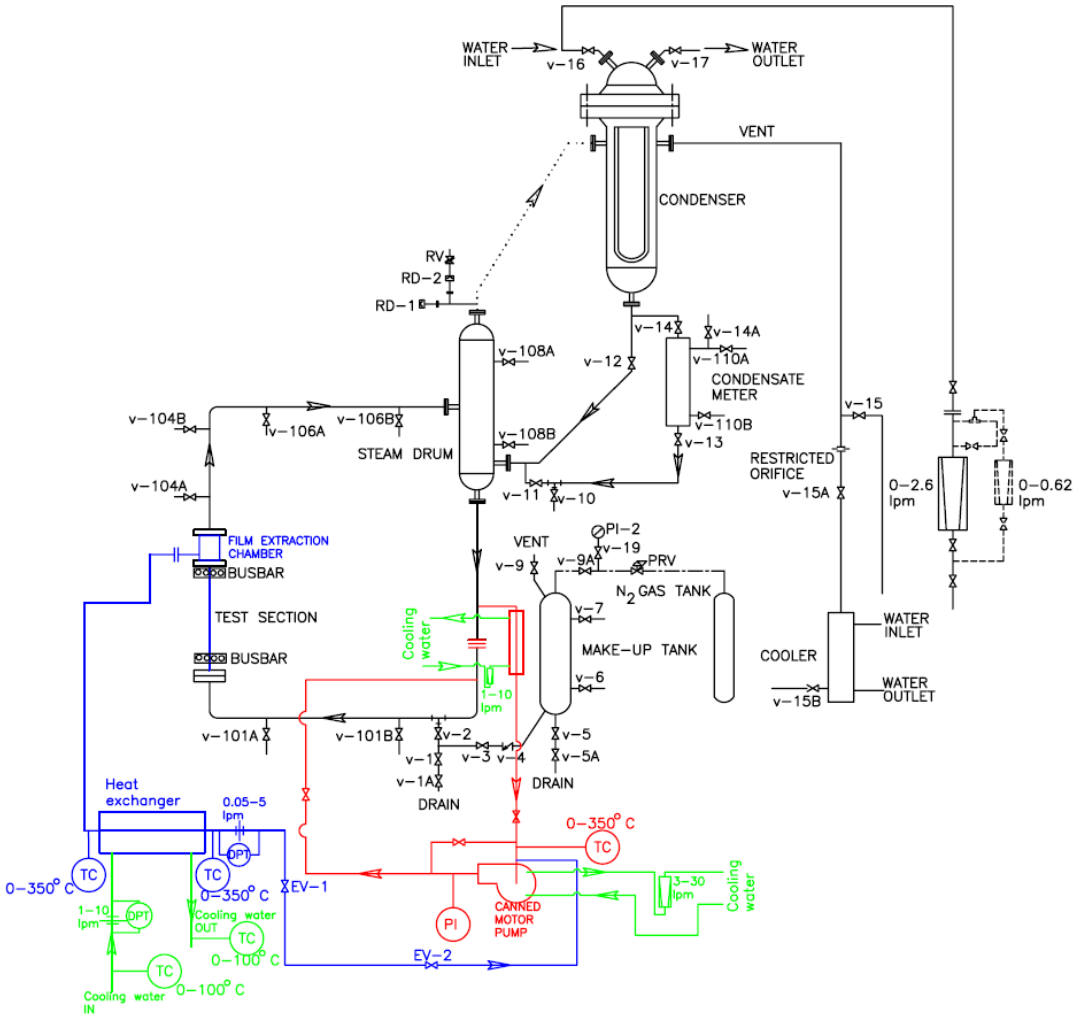

Figure 56
The piping, flow and instrumentation diagram of the facility

10.3 Fuel vendor 'full scale' rigs

As noted above, all fuel vendors operate full reactor conditions, full-length, rod bundle CHF test facilities, albeit they are more commonly scaled to test a small subsection of the assembly, perhaps 5 x 5, rather than a full 17 x 17 rods.

10.3.1 Westinghouse

Westinghouse[63] have now concentrated their thermal hydraulic testing of this kind at their Vasteras facility in Sweden, which inter alia houses their two CHF rigs ODEN and FRIGG[†]. ODEN is a PWR Loop for critical heat flux (DNB), pressure drop and mixing. FRIGG is a BWR Loop for critical heat flux (dryout) and pressure drop, both static and transient measurements, as well as hydraulic stability and void.

[†] Named after Norse gods, apparently.

The FRIGG loop, a much upgraded facility dating originally from the mid-1960's, has characteristics:-

- Power: 15 MW

- Pressure: 10 MPa

- Temperature: 311 C

- Flow: 25 kg/s

- Sub bundle or full bundle

- Production spacers & channel

The PWR ODEN facility is more recent, and is intended to be a successor to the Columbia University HTRF (Heat Transfer Research Facility).

- Power: 12 MW

- Pressure: 20 MPa

- Temperature: 366 C

- Steam quality up to 40%

- Flow: 0.7 - 22 kg/s

- 12 and 14 ft designs

- Up to 6x6 arrays

- Directly heated rods

10.3.2 Areva

The main Areva facility is KATHY[64, 65]. This too is a large and sophisticated facility, with main characteristics:

Electrical DC power: 20 MW, 83 kA

Design pressure: 185 bar

Design temperature: 360 °C

Flow rate: max. 250 m^3/h

Precise, automated power control system

620 data channels (easily extendible)

Test bundle geometries: 5x5, 9x9, 10x10, 11x11, 12x12

Axial power profiles: Cosine, top-, down-peak, uniform

A sense of the scale and complexity is gained from the three dimensional depiction of the facility in Figure 57.

10.4 Closing remarks

We are not aware of any facilities that have been developed to investigate the rather particular circumstances that are the subject of the present study. It is quite possible that they might exist, and being commercial facilities we would not have become aware of them. Indeed, we have been informed by ONR of some measurements at least attempting to

address the issue. Nonetheless, from such contact as we do have, we would not expect that this is an issue that has received the kind of attention that would be needed to address it properly.

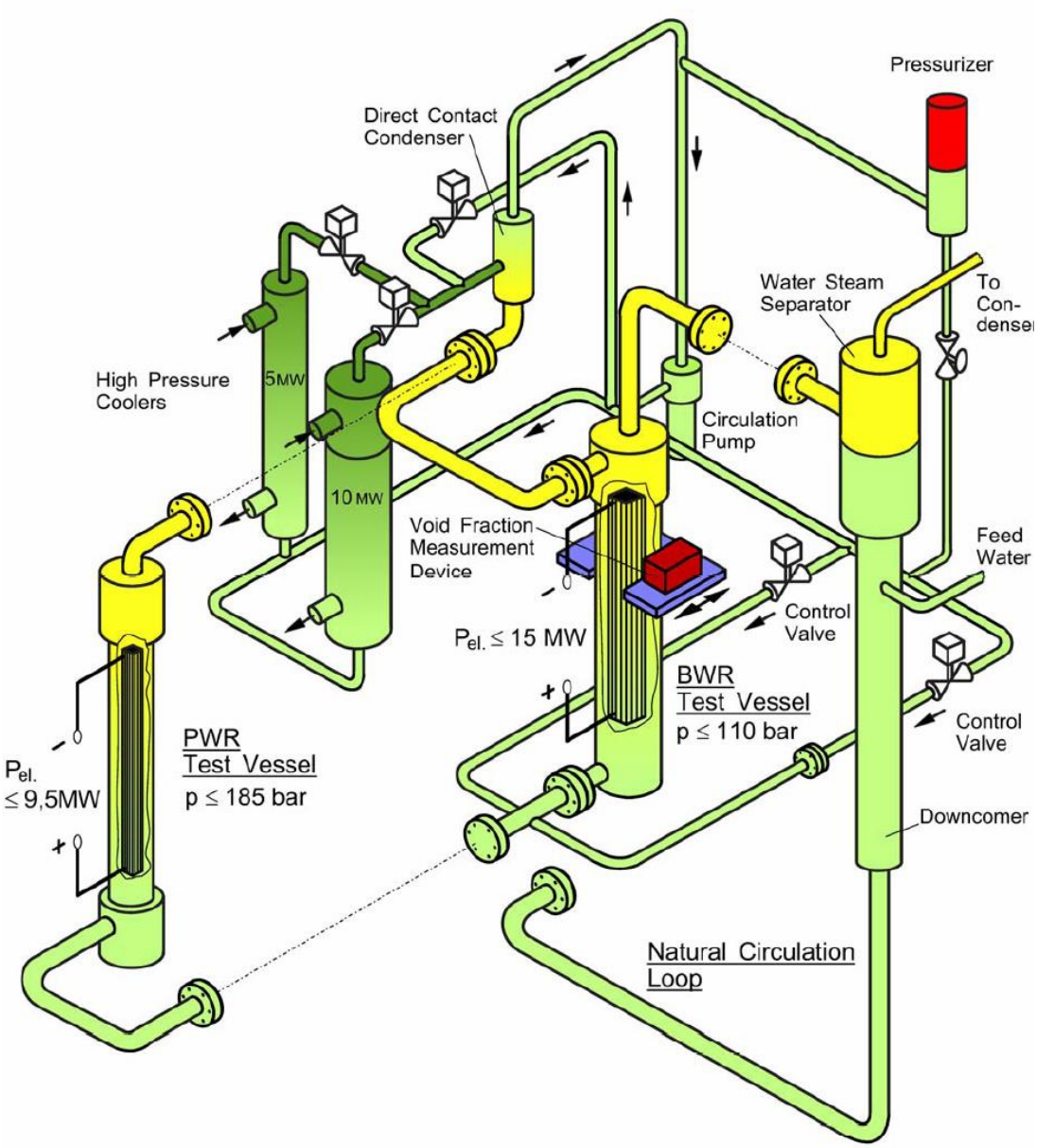

Figure 57
The KATHY CHF facility[65]

11 APPROACHES TO ASSESSING THE HEAT TRANSFER CONDITIONS DOWNSTREAM OF TOUCHING SPACER GRIDS

Drawing on the above, in the following sections we will try to identify what in our view might be sensible approaches to characterising the cooling of the fuel downstream of a pair of touching spacer grids.

Obviously, the approach one might take would depend upon how big a problem it was thought to be, and on how much one was prepared to spend, although of course these two issues themselves are coupled. Also of course, it is hard to know how big problem it is till one has reliably done this assessment. There is an element of Catch-22 here.

In the following sections we will discuss approaches largely independently of this, albeit we will attempt to indicate which of the more expensive and less practicable ones, and which are the more accessible.

11.1 Measurement

As has been indicated above, most CHF measurement facilities are capable of studying bundles that are very much a subset of a typical (e.g. 17 x 17) subassembly. In general, such reduced-size bundles still cause the behaviour their central regions to be sufficiently like that in full-size subassemblies such that results can be relied upon. Also, the more detailed and refined is instrumentation and observation that is desired, the harder it is to achieve in the centre of a large group of rods.

We reproduce here the earlier figure of the typical Areva spacer grid, showing the assembly-edge tabs turned over to form the flow blockages that are at the heart of the present discussion.

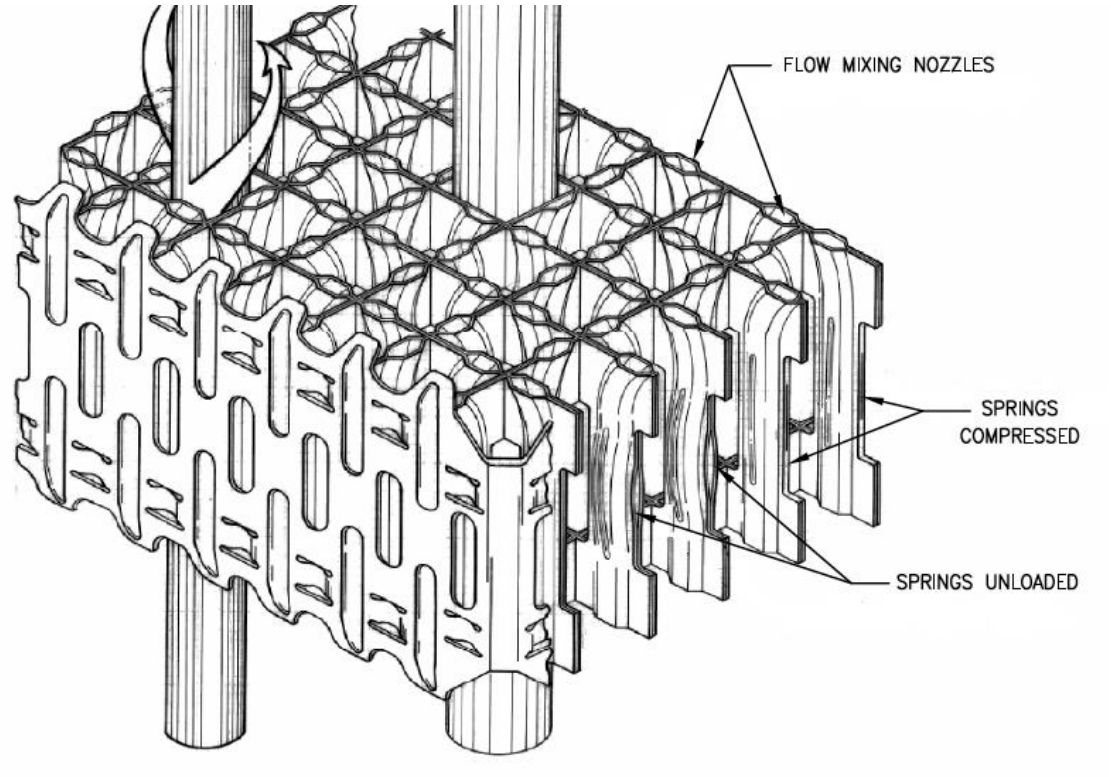

Figure 58
A typical Areva spacer grid, showing the turned-inwards tabs on the periphery.

One obvious approach would seem to be to make a "special" spacer grid, 5 x 5 or whatever was needed for that particular test facility.

This could be done by taking the outer "2 1/2 rod's worth" of two normal spacer grids, and bonding them together as if they had touched through subassembly distortion.

In the 5 x 5 assembly so formed, that would provide for those two central rows of pins conditions that were really quite similar to those expected to be experienced by the real pins at issue. Comparison of measurements made with this special part-subassembly, and a standard part-subassembly, would allow a very direct and convincing assessment to be made of the significance of the issue.

We understand that some measurements have been made in a 5 x 5 rod bundle with some attempt to simulate the flow blockage at issue. We do not have details, but understand the similarity to the real geometry was very much less.

All in all would seem to provide a really rather cheap and simple way to simulate the real geometry quite accurately. This should provide results more than good enough to decide if this is a significant issue that should be pursued. As evidenced from some of the earlier validation measurements discussed above, the making of non-standard spacer grids is really quite a routine issue (see Figure 48), and simply using a cut-about and re-fixed standard one would seem at the simpler end of this.

11.2 Single phase CFD analysis

There is evidence that a certain amount of crud has formed on the surface of the fuel rods about 10 diameters downstream of the spacer grid. This is an indication that at that location a

degree of nucleate boiling has occurred, as initial crud formation is commonly associated with this. That is obviously an indication that turbulence and/or mass flow rate of coolant there has been reduced by the blockage upstream.

We have seen above that the ability to model turbulent single phase flow in rod bundles and spacer grids is now rather good. A natural first modelling step might be to construct two single-phase CFD analyses, of a portion of two normally-separated, and of two touching spacer grids.

Whilst the prediction of flow around the two normal, separate part rod bundles will not be exact, it is likely to be quite good. Rather more importantly, the perturbation caused by the closure of the separation between the two assemblies should be predicted rather well.

Together, these results would allow the changed mass flow rate and turbulence, wall shear stress and so on in the region downstream of the spacer grid to be assessed. One would obviously look to see if the area of greatest heat transfer reduction was reasonably coincident with the area over which crud deposition has been observed.

It might be prudent to do this initially with an unheated, adiabatic model, just studying the flow. It would be a straightforward matter then to apply an appropriate heat flux distribution, and examine the predicted wall temperatures.

11.3 Two phase boiling CFD analysis

The same analyses could then be conducted, but invoking a wall-boiling, heat flux partitioning model.

In an ideal world, one might expect to see a small void fraction generated on the surface of external pins, a few diameters downstream of the spacer grid. It might in practice be necessary to raise the heat flux in the model in order to begin to generate noticeable void (as the amount of void required, over time, to generate a small amount of crud is probably rather tiny).

In either case, observing the spatial distribution over the surface of the first generation of void, as heat fluxes are raised, would be of great interest. This spatial distribution could then be compared to the observed distribution of crud formation.

11.4 Bubble-crowding CHF analysis

The natural next step would be steadily to increase the linear power throughout the model (for both models, normal and touching), and observe the distribution of void fraction over the surface. Again, whilst there are inevitably significant uncertainties with absolute values and so on, one would expect that the *difference* between the performance of the two models would give a reasonably reliable indication of the increased propensity to form near-surface void in the case of the touching space grids compared to the normal case.

We do not want to revisit here the difficulties and logical inconsistencies associated with the quantity "DNBR", but evaluation of the likely degree of the change to this quantity would be interesting. This could be achieved by steadily raising the linear power, along probably with judicious raising of the inlet temperature to the region modelled, to achieve conditions of high local near-wall void fraction in the vicinity of the spacer grid. The differences in power level, and all the extent and degree of void, between the two cases, would provide some indication of the degradation of DNBR performance caused by the touching spacer grids.

11.5 High quality, film-dryout CHF

We understand that the most likely form of critical heat flux to occur in this location is of the film-dry out form, occurring probably at low flow, low pressure and maybe low power.

We have discussed fairly extensively above the issues involved in attempting to predict the underlying fundamental processes, of droplet deposition, droplet entrainment and film flow, and the way in which these are complicated by "normal" spacer grids. We have mentioned some of the attempts, some which really represent frontiers in current methods development, to improve the handling of spacer grids in this context.

Plainly these issues are all rather more acute for the "non-standard" case of the spacer grid touching its neighbour, and in particular where such touching results in the quite significant blockage that seems the case here.

It is probably helpful to separate the problem into two (and arguably it needs to be three) parts; the disruption of the flow of the thin liquid film, any modifications to the rate of deposition, and possibly modifications to the rate of entertainment.

11.5.1 Entrainment and deposition

As we have indicated above, there is experience, and a degree of acceptance, of the approach of using deposition rates downstream of spacer grids that are semi--mechanistically and semi-empirically modified to account for the geometrical disturbance the grid presents. To the extent that "all" we have here is a slightly different geometry of spacer grid, in principle one can imagine doing something similar. Just as deposition downstream of conventional spacer grids has been informed by single phase CFD analyses of the associated flow, this would need to be informed by CFD analysis of the single phase flow in the touching spacer grid region. (The analyses suggested in the section above, and perturbations on those, would be appropriate.)

In principle one could attempt to make modifications of entrainment rate along the same lines, but this is rather more uncertain. However, since we are concerned with CHF, the entrainment rate will be relatively low because the film will be thin, and entrainment from thin films is small. It may be that one could get away with no modification. More generally, there is great scope to take the enormously powerful one-dimensional phenomenological capability that forms a major plank of CHF prediction and incorporate the approach into modern three dimensional CFD.

11.5.2 Film flow

The flow of the film, and its possible disruption by the spacer grid, possibly represents a greater challenge, but this may well depend acutely on the detailed design of the grid. Examination of Figure 58 shows that there is minimal contact between a fuel rod at the periphery of the assembly, and the outer face of the spacer grid. There are two short regions of line contact, where the pressed-in small "thumbnail" pieces touch the rod. If that is the only mechanical contact between the spacer grid and the fuel rods, one might expect that the film would flow more or less undisturbed. The remaining major opportunity for film disruption is via the folded-in tabs. If these are folded in such that there is significant contact around the perimeter of the pin, there will be film disruption, obviously. If they retain a modest (mm) clearance, the film again may well pass relatively undisturbed.

If there is significant contact, such that film disruption cannot be argued away, it is hard to see how modelling could be relied upon, without a significant development and validation programme.

12 SUMMARY OF RECOMMENDATIONS

We summarise in tabular form below the suggestions made above. We also indicate, very approximately, the likely duration in years of each activity; the time likely to be required for the activity to produce useful results. In the third column we give an approximate indication of effort in man-years.

Activity	Time	Cost	Section
Measurement: A partial (say 5 x 5) rod bundle, such as is used for CHF testing, could be built with a spacer grid formed from two '2 ½ rod's worth' of spacer grids joined together such as to engineer the blockage to be in the centre of the bundle. Otherwise-routine CHF testing of this assembly would provide quite direct evidence of the likely behaviour of the touching subassembly peripheries.	0.5	2.0	11.1
Single phase CFD analysis One could run what is by now more or less a conventional single-phase CFD analysis (using 'best practice' as discussed in the body) of an appropriate portion of a pair of spacer grids and partial bundles in both "touching" and normal configuration. This will allow flow perturbations, changed turbulence intensities and someone associated with the bowing to be investigated. As part of this one would see if significant changes were predicted in the region in which crud has been observed to form.	0.25	0.25	11.2
Two-phase boiling CFD analysis It would be straightforward to extend the above study by the inclusion of a wall heat flux, and the invoking of a wall-boiling (heat flux partitioning) model in the CFD. Again, the objective would be to see if the predicted propensity to nucleate boiling was observed to be in regions broadly corresponding to the observations of crud.	0.25	0.25	11.3

Bubble-crowding CHF analysis Building on the wall boiling model, studying void distributions as heat fluxes are raised would give an indication of where DNB was likely to be observed first (to a degree independently of the ability to predict the level of heat flux that causes DNB). Interest would of course focus on whether this was indeed downstream of the touching spacer grids.	0.25	0.25	11.4
Film disruption by spacer grids This is a generic issue, about which we have reasonable, albeit rather 'assertion-based', confidence that it is in practice not too much of a problem, but which becomes more uncertain and more acute in the present problem. CFD capabilities are now such that there would be great benefits from a focused program of observation / measurement of this to provide validation and model building support to a parallel program of development of models of film disruption to incorporate into CFD. In the context of this present study, *differences* in predictions film disruption between regular and touching spacer grids would be of great interest. This work, however, would have benefits well beyond this rather particular problem. In a nuclear context, there would be benefits in the many places and circumstances that thin film dryout needs to be predicted reliably in complex geometries.	5	10	11.5.2
Phenomenological modelling via CFD This could then feed into a broader program of the building of the next generation of phenomenological models, based on CFD, and able to deal more convincingly with three-dimensional effects in general. As with the work above, there would be benefits in the many places and circumstances that thin film dryout needs to be predicted reliably in complex geometries.	5	10	11.5.1

13 CONCLUSIONS

Having attempted to identify and describe the physical phenomena governing conditions downstream of spacer grids, and having reviewed our current capabilities ability to model the circumstances, we have attempted to identify how one might set about assessing whether or not the touching spacer grids present a problem, and how one might make a case that they do not (if that were to be one's conclusion).

One approach might involve purely measurement and demonstration. We suggested above that partial spacer grids could be combined to cause the geometry at issue to be constructed within the central region of a normal small bundle in the CHF facility. This could be done in a way that (more or less) replicated two un-deformed assemblies, and then in a way that replicated two deformed assemblies where their spacer grids were touching.

From a modelling point of view, the position seems less difficult as regards assessing low quality, bubble-crowding critical heat flux. We have outlined a series of calculations that one might contemplate. Whilst we do not suggest that these will generate in any sense "perfect" results, it seems that, carefully performed, they should allow the perturbation associated with this particular condition to be identified and characterised with reasonable credibility.

We understand, though, that film dryout, high quality, critical heat flux is more likely to be relevant here. We feel that the main determinant of whether a reasonable modelling-only case could be made depends upon the details of the geometry of the spacer grid. It seems to us that if the geometry offers the prospect of significant disruption of the liquid film, either a dedicated measurement program, or a program to develop and validate fairly sophisticated computational tools, would be required.

14 REFERENCES

[1] ONR, "Statement of service requirement for the provision of research support on study of local heat transfer coefficient on peripheral pwr assembly fuel in the event of touching spacer grids," Office for Nuclear Regulation ONR/T2888, 2016.

[2] G. F. Hewitt, *Handbook of Multiphase System: Chapter 6.4 'Burnout'*: Hemisphere/McGraw Hill, 1982.

[3] L. S. Tong and Y. S. Tang, *Boiling Heat Transfer and Two-phase Flow*, 2 ed.: Taylor and Francis, Washington, 1997.

[4] G. F. Hewitt, *Handbook of Heat Transfer: Chapter 15 'Boiling'*, 3rd ed. New York: McGraw-Hill, 1998.

[5] J. G. Collier, "Boiling within vertical tubes," in *Heat Exchanger Design Handbook*. vol. 1, G. F. Hewitt, Ed., ed New York: Begell House, 1998.

[6] J.-M. Le Corre, S.-C. Yao, and C. H. Amon, "Two-phase flow regimes and mechanisms of critical heat flux under subcooled flow boiling conditions," *Nuclear Engineering and Design,* vol. 240, pp. 245-251, 2010.

[7] G. Hestroni, *Handbook of Multi-Phase Systems*: Hemisphere, 1982.

[8] D. Groeneveld, J. Shan, A. Vasic, L. Leung, A. Durmayaz, J. Yang, *et al.*, "The 2006 CHF look-up table," *Nuclear Engineering and Design,* vol. 237, pp. 1909-1922, 2007.

[9] J. G. Collier, *Convective Boiling and Condensation*. Maidenhead: McGraw-Hill, 1972.

[10] R. V. Macbeth, "Burnout analysis. Part 5. Examination of published world data for rod bundles," UKAEA AEEW-R358, 1964.

[11] L. Biasi, "Studies in Burnout, Part 3: A New Correlation for Round Ducts and Uniform Heating and Its Comparison with World Data," *Energia Nuclaire,* vol. 14, pp. 530-536, 1967.

[12] USNRC, "TRACE v5.0 Theory Manual," US Nuclear Regulatory Commission.

[13] D. D. Hall and I. Mudawar, "Critical heat flux (CHF) for water flow in tubes - II. Subcooled CHF correlations," *International Journal of Heat and Mass Transfer,* vol. 43, pp. 2605-2640, 2000.

[14] D. D. Hall and I. Mudawar, "Critical heat flux (CHF) for water flow in tubes - I. Compilation and assessment of world CHF data," *International Journal of Heat and Mass Transfer,* vol. 43, pp. 2573-2604, July 2000.

[15] M. Ferrouk, S. Aissani, F. D'Auria, A. DelNevo, and A. B. Salah, "Assessment of 12 CHF prediction methods, for an axially non-uniform heat flux distribution, with the RELAP5 computer code," *Nuclear Engineering and Design,* vol. 238, pp. 2718-2725, 2008.

[16] W. Wong, "Effect of diameter on the critical heat flux," MSc, Department of Mechanical Engineering, Ottawa, 1994.

[17] A. W. Bennett, G. F. Hewitt, H. A. Kearsey, R. K. F. Keeys, and D. J. Pulling, "Studies of burnout in boiling heat transfer," *Transactions of Institution of Chemical Engineers,* vol. 45, pp. 319-333, 1967.

[18] L. S. Tong, H. B. Currin, P. S. Larsen, and O. G. Smith, "Influence of axially non-uniform heat flux on DNB," Westinghouse WCAP-2767, 1966.

[19] B. S. Shiralkar, "Analysis of non-uniform flux CHF data in simple geometries," NEDM-13279, 1972.

[20] R. K. F. Keeys, J. C. Ralph, and D. N. Roberts, "The effect of heat flux on liquid entrainment in steam-water flow in a vertical tube," UKAEA AERE-R6294, 1971.

[21] G. F. Hewitt and A. H. Govan, "Phenomena and Prediction in Annular Two Phase Flow," presented at the Advances in Gas-Liquid Flows; Presented at the Annual Winter Meeting of ASME, Dallas, 1990.

[22] J. Weisman and B. S. Pei, "Prediction of Critical Heat-Flux in Flow Boiling at Low Qualities," *International Journal of Heat and Mass Transfer,* vol. 26, pp. 1463-1477, 1983.

[23] S. Haensch, S. P. Walker, and C. Narayan, "Mechanistic studies of single bubble growth using interface-tracking methods," *Nuclear Engineering and Design (in press),* 2016.

[24] G. Yadigaroglu, "CMFD and the critical-heat-flux grand challenge in nuclear thermal–hydraulics," *International Journal of Multiphase Flow,* vol. 67, pp. 3-12, 2014.

[25] V. K. Dhir, "Mechanistic Prediction of Nucleate Boiling Heat Transfer–Achievable or a Hopeless Task?," *Journal of Heat Transfer,* vol. 128, 2006 2006.

[26] S. G. Kandlikar, "Heat Transfer Characteristics in Partial Boiling, Fully Developed Boiling and Significant Void Flow Regions of Subcooled Flow Boiling," *Journal of Heat Transfer,* vol. 120, pp. 395-401, 1998 1998.

[27] N. Kurul and M. Z. Podowski, "On the modeling of multi-dimensional effects in boiling channels," presented at the 27th National Heat Transfer Conference, Minneapolis, 1991.

[28] B. B. Mikic and W. M. Rohsenow, "A New Correlation of Pool-Boiling Data Including the Effect of Heating Surface Characteristics," *Journal of Heat Transfer,* vol. 91, pp. 245-250, 1969.

[29] M. Colombo and M. Fairweather, "Accuracy of Eulerian–Eulerian, two-fluid CFD boiling models of subcooled boiling flows," *International Journal of Heat and Mass Transfer,* vol. 103, pp. 28-44, 2016.

[30] L. S. Tong, "Prediction of departure from nucleate boiling for an axially non-uniform heat flux distribution," *Journal of Nuclear Energy,* vol. 21, pp. 241-248, 1967.

[31] G. P. Gaspari, C. Lombardi, G. Peterlongo, M. Silvestri, and F. A. Tacconi, "Heat transfer crisis with steam-water mixtures," *Enerqia Nucleare,* vol. 12, pp. 121-133, 1965.

[32] C. Lifante, T. Frank, and A. Burns, "Wall boiling modeling extension towards critical heat flux," presented at the NURETH-15, Pisa, Italy, 2013.

[33] J. Barbosa, G. F. Hewitt, G. Konig, and S. M. Richardson, "Liquid entrainment, droplet concentration and pressure gradient at the onset of annular flow in a vertical pipe," *International Journal for Multiphase Flow,* vol. 28, pp. 943-961, 2002.

[34] M. Ahmad, D. J. Peng, S. P. Walker, C. P. Hale, and G. F. Hewitt, "Droplet entrainment in churn flow," in *International Conference of Multiphase Flow*, Florida, USA, 2010.

[35] V. I. Milashenko, B. I. Nigmatulin, V. V. Petukhov, and N. I. Trubkin, "Burnout and distribution of liquid in evaporative channels of various lengths," *International Journal of Multiphase Flow,* vol. 15, pp. 393-401, 1989/6// 1989.

[36] M. Ahmad, D. Chandraker, G. F. Hewitt, P. Vijayan, and S. P. Walker, "Phenomenological modeling of critical heat flux: The GRAMP code and its validation," *Nuclear Engineering and Design,* vol. 254, pp. 280-290, 2013.

[37] D. Chandraker, A. Dasgupta, A. K. Nayak, P. K. Vijayan, S. P. Walker, and K. S. Deshpande, "Validation of the Dryout Modelling Code, FIDOM," in *16th International Topical Meeting on Nuclear Reactor Thermal Hydraulics (NURETH 16)*, ed. Chicago, 2015.

[38] L. Sanmiguel Gimeno, S. P. Walker, G. F. Hewitt, J.-M. Le Corre, A. Dasgupta, and M. Ahmad, "Validation and cross-verification of three mechanistic codes for annular two-phase flow simulation and dryout prediction," in *NURETH-16*, ed. Chicago, IL, 2015.

[39] A. Dasgupta, O. Patel, D. Chandraker, A. K. Nayak, S. P. Walker, and A. R. Rao, "Measurement of Film Flow Rate and Estimation of Dryout Power in Annular Flow," in *6th International and 43rd National Conference on Fluid Mechanics and Fluid Power*, ed. Allahabad, U.P., India, 2016.

[40] A. Dasgupta, D. Chandraker, S. Walker, and P. Vijayan, "An Assessment of the Correlations for Entrainment and Deposition Rates in Annular Flow for Dryout Prediction," in *Multiphase Science and Technology (submitted)*, ed, 2016.

[41] C. Adamsson and H. Anglart, "Influence of axial power distribution on dryout: Film-flow models and experiments," *Nuclear Engineering and Design,* vol. 240, pp. 1495-1505, 2010.

[42] A. Ioilev, M. Samigulin, V. Ustinenko, P. Kucherova, A. Tentner, S. Lo, *et al.*, "Advances In The Modeling Of Cladding Heat Transfer And Critical Heat Flux In Boiling Water Reactor Fuel Assemblies," presented at the The 12th International Topical Meeting on Nuclear Reactor Thermal Hydraulics (NURETH-12) September 2007, Pitsburgh, 2007.

[43] A. Tentner, E. Merzari, and P. Vegendia, "Computational fluid dynamics modeling of two-phase boiling flow and critical heat flux," in *ICONE22*, ed. Prague, Czech Republic, 2014.

[44] A. Tentner, P. Vegendia, A. Obabko, A. Tomboulides, P. Fischer, O. Marin, *et al.*, "Modeling of two-phase flow in a BWR fuel assembly with a highly-scalable CFD code," in *NURETH-16*, ed. Chicago, IL, 2015.

[45] J. Gong, S. Markidis, M. Schliephake, E. Laure, D. Henningson, P. Schlatter, *et al.*, "Nek5000 with OpenACC," in *Solving Software Challenges for Exascale*. vol. 8759, S. Markidis and E. Laure, Eds., ed Berlin: Springer-Verlag Berlin, 2015, pp. 57-68.

[46] K. Ikeda, J. Shimizu, Y. Yamaguchi, and K. Okamoto, "Study of spacer grid span pressure loss under high Reynolds number flow condition," in *ICONE17*, ed. Brussels, Belgium, 2009.

[47] K. Ikeda and M. Hoshi, "Development of Mitsubishi High Thermal Performance Grid (CFD Applicability for Thermal Hydraulic Design)," *JSME International Journal,* vol. 45, pp. 586-591, 2002.

[48] R. Sugrue, M. Conner, J. Yan, and E. Baglietto, "Pressure Drop Measurement and CFD predictions for PWR structural grids," in *TopFuel-2013*, ed. Charlotte, NC, 2013.

[49] D. M. Wells, P. Peturaud, and S. K. Yagnik, "Overview of CFD Round Robin Benchmark of the High Fidelity Fuel Rod Bundle NESTOR Experimental Data," in *NURETH-16*, ed. Chicago, IL, 2015.

[50] M. Martin, T. Keheley, K. Vogel, K. Goodheart, A. Hatman, and A. Chatelain, "Validation of AREVA's Best Practices in the EPRI Round Robin Benchmark," in *NURETH-16*, ed. Chicago, 2015.

[51] M. E. Conner, Z. E. Karoutas, and Y. Xu, "Westinghouse CFD Modeling and Results for EPRI NESTOR CFD Round Robin Exercise of PWR Rod Bundle Testing," presented at the NURETH-16, Chicago, 2015.

[52] B. Han, B. W. Yang, H. Zhang, H. Mao, and Y. Zha, "The effect of spacer grid critical component on pressure drop under both single and two phase flow conditions," *Kerntechnik,* vol. 81, pp. 257-267, Jun 2016.

[53] H. Mao, B. W. Yang, and B. Han, "Study on effects of mixing vane grids on coolant temperature distribution by subchannel analysis," *Kerntechnik,* vol. 81, pp. 244-250, Jun 2016.

[54] D. Chen, Z. Yang, Y. Zhong, Y. Xiao, and L. Hu, "Numerical investigation on the characteristics of two-phase flow in fuel assemblies with spacer grid," *Kerntechnik,* vol. 81, pp. 276-285, Jun 2016.

[55] S. Lo and J. Osman, "CFD Modeling of Boiling Flow in PSBT 5x5 Bundle," *Science and Technology of Nuclear Installations,* vol. 2012, p. 8, 2012.

[56] J. Yan, Z. E. Karoutas, L. D. Smith III, P. F. Joffre, and M. E. Conner, "Evaluating spacer grid CHF performance by high fidelity 2-phase flow modeling," in *TopFuel-2013*, ed. Charlotte, NC, 2013.

[57] J. Yan, L. D. Smith III, and Z. Karoutas, "Departure from Nucleate Boiling Modeling Development for PWR Fuel," in *ICONE21*, ed. Chengdu, China, 2013.

[58] J. Yan, P. Yuan, P. F. Joffre, Z. E. Karoutas, and L. D. Smith III, "CHF model development in Westinghouse," in *International seminar on subchannel analysis CFD modelling and verification, CHF experiment and benchmarking (ISACC-2013)*, ed. Xian, China, 2013.

[59] A. Rubin, A. Schoedel, M. Avramova, H. Utsuno, S. Bajorek, and Velazquez-Lozada, "OECD/NRC Benchmark Based on NUPEC PWR Sub-channel and Bundle Tests (PSBT), Volume I: Experimental Database and Final Problem Specifications," Nuclear Energy Agency, OECD2012.

[60] N. Alleborn, R. Reinders, S. Lo, and A. Splawski, "Analysis Of Two-Phase Flows In Pipes And Subchannels Under High Pressure," presented at the 7th World Conference on Experimental Heat Transfer, Fluid Mechanics and Thermodynamics: ExHFT-7, Krakow, Poland, 2009.

[61] R. J. Weatherhead, "Nucleate boiling characteristics and the critical heat flux occurrence in sub-cooled axial flow water systems," Argonne National Laboratory ANL 6675, 1963.

[62] K. Goodheart, N. Alleborn, A. Chatelain, and T. Keheley, "Analysis of the Interfacial Area Transport Model for Industrial 2-Phase Boiling Flow Applications," in *NURETH-15*, ed. Pisa, Italy, 2013.

[63] S. Andersson, A. Mingo, and M. Majed, "Westinghouse BWR and PWR Fuel Thermal Hydraulic Test Facility in Sweden," presented at the International Conference Nuclear Energy for New Europe, Portorož, Slovenia, 2008.

[64] O. Wieckhorst, J. Kronenberg, H. Gabriel, S. Opel, D. Kreuter, T. Berger, *et al.*, "AREVA'S TEST FACILITY KATHY: ROBUST CRITICAL HEAT FLUX MEASUREMENTS, A PREREQUISITE FOR RELIABLE CHF PREDICTION," presented at the Proceedings of the 22nd International Conference on Nuclear Engineering - 2014, Vol 2b, Prague, 2014.

[65] Areva. (2016). *The Areva KATHY CHF test facility*. Available: http://de.areva.com/EN/customer-550/kathy-loop-for-critical-heat-flux-tests.html